HYDRONAUTICS, incorporated

research in hydrodynamics

Research, consulting, and advanced engineering in the fields of NAVAL and INDUSTRIAL HYDRODYNAMICS. Offices and Laboratory in the Washington, D. C., area: 200 Monroe Street, Rockville, Md.

TECHNICAL REPORT 001-7

LOW DRAG SUPERCAVITATING HYDROFOIL SECTIONS

By

Jakob Auslaender

April 1962

Prepared Under

Bureau of Ships
Department of the Navy
Contract No. NObs-78396
Index No. SF-013-02-01

ABSTRACT

Existing theory and experimental information on the design and performance of two-dimensional, low-drag, supercavitating and fully ventilated hydrofoils is reviewed and summarized. The results of detailed calculations based on linearized cavity flow theory (neglecting gravity) at zero cavitation number are presented in the form of lift-cavity drag ratio vs. lift coefficient and non-dimensional bending modulus vs. lift coefficient of low-drag foils designed specifically for operation at depths of 1/2, 1, 2 and 5 chords, as well as infinite depth. The design of foils for arbitrary depths, including methods of interpolation between depths for which detailed plots are available is described. The necessary non-linear corrections and the effect of finite cavitation number are discussed and evaluated. The theory is shown to be in good agreement with experimental information found in the literature. A Summary Table of both experimental and theoretical work heretofore performed in this field is provided.

TABLE OF CONTENTS

LIST OF FIGURES

Figure No. Page No.

LIST OF TABLES

NOTATION

a	A depth dependent constant in the hydrofoil-airfoil transformation
c_D	Two dimensional non-linear drag coefficient = $\frac{D}{\frac{1}{2}\rho U_\infty^2 c}$
c_L	Two dimensional non-linear lift coefficient = $\frac{L}{\frac{1}{2}\rho U_\infty^2 c}$
c	Chord length
$c_d(h,k,\delta,\tau)$	Two-dimensional, linearized drag coefficient of a two-term foil designed for depth chord ratio h, with camber index k, design angle of attack δ and quasi-parabolic thickness coefficient τ, at $\sigma = 0$
$c_\ell(h,k,\delta)$	Lift coefficient of a two-term foil designed for depth chord ratio h, with camber index k and design angle of attack δ, at $\sigma = 0$, (linearized)
c_{L_σ} , c_{D_σ}	Lift and drag coefficient for $\sigma \neq 0$, (non-linear)
D	Two dimensional cavity drag
h	Depth of submersion/chord
k	Two term camber index. In a two term foil designed for infinite depth, $k = c_\ell(\infty,k,0)$
L	Two dimensional lift
m	Non-linear two dimensional lift coefficient/α_e
p_c	Cavity pressure
p_∞	Static pressure in the free stream
$T(\delta)$	Total thickness, at the trailing edge, due to angle of attack only = $y_c(h,1,0,\delta,0) + \delta$

$T(\tau)$ Total thickness, at the trailing edge, due to τ only $= y_c(h,1,0,0,\tau) - y_o(h,1,0,0,\tau)$

U_∞ Free stream velocity

x Distance along the chord measured from the leading edge as a fraction of c. The x axis is the foil reference line from which y_o and y_c are measured.

y_c Ordinate of the top cavity boundary, measured from the x-axis, expressed as a fraction of the chord length

y_o Ordinate of the bottom surface of the hydrofoil, measured from the x axis, expressed as a fraction of the chord length.

$y_c(h,x,k,\delta,\tau)$ y_c at chordwise location x, in a two term foil designed for operation at h, with camber index k, design angle of attack δ and quasi-parabolic thickness coefficient τ

$y_o(h,x,k,\delta,\tau)$ y_o at chordwise location x, in a two term foil designed for operation at h, with camber index k, design angle of attack δ and quasi-parabolic thickness coefficient τ

Z Hydrodynamic section modulus of the hydrofoil. This is the section modulus of a solid supercavitating foil whose top surface coincides with y_c

$\overline{Z}$ Non-dimensional section modulus $= Z/c^3$

α Angle of attack; the angle between U_∞ and the foil reference line (see Figure 3)

α_c Camber equivalent angle of attack, i.e., the angle of incidence of a flat plate which develops the same lift coefficient as a given, pure camber $= \dfrac{c_\ell(h,k,0)}{c_\ell(h,0,\delta)/\delta}$

α_e Effective angle of attack $= \delta + \alpha_c$

γ A measure of circular arc camber = 1/2 the central angle subtending the chord of a circular arc hydrofoil

δ Design angle of attack of a supercavitating hydrofoil; the angle between U_∞ and the x-axis (the foil reference line). The actual shape of the foil depends on δ (see Figure 3)

ξ The real coordinate in the airfoil plane

ρ Mass density of water

σ Cavitation number = $\dfrac{p_\infty - p_c}{\frac{1}{2}\rho U_\infty^2}$

τ Quasi-parabolic thickness coefficient. In a foil designed for infinite depth $T(\tau) = 2\tau$; in a foil designed for finite depth, $T(\tau) > 2\tau$.

LOW DRAG SUPERCAVITATING HYDROFOIL SECTIONS

INTRODUCTION

The requirement for increasing speeds of marine vehicles has focused attention on the design of high speed lifting surfaces. Such surfaces may serve as hydrofoil wings and thus be required to develop sufficient dynamic lift to raise an entire ship's hull clear of the disturbed surface of the sea. They may also serve as the means of horizontal control (rudders) of submerged, surface and over-the-surface high speed craft or to control the vertical motions (diving planes) of submerged vehicles.

Hydrofoils designed for low speed applications consist of the well known fully wetted sections which very closely resemble the cross sections of subsonic airfoils. Such airfoil sections, with their blunt, well rounded leading - and sharp trailing-edges have been used successfully for decades in the design of low speed propellers, pumps, rudders, and diving planes. More recent years have also seen the application of fully wetted hydrofoils to the design of wings for a number of relatively low speed hydrofoil craft. At sufficiently high speeds, however, the classical fully wetted section suffers severe loss in performance due to the onset of cavitation. The cavities that form due to high speeds or low ambient pressures are filled with the vapor of the surrounding liquid, or - in case air has access to the cavity - a mixture of air and liquid vapor. In a foil designed for fully wetted operation the onset of cavitation has the immediate effect of reducing the lift effectiveness of the foil

while generally increasing its total drag. In addition, the violent collapse of cavities whose length is smaller than the foil chord causes severe erosion of the hydrofoil surface.

One of the most important parameters that characterize the behavior of a foil after the onset of cavitation is the cavitation number σ, expressed as the difference between the static pressure in the undisturbed stream and the pressure in the cavity (vapor pressure, in the case of pure-vapor cavities), normalized with respect to the free stream dynamic pressure. The effect of the cavitation number on the flow pattern about a hydrofoil is schematically illustrated in Figure 1. Once a cavity is formed (the value of σ associated with this condition is known as the incipient cavitation number) its length increases with decreasing cavitation number until, at $\sigma = 0$ (i.e., when the pressure in the cavity equals the pressure in the undisturbed flow or, when the speed of the foil through the liquid becomes infinite) the cavity, in theory, becomes infinite in length. At values of σ for which the cavity is just sufficiently long so that the pressure pulses created by its collapse clear the surface of the foil, the latter is no longer subject to cavitation erosion. In that condition, however the eddies and the re-entrant jet which exist at the downstream end of the cavity may impinge upon the foil trailing edge and cause severe buffeting and foil vibrations. Upon further reduction of the cavitation number the cavity length increases to the point where the reentrant jet is dissipated before it reaches the trailing edge of the foil. In that condition the flow is said to be supercavitating. Thus

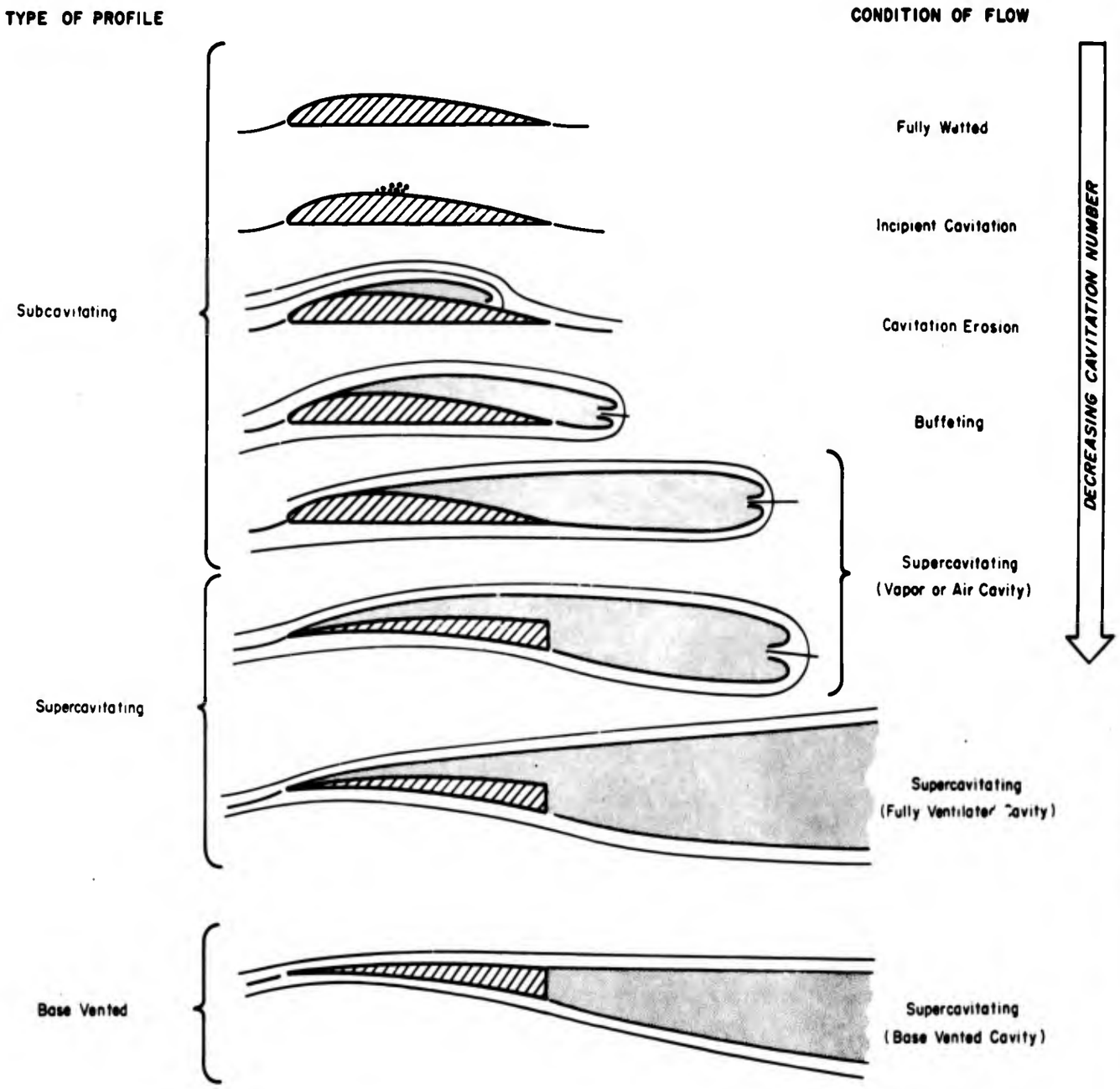

Figure 1- The Effect of Cavitation and Ventilation on the Hydrofoil Flow Pattern.

cavities associated with supercavitating flows are very long (at least two foil chords but, usually, much longer); they may be filled with liquid vapor or with a foreign gas or a mixture of both. Flows in which the cavity is filled with atmospheric air have come to be called ventilated or vented flows. The term "supercavitating" is, however, applied herein to all cases of sufficiently long cavities, regardless of whether these are filled with water vapor or air.

Ventilated flows are of extreme importance in connection with hydrofoil craft, propellers and rudders. The proximity of all these devices to the free water surface is particularly conducive to the phenomenon of spontaneous ventilation. At quite moderate speeds (say, 25-30 knots) sufficiently low pressures may exist on the underwater lifting devices to create adequate potential for ventilation which will occur very rapidly when the necessary path for air rushing in from the surface is created during turning maneuvers (yawed struts) or during operation in rough water. As has been pointed out by Johnson and Tulin (1), the consequences of spontaneous ventilation may well have catastrophic consequences for hydrofoil boats utilizing fully wetted foils because the severe loss of support (as much as 75 percent of the pre-ventilation lift) may cause the hull of the craft to crash into the water.

The difficulties associated with the prevention of cavitation and ventilation can be avoided by inducing a properly designed hydrofoil system to ventilate at a sufficiently low speed. If the maximum speed of such a foil is only moderately high (say, 40-50 knots) the optimum configuration may be one in which only part of the suction side or only

the blunt trailing edge of the foil is ventilated. Such configurations are known as Base Vented hydrofoils. For higher speeds, however, the optimum configuration is often one in which the air-filled cavity springs from the leading edge. The advantage of a system incorporating such Fully Ventilated hydrofoils is that they can be designed so that once ventilated, no further ventilation, nor any cavitation can occur, resulting in a stable lifting surface free from force discontinuities, erosion or buffeting.

In Figure 2 an NACA photograph of a vapor cavitating, cambered hydrofoil (Figure 2a) at a speed of 80 fps and a cavitation number of 0.33 is compared with a photograph of the same foil (Figure 2b) operating fully ventilated, at the same angle of attack, a somewhat higher cavitation number (σ = 0.48) and a speed of only 20 fps. It is to be noted that except for a slight lengthening of the cavity associated with the drop in cavitation number the flows are very similar in appearance. The foil shown in Figure 2b is an example of natural ventilation in which air is being bled to the foil upper surface from the atmosphere. Figure 2c, a photograph made recently at the David Taylor Model Basin, shows a cambered foil operating fully ventilated at a depth of two chords and a cavitation number of 0.10. As can be seen a much longer cavity is associated with the low cavitation number which, in this case, was obtained by pumping air to the upper surface of the foil.

An excellent general discussion of cavitation and ventilation phenomena, employing interesting parallels between hydrofoil and airfoil design has been given in Reference (1) as part of the present series of BuShips sponsored

reports. For an interesting discussion of the mechanics of cavitation and on the behavior of bodies in supercavitating flow the reader is referred to Eisenberg (2), and Tulin (3), and to the extensive bibliography therein.

In order to obtain satisfactory performance characteristics in supercavitating (or fully ventilated) operation it is, of course, necessary to design foils specifically for that condition. The pressure surface of such a foil must be so designed as to insure the absence of cavitation thereon, and so as to minimize the form drag that results from the presence of a trailing low pressure region (the cavity). Its upper surface should be shaped so as to fall within the cavity generated by the pressure surface so that frictional drag is minimized. These foils, which are generally wedge shaped with relatively thin leading edges, moderately cambered lower (or pressure) surfaces and blunt trailing edges, have come to be known as supercavitating foils.

The study of supercavitating flows has reached the point at which it is possible to establish methods of designing practical, low-drag, two dimensional hydrofoil sections that are prerequisite to the design of optimum supercavitating hydrofoil systems. It is the purpose of this paper, after a brief review of the pertinent studies of supercavitating flow about two-dimensional lifting surfaces, to present the results of detailed studies of the behavior of a family of such foils, designed to give optimum performance (i.e., minimum cavity drag) while delivering a desired lift and maintaining a desired section bending modulus. This report is concerned only with the two dimensional aspects of the problem; the methods of using

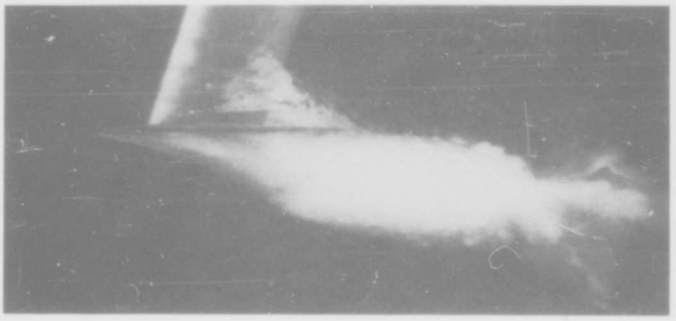

(a)- Vapor; 80 fps, σ = 0.33

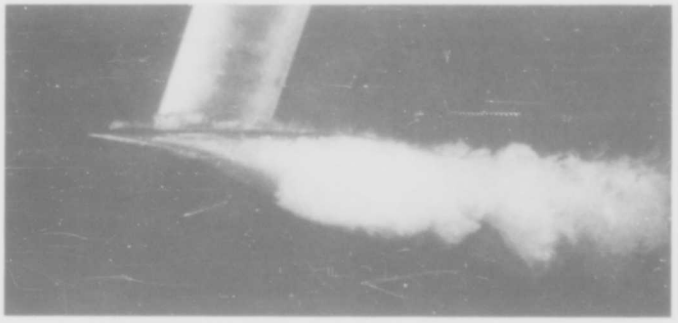

(b)- Air (Natural Ventilation); 20 fps, σ = 0.48

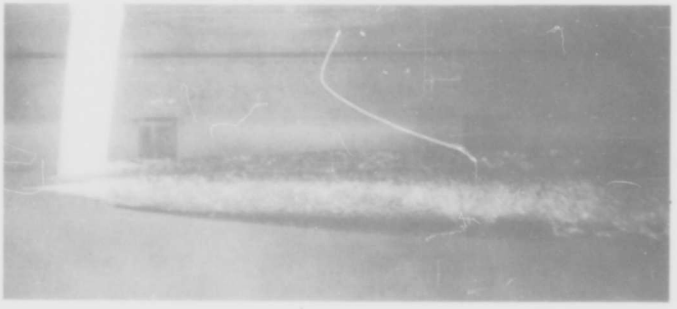

(c)- Air (Forced Ventilation); 30 fps, σ = 0.10

Figure 2- Photographs of Air and Vapor Cavities on Supercavitating Cambered Hydrofoils

the two-dimensional information in the design of actual, three-dimensional wings are subject to separate study.

The cavitation number associated with adequately ventilated foils operating at reasonably high speeds is very small. For example, a foil fully vented to the atmosphere, moving at 60 knots at a depth of 5 ft. operates at $\sigma = 0.031$ and at 80 knots the cavitation number is only 0.018. The σ of a pure vapor cavity under the same conditions (at 60 knots) is approximately 0.18; and the value of σ associated with a pure vapor cavity at the 0.5 radius of a 3 ft. diameter, supercavitating propeller operating at 2000 rpm at a shaft submergence of 5 ft. and a forward speed of 60 knots is approximately 0.044. Since the effect of small values of σ is very small (up to, say, $\sigma = 0.03$ it is very nearly negligible) a major part of this study is concerned with foils designed for zero cavitation number and the effect of finite σ (< 0.4) is evaluated separately.

The early mathematical investigations of cavity flows such as those performed by Kirchoff (4), Helmholtz (5), and Levi-Civita (6), (see Milne-Thomson (7), chapter 12 and Birkhoff (8), chapter 2) are almost all concerned with exact (non-linearized) solutions. It is an unfortunate fact, however, that exact solutions in closed form to the direct problem (i.e., the problem of ascertaining the characteristics of a given shape) have been obtained only for the very simple case of a flat plate at incidence. The exact solution of the latter was obtained by Rayleigh (9) for the case of an infinite fluid and by Green (10), and Chapligin (11), for the case in which a free surface is present in the vicinity of the suction side of the plate.

The dilemma is resolved by the acceptance of two basic changes in the method of attack on the problem. The first of these, suggested by Levi-Civita (6), is that we consider what is normally regarded as the inverse problem. In this method we construct fully cavitating flows without initially specifying the shape of the hydrofoil. Instead, we specify the pressure on the streamline which forms the loaded side of the hydrofoil and on the cavity boundaries (the free streamlines) and then proceed to calculate the hydrofoil shape that produces these pressures, and the shape of the free streamlines. If the resulting shape is a practical one, we use the initially prescribed pressure distribution to calculate the performance characteristics. The second necessary step in the direction of obtaining practical methods for the design of supercavitating hydrofoils was accomplished when Tulin (12) introduced a first order linearized cavity flow theory. The loss of accuracy caused by the linearization is insignificant as long as the requirements of linear theory (small slopes and small velocity perturbation) are satisfied and is, at any rate, overwhelmingly overshadowed by the fact that without linearization the detailed design of low-drag foils, especially for the case of finite operating depths, is not within the realm of practical possibility.

The practical possibilities of designing low drag supercavitating foils were first discussed by Tulin and Burkart (13). They applied the linearized cavity flow theory to the inverse problem and showed that the hydrofoil problem may be transformed into the problem of an equivalent thin airfoil. Thus they produced a linearized theory for determining the forces and moments on fully cavitating hydrofoils of arbitrary shape and specified

pressure distribution, operating at zero cavitation number and proceeded to show what kind of pressure distributions lead to effective, practical foils.

The pressure (or vorticity) distribution on the equivalent airfoil may be expressed in terms of a Fourier Series. Tulin and Burkart (13) chose a low drag shape by specifying the first two terms in the Fourier expression so as to result in the lowest cavity drag that is commensurate with the condition that the pressures on the pressure side of the foil be nowhere less than the static pressure in the undisturbed stream. This shape has since come to be known as the Two-Term Camber and foils in which it is combined with angle of attack and, if necessary, with an appropriate thickness distribution, have come to be known as Two-Term Supercavitating Hydrofoils.

Although Tulin and Burkart (13) presented general expressions for the location of cavity boundaries they specifically calculated only the cavity boundary (and thus, the maximum foil thickness) due to a flat plate at incidence. They did not, in that reference, calculate the minimum design angle of attack that must be combined with a given amount of two-term camber in order to obtain a finite cavity thickness over the entire chord length. This problem was, however, treated by Tulin and Burkart at the David Taylor Model Basin at about the time of publication of the previous reference in connection with the design of supercavitating propellers. The results were later incorporated into a propeller design paper by Tachmindji, Morgan, Miller and Hecker (14) which thus reported on the first practical application of low drag supercavitating hydrofoil sections. Figure 3 shows a typical flow pattern on a supercavitating propeller at the David Taylor Model Basin. It is to be noted that a large,

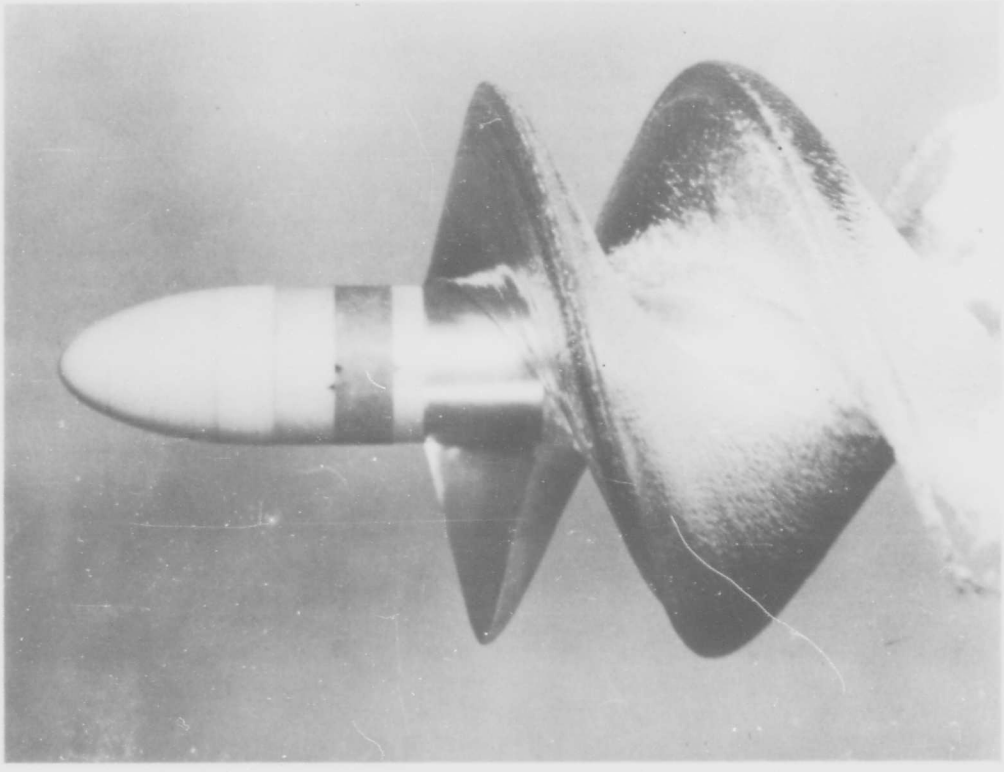

Figure 3 - A Two-Bladed Supercavitating Propeller

fully developed cavity emanates from each leading edge, covers the entire back of each blade and extends far downstream, and that the blade faces (pressure sides) are entirely free from cavitation.

Johnson (15) extended the work of Tulin and Burkart to include camber distributions (for infinite depth) derived from, in one case, the first three and, in a second case, the first five terms of the vorticity series expansion and presented approximate calculations of the upper cavity streamline. Foils incorporating the camber distributions resulting from the first three and the first five terms are known as Three- and Five-Term Supercavitating Hydrofoils. In later papers, Johnson (16) and (17) also developed a method for estimating the effect of finite depth on the lift of two-, three-, and five-term foils designed for infinite depth. The three- and five-term foils deliver higher lift-cavity drag ratios than the two term foils. It will be seen below, however, that this statement is strictly correct only when foil strength is not taken into account.

The effect of depth on cavity drag was evaluated for the first time in Reference (18). In that report it was also shown that the transformation between the hydrofoil and its equivalent airfoil is a function of the operating depth and since the derivation of the appropriate hydrofoil shape (i.e., the shape that will produce the specified pressure distribution) is dependent upon the hydrofoil-airfoil transformation, it is clear that the methods of (18) result in foils which are designed for a specific operating depth. The original two-term foils (13), as well as the original three- and five-term foils (15), are specifically designed for the condition that the liquid medium extend to

infinity along a line parallel to the lift vector. Hence they are specifically applicable to supercavitating hydrofoils operating at depths that are very large compared to their chord length and to supercavitating propellers whose thrust is directed along a line parallel to the surface. Despite the importance of the free surface upon foil performance, low drag foils designed for finite depths are generally similar in shape to those designed for infinite depth, differing from the latter only in detail.

When considering supercavitating hydrofoils that are to operate at a finite depth below a free surface, two choices are presently available. In the first of these a foil whose shape is designed for infinite depth is operated as efficiently as possible at the desired, finite depth by making appropriate changes in the geometric angle of attack. When such an infinite-depth foil approaches the surface, its effective angle of attack increases. Since it is necessary to maintain the condition in which the dividing streamline coincides with the leading edge (the condition of "shock free entry"), the foil must be operated at an angle of attack which is smaller than the infinite depth design angle. The lift due to camber and the chordwise pressure distribution due to camber also change as the depth of submersion is varied. Since the shape of the foil is fixed, the precise evaluation of its characteristics amounts to solving the direct problem which, as stated above, is a very difficult task indeed, even when only the linearized theory is used. As mentioned previously, Johnson (16, (17, and (19) developed an approximate method for calculating the effect of depth on angle of attack and on the lift due to camber of a foil whose shape is initially fixed. The method is quite

adequate and very useful in ascertaining the effect of depth variation on the performance of a foil of given shape.

It is quite clear, however, that foils whose shape is specifically designed for their anticipated operating depth deliver better performance than infinite depth foils whose incidence has been corrected for finite depth operation. For this reason, a comprehensive study of two-dimensional, supercavitating ($\sigma = 0$), depth-adapted hydrofoils was initiated at HYDRONAUTICS, Incorporated. This study utilized the depth dependent conformal transformation (18) to derive the linearized general expressions for the foil lower surface shape, cavity shape, lift, drag and moment of hydrofoils whose pressure (or vorticity) distributions are specified in the plane of the equivalent airfoil. These general expressions were used to derive analytical expressions for the shapes and performance of foils which have the following types of pressure distribution: (a) two-term camber, (b) three-term camber, (c) five-term camber, (d) constant pressure camber, (e) the pressure distribution on a flat plate at incidence, and (f) the pressure distribution associated with a symmetric parabola at infinite depth and a similar, non lifting shape at finite depths, which has, hence, been called "quasi-parabolic thickness". The results of this study were published in a previous HYDRONAUTICS, Incorporated Report (20). Semi-parabolic thickness was introduced because its use makes it possible -- usually but not always at the cost of some additional drag -- to round the otherwise extremely sharp leading edges of supercavitating foils. Recently accumulating experimental evidence has shown that the extremely sharp leading edges associated with angle of attack are prone to excessive vibration. Figure 4, reproduced here

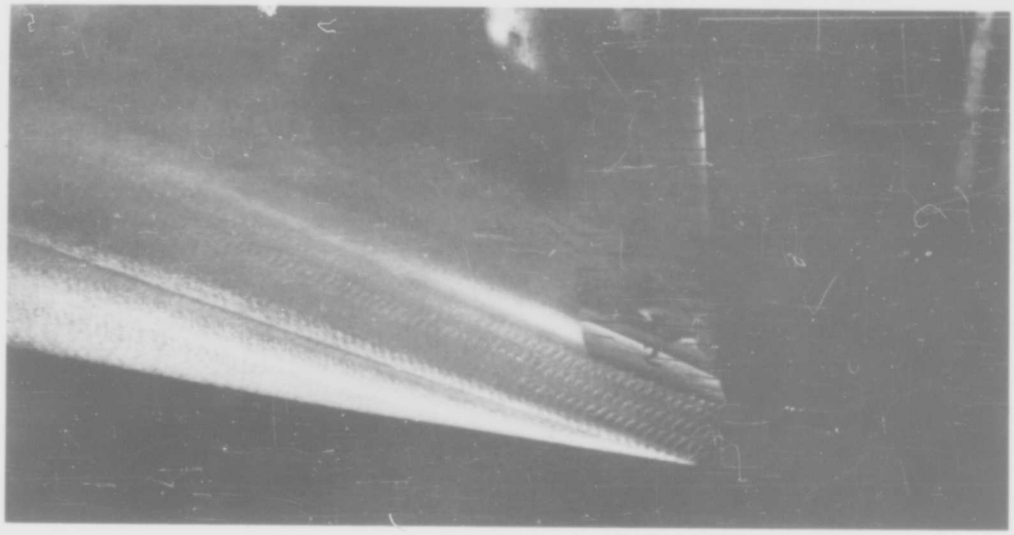

Figure 4- Photograph of the Flow about a Flat Bottomed Hydrofoil, Illustrating Leading Edge Vibration
$\alpha = 8°$, $h = 0.21$, $U_\infty = 148$ fps

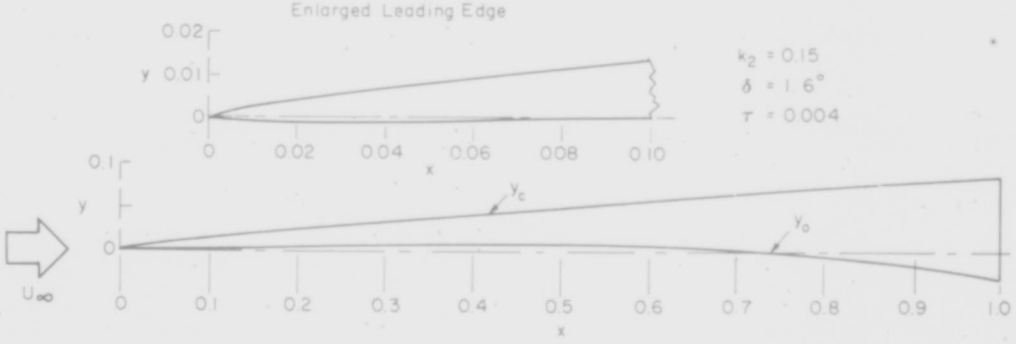

Figure 5- Typical Two Term Hydrofoil Section Designed for a Depth of One Chord;
$c_\ell = 0.195$, $\frac{L}{D} = 34.5$, $\bar{z} = 4.1 \times 10^{-4}$

from Reference (21) illustrates the type of leading edge vibration that has been observed; Figure 5, reproduced from Reference (20), shows a typical two-term foil with angle of attack (δ) and a moderate amount of quasi-parabolic thickness (denoted by τ). As can be seen in the enlarged view of the forward part of the foil, the leading edge is quite nicely rounded. A two-term foil designed for the same depth, producing the same (linearized) lift coefficient and obtaining the same section modulus (see definition on page 26) without benefit of quasi-parabolic thickness has a much sharper leading edge* and its lift drag ratio is 36 versus the L/D = 34.5 of the foil in Figure 5. As mentioned in Reference (20) a high-speed digital computer at the David Taylor Model Basin was used to calculate the performance characteristics and the section bending moduli of foils that were composed of all reasonable combinations of the pressure distributions listed above. The section moduli thus calculated were based on the assumption that the entire volume of the cavity would be solidly filled with metal. This computer study was done for the purpose of ascertaining, by means of a computer-programmed optimization procedure, which combination, if any, of types of pressure distribution will result in foils whose lift-drag ratio is highest for given values of lift and section bending modulus (see definition on page 26) at a given depth. The study was carried out for five finite depths, ranging from 1/4 to 5 chords, as well as for infinite depth. At each depth, a potential total of 4980 different foils was taken into consideration by the optimization procedure. The optimization process indicated that

---

*The thickness-chord ratio at 2% chord of the foil without quasi-parabolic thickness ($\delta = 2.05^{\circ}$, $k = 0.132$, $\tau = 0$) is 0.356% while that of the foil with quasi-parabolic thickness (Figure 5b) is 0.493% - an increase of 38% over the previous value.

for practical values of the depth chord ratio h, the section modulus coefficient $\overline{Z}$, and the lift coefficient c_ℓ (i.e., $h \geq 0.5$, $0.0002 \leq \overline{Z} \leq 0.0006$ and $0.05 \leq c_\ell$ 0.50), foils comprised of two-term camber, angle of attack and quasi-parabolic thickness are almost always preferable to any other combination of pressure distributions. In the very few cases that form an exception to this rule, the difference between the optimum lift-drag ratio of some other combination of pressure distributions and that of the appropriate two term foil is insignificant. It was concluded that within the applicability range of the linearized theory, at nearly vanishing cavitation number and very high Froude numbers, when strength is taken into account, the two term supercavitating hydrofoil is superior, for all reasonable values of lift coefficient, section modulus and operating depths, to the other combinations of the pressure distribution under investigation.

The detailed characteristics of two-term supercavitating sections designed for operation at a finite depth are presented in the next section.

TWO-TERM SUPERCAVITATING HYDROFOILS FOR FINITE DEPTH

The derivation of two dimensional, two-term supercavitating hydrofoils for operation at a specified depth below a free surface at zero cavitation number and very high Froude numbers has been described in Reference (20). In this section the results of numerical computations, based on the expressions for lift, drag, foil shape and cavity shape, will be presented in tabular and graph form. Before proceeding with that presentation, however, it will be necessary to reiterate some of the

principles of the linearized theory and to explain the notation involved in the description of the foils and their characteristics.

The supercavitating sections under discussion are designed by means of the linearized solution to the so called "inverse problem" of classical airfoil theory. In the inverse problem the pressure distribution, rather than the shape of the foil is initially specified and the hydrodynamic characteristics as well as the shape are calculated in terms of the given pressure distribution.

The hydrofoil is first transformed by means of a suitable conformal transformation into its equivalent airfoil. The shape and characteristics of the latter are then calculated in terms of the pressure distribution in the airfoil plane and the solution is then transformed back and obtained, finally, in the physical (hydrofoil) plane. The transformation is a function of the hydrofoil operating depth and is given by

$$\frac{dx}{d\xi} = \frac{h\xi}{a\pi(\xi+a)} \qquad [1]$$

where

h = the depth-chord ratio

x = the chordwise coordinate in the hydrofoil plane along an axis through the leading edge, parallel to the direction of the undisturbed stream. x is normalized with respect to the chord length.

ξ = the chordwise coordinate in the plane of the equivalent airfoil, normalized with respect to the chord length.

a = a real constant, dependent on depth.

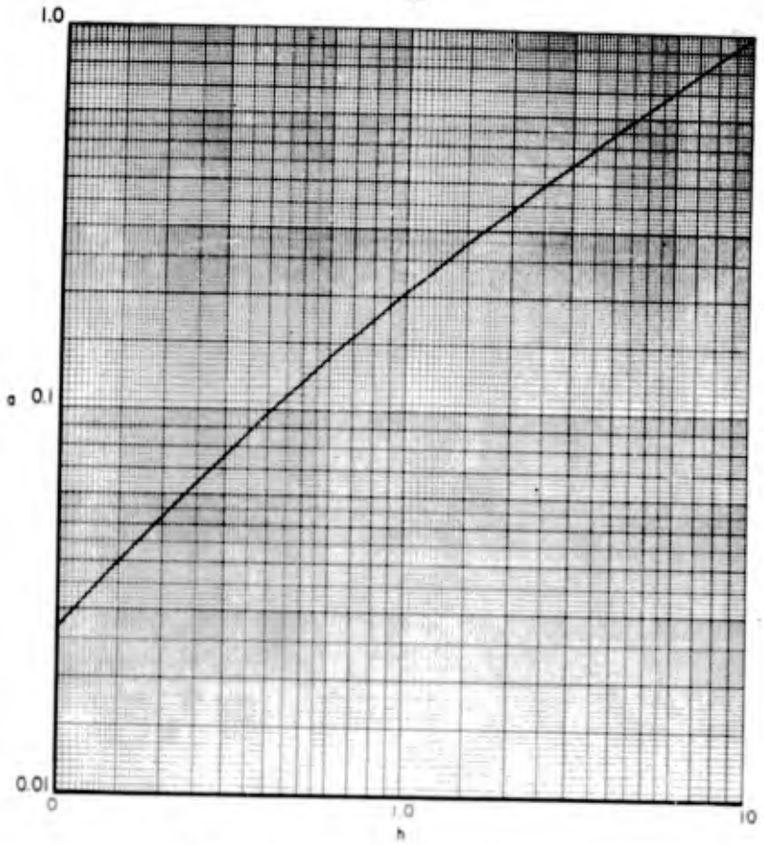

Figure 6- The Influence of Depth on the Parameter a

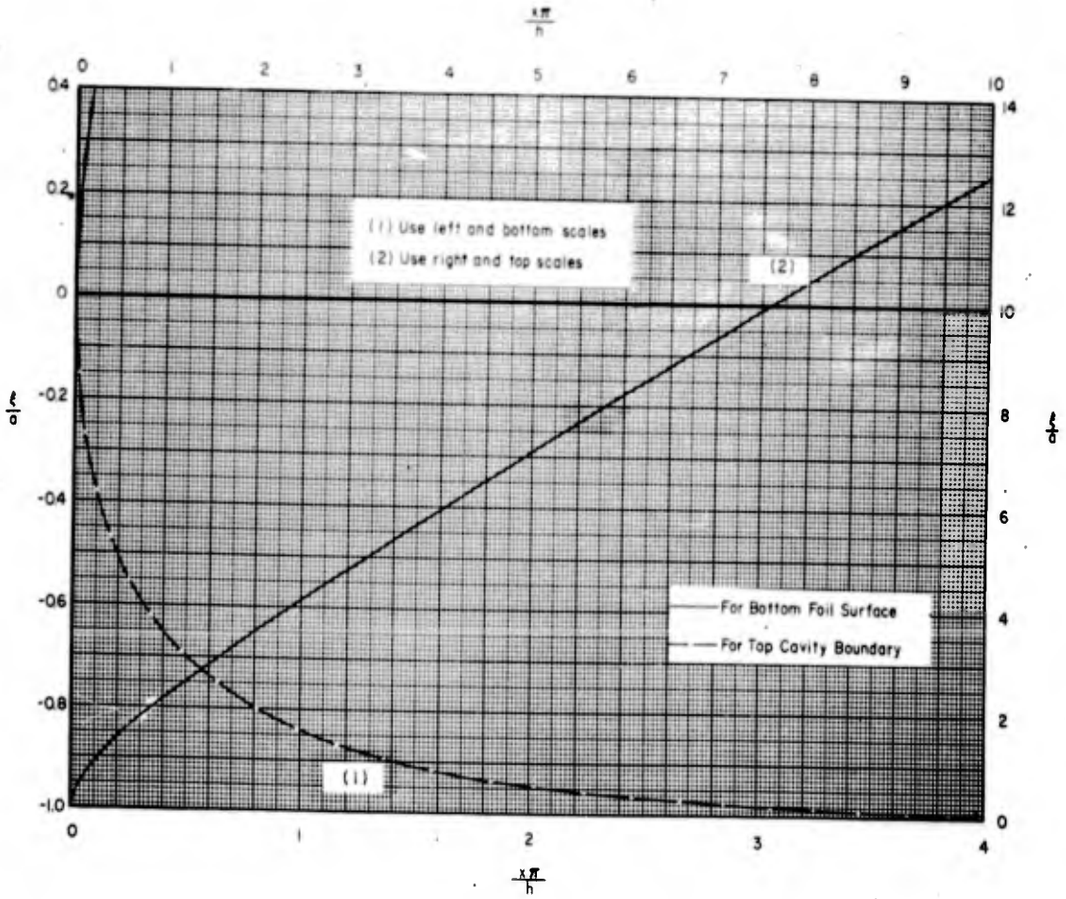

Figure 7- The $x-\xi$ Transformation

The value of a is given implicitly in terms of h by

$$h = \frac{a\pi}{1-\ell n(\frac{1+a}{a})} \qquad [2]$$

and the relationship between x and ξ is given by

$$x = \xi^2 \qquad (h = \infty)$$

$$x = \frac{h}{\pi}\left[\frac{\xi}{a} - \ell n\ (1 + \frac{\xi}{a})\right] \quad (0 < h < \infty) \qquad [3]$$

where $\xi < 0$ for points on the upper cavity boundary and $\xi > 0$ for points on the lower surface of the foil and on the lower cavity boundary.

The values of a vs h and $\frac{x}{h/\pi}$ vs $\frac{\xi}{a}$ are plotted in Figures 6 and 7, respectively. Accurate values of a for a number of discrete depth-chord ratios are given in Table I. Tabulations of ξ vs x for the calculation of ordinates on the foil lower surface and on the upper cavity boundary, at h = 1/4, 1/2, 1, 2, 5 and ∞ are given in Table II.

Two term supercavitating hydrofoils are composed of the two term camber distribution whose magnitude is denoted by the camber index k, a quasi-parabolic thickness distribution denoted by τ and an angle of attack denoted by δ. Since δ is built into the foil (the shape of the upper cavity boundary and hence - the shape of the upper foil surface - depends on δ) it is called the design angle of attack. The lift developed by a given foil depends on the depth, the camber index and the operating angle of attack $\alpha + \delta$. The drag depends on h, $\alpha + \delta$, k and on the quasi-parabolic thickness, τ. In the design condition, the ordinates of the foil bottom surface and the ordinates of the top cavity boundary depend on h, k, δ, τ, and, of course, on the abscissa x. Hence the notation $c_\ell(h,k,\ \alpha + \delta)$, $c_d(h,k,\ \alpha + \delta,\ \tau)$, $y_o(h,x,k,\delta,\tau)$

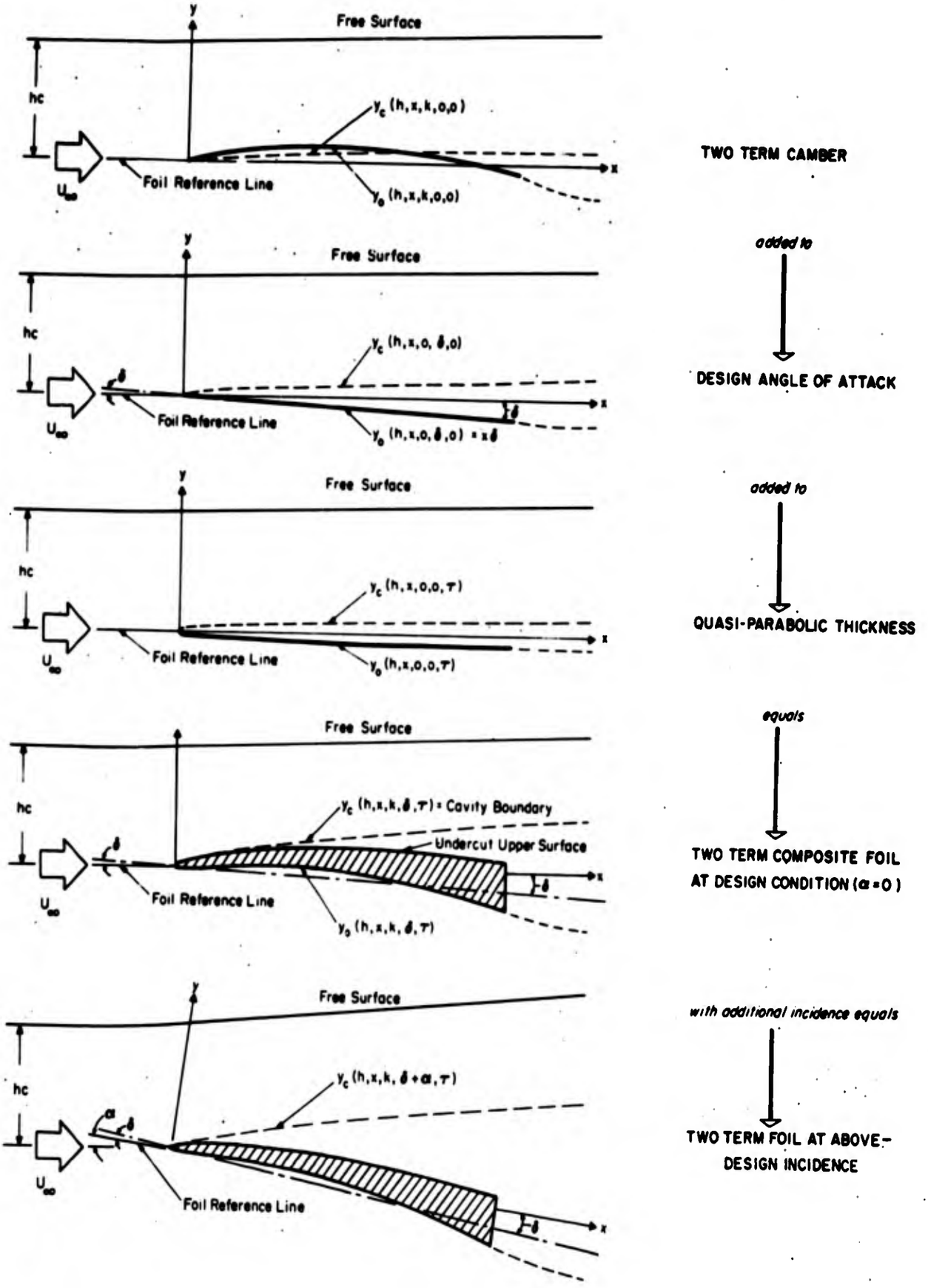

Figure 8- Schematic Showing Composition of Supercavitating Hydrofoils *(not to scale)*

and $y_c(h,x,k,\delta,\tau)$ has been adopted to denote, respectively, the lift coefficient, drag coefficient, bottom (foil) shape and top (cavity) shape of two term supercavitating hydrofoils. y_o and y_c are both measured from the x-axis and normalized with respect to the chord length. To illustrate, $c_d(2.3, 0.15, 3.0^o, 0.004)$ denotes the drag coefficient of a foil with $k = 0.15$ and $\tau = 0.004$ operating at an angle of attack of 3.0 degrees, at a depth of 2.3 chords; $y_o(0.8, 0.6, 0.12, 2^o, 0)$ denotes the ordinate, at 0.6 chord, of the bottom surface of a foil whose $k = 0.12$, that has been designed to operate at an angle of attack of 2^o, at a depth of 0.8 chords; this foil contains no quasi-parabolic thickness.

The exact definitions of and the distinction between the angles δ and α are illustrated in Figure 8. The two term foil is built with reference to the "foil reference line" (the x-axis) - an arbitrary line in space. If a pure camber line is subjected to uniform flow U_∞ in such a way that the reference line is parallel to U_∞, it will - according to the linearized theory - develop a lift per unit span equal to $\frac{1}{2}\rho U^2 c\, c_\ell\,(h, k, 0)$. When $\tau = 0$ this camber line forms the bottom surface of the foil. In order to develop a cavity large enough to contain a foil of sufficient strength the camber line must be rotated through an angle of attack which is large enough to cause the generation of such a cavity. That angle is δ. If we assume, for the sake of explanation, that the entire cavity will be filled with metal it is clear that the top and bottom surfaces of the foil are found by adding, respectively, the top and bottom surfaces generated by δ and k. If such a foil were ever to operate at an angle of

attack smaller than δ, its top surface would wet. When quasi-parabolic thickness is incorporated into the design of the foil, the top and bottom surfaces due to τ are also added linearly to those due to δ and k. A foil designed with a built-in angle of attack δ may, of course, be operated at some other incidence. The actual operating angle of attack is denoted by $\alpha + \delta$, and the lift and drag are functions of $\alpha + \delta$. In a foil whose upper surface coincides with $y_c(h,x,k,\delta,\tau)$, the condition ≥ 0 must hold if the cavity is to begin at the leading edge. α and δ are both measured from the foil reference line, and α is thus the difference between the operating angle of attack and the design angle of attack.

The analytical expressions for the foil and cavity ordinates and for the lift and drag coefficients due to two-term camber, angle of attack and quasi-parabolic thickness have been published previously (20). The values of y_c and y_o due to camber, y_c due to pure incidence and y_c and y_o due to quasi-parabolic thickness are plotted in Figures 9 and 10*, and listed in Table III, for a number of discrete depth-chord ratios. The influence of depth on the lift- and drag-coefficient due to camber, angle of attack and τ is shown in Figure 11 and listed in Table I.

It is important to note that for a given value of τ the foil thickness (i.e. $y_c - y_o$ when the entire volume of the cavity is filled with metal) due to τ alone decreases with depth at a faster rate than the drag coefficient due to τ. The significance of this is illustrated by a plot of $c_d(h,0,0,\tau)$ for a given thickness $T(\tau)$, where $T(\tau) = y_c(h,1,0,0,\tau) - y_o(h,1,0,0,\tau)$. As seen in Figure 11 the value of $\dfrac{c_d(h,0,0,\tau)}{[T(\tau)]^2}$ decreases as the surface

*Figures 9 and 10 are located at the end of the report.

is approached while the value of $\frac{c_d(h,0,0,\tau)}{\tau^2}$ exhibits a sharp rise. The same situation exists with respect to the foil thickness due to angle of attack alone: While the drag coefficient of a flat plate at a given angle of attack increases as the surface is approached (see Figure 11), the more rapid concurrent increase in cavity thickness (Figure 10a) results in an accompanying decrease in the drag for a given thickness due to angle of attack. Since the drag-lift ratio of a flat plate is independent of depth, we find that for a given cavity thickness the drag-lift ratio of a flat plate at incidence also decreases as the plate approaches the surface. This is illustrated by the plot of $\frac{D/L(h,0,\delta,0)}{T(\delta)}$ vs h in Figure 11, where D/L is the ratio of cavity drag to lift and $T(\delta) = y_c(h,x,0,\delta,0) - y_o(h,x,0,\delta,0)$.

According to the linearized theory the lift, foil shape and cavity shape of a composite foil (i.e., a foil which is a combination of camber, angle of attack and quasi-parabolic thickness) is obtained by adding the respective properties of the separate components. The drag of such a foil is obtained from the square of the sum of the square roots of the component drags. Thus,

$$c_\ell(h,k,\alpha+\delta) = c_\ell(h,k,0) + c_\ell(h,0,\alpha+\delta) \qquad [4]$$

$$c_d(h,k,\alpha+\delta,\tau) = \left(\sqrt{c_d(h,k,0,0)} + \sqrt{c_d(h,0,\alpha+\delta,0)} + \sqrt{c_d(h,0,0,\tau)}\right)^2 \qquad [5]$$

$$y_o(h,x,k,\delta,\tau) = y_o(h,x,k,0,0) + y_o(h,x,0,\delta,0) + y_o(h,x,0,0,\tau) \qquad [6]$$

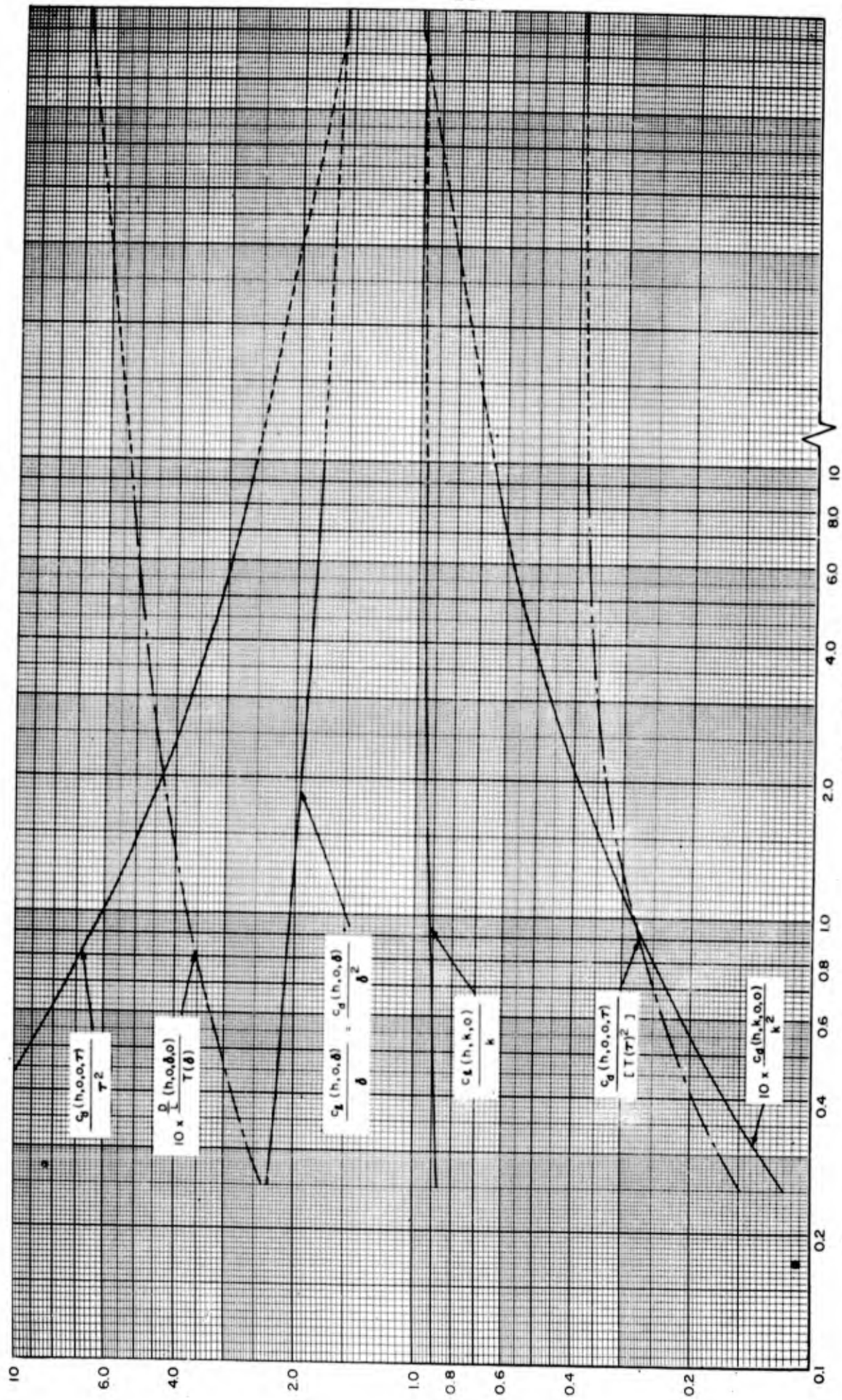

Figure 11- The Influence of Depth on the Lift and Drag Due to Two-Term Camber, Angle of Attack and Quasi-Parabolic Thickness

$$y_c(h,x,k,\delta,\tau) = y_c(h,x,k,0,0) + y_c(h,x,0,\delta,0) + y_c(h,x,0,0,\tau) \qquad [7]$$

The values of the lift and drag coefficients as well as the section moduli that would result if the entire cavity were to be filled with metal, were calculated for foils designed for depths of 1/2, 1, 2, 5 and ∞ chord lengths. The results are shown in Figures 12 through 16*. The section modulus was calculated by assuming that the neutral axis is parallel to the direction of the undisturbed stream. The actual location of this neutral axis was calculated and the area moment of inertia about it was divided by the distance between the neutral axis and the "furthest fiber" to give the section modulus Z. The parameter $\overline{Z}$ in Figures 12 through 16 is the non-dimensional section modulus coefficient defined by

$$\overline{Z} = \frac{Z}{c^3} .$$

The foil section properties are presented in the form of lines of constant δ and constant k on a grid of (a) L/D vs c_ℓ and (b) $\overline{Z}$ vs c_ℓ, for a given value of τ and a given value of the depth-chord ratio h. In assembling the data for the Figures, all possible combinations of k, δ and τ were considered, with k assuming 10 values between 0 and 0.6, δ assuming 13 values between 0 and 3 degrees and τ assuming 9 values between 0 and 0.1. These combinations of k, δ and τ that result in zero or negative foil thicknesses were, of course, discarded. Since the linear theory is not valid for large lift coefficients

---

*Figures 12 through 16 are located at the end of the report.

it must be kept in mind that the information in Figures 12 through 16 is valid only for c_ℓ smaller than approximately 0.4.

Figures 12 through 16 are intended, generally, for one of two different uses. In the first of these the lift, drag and section modulus of a foil with given angle of attack, camber index and τ, designed for one of the discrete, plotted values of depth-chord ratio, is found, directly, from a particular plot. When using the curves for this purpose care must be taken not to extrapolate indiscriminently beyond the envelope of the curves in the direction of decreasing $\overline{Z}$. Interpolation between plotted values of k, δ, τ and h will yield reasonably accurate results. The second common use of Figures 12 through 16 is that of ascertaining which values of k, δ and τ will result in a foil designed for a given depth, with given values of c_ℓ and $\overline{Z}$. When using the curves for this purpose it must be remembered that the lift coefficient is independent of the quasi-paraboli thickness τ and that the latter is intended for the purpose of increasing the section modulus and the nose thickness of the section. It will further be remembered that a given value of τ contributes more towards increased $\overline{Z}$, nose thickness and drag as the depth chord ratio becomes smaller, while the drag associated with a given thickness due to τ diminishes with decreasing depth. Thus the choice of τ for a particular design, while based almost entirely on experience acquired through manipulation of the various parameters involved, can be made independently of the desired lift. After a value of τ has been chosen, there is one and only one combination of k and δ that will result in a given c_ℓ and $\overline{Z}$ at a given depth.

It is highly unlikely, of course, that in a practical case the desired operating depth will correspond exactly to one for which a curve is presented. The indicated interpolation across depth must be done with great care. The suggested method is that of constructing a plot of δ vs h for the desired values of c_ℓ and $\bar{Z}$ and the predetermined value of τ. After the design angle of attack δ is determined with such a plot, the appropriate value of k may be calculated with the aid of Equation [4], and Figure 11. The cavity drag is then found from Equation [5] and Figure 11. Due to the impracticability of presenting such δ vs h curves for all likely combinations of c_ℓ, $\bar{Z}$ and τ, this task must be left to the designer in each case.

It must be reemphasized that the design procedure described herein applies, strictly speaking, only to foils of infinite aspect ratio. In order to apply this information to practical (finite aspect ratio) wings, three dimensional corrections must be incorporated into the design procedure. In general terms, three dimensional hydrofoil wing design is patterned after the methods used in the design of marine propellers: First the camber index, the design angle of attack and the amount of quasi-parabolic thickness are chosen for the spanwise sections of a postulated wing subjected to two dimensional flow, so as to result in desired values of lift coefficient and section moduli. When that is done appropriate corrections which depend on aspect ratio, depth, and spanwise load distribution are applied to k, δ and τ in such a manner that the finite aspect ratio wing will have the same lift distribution and the same $\bar{Z}$ distribution as the two-dimensional wing. Additional drag due to finite aspect ratio is then calculated and added

to the two-dimensional drag.

The actual performance characteristics of the two dimensional sections resulting from the design procedures described heretofore are, of course, strictly relevant only within linear ranges of operation and must at times be suitably corrected for non-linear effects. A very successful, approximate method for correcting the predicted performance for non-linear effects is described in the next section.

NON-LINEAR CORRECTIONS

Within the currently practical range of lift coefficient (say, $0.05 < c_L < 0.20$) the linearized theory predicts lift and drag coefficients which are approximately 2-1/2 percent too high at $c_L = .05$ and 10 percent too high at $c_L = 0.20$. For more heavily loaded foils the error is proportionately increased. These errors are corrected by means of the method presented by Johnson (16, 17, 19). Johnson's method utilizes Green's (10) exact solution for the lift curve slope of a two-dimensional supercavitating ($\sigma = 0$) flat plate near a free surface. The lift due to angle of attack is treated directly by Green's method. To evaluate the non-linear effects on the lift contributed by camber, Johnson used the concept of a camber-equivalent angle of attack, α_c. The curves representing Green's solution are reproduced here from Reference (16), as Figure 17. The corrected two-dimensional lift of a given combination of camber and angle of attack is given by

$$c_L = m\,\alpha_e \frac{\cos(\alpha+\delta)}{\cos\,\alpha_e} \qquad [8a]$$

where

$m = \dfrac{c_L(h,0,\alpha_e)}{\alpha_e}$ obtained from Figure 17, for given values of α_e and h = non-linear lift of a flat plate $/\alpha_e$

$\alpha+\delta$ = operating angle of attack measured from foil reference line

$\alpha_e = \alpha + \delta + \alpha_c$

α_c = camber-equivalent angle of attack = $\dfrac{c_\ell(h,k,0)}{[c_\ell(h,0,\alpha)/\alpha]}$

As shown in Figure 17, Green's solution was, necessarily, given in terms of the spray thickness rather than the depth-chord ratio h. The relationship between h and the spray thickness is very complex and depends on three dimensional as well as gravity effects. Fortunately, however, Johnson (16) has determined this relationship experimentally for some specific aspect ratios and types of lifting surfaces. It is quite clear from this experimental information that in assuming the spray thickness to be equal to the depth chord ratio when using Figure 17, the error incurred in the value of m is no larger than 1.5 percent.

In the case of infinite depth, Green's solution reduces to that given by Rayleigh (9), namely,

$$c_L = \frac{2\pi \sin \alpha_e \cos (\alpha+\delta)}{4 + \pi \sin \alpha_e} \quad (h = \infty) \qquad [8b]$$

In a practical design case, then, one must first determine the values of k, δ and τ which, according to the linearized theory, will result in the desired lift coefficient c_ℓ and section modulus and proceed to calculate the value of c_L (non-linear)

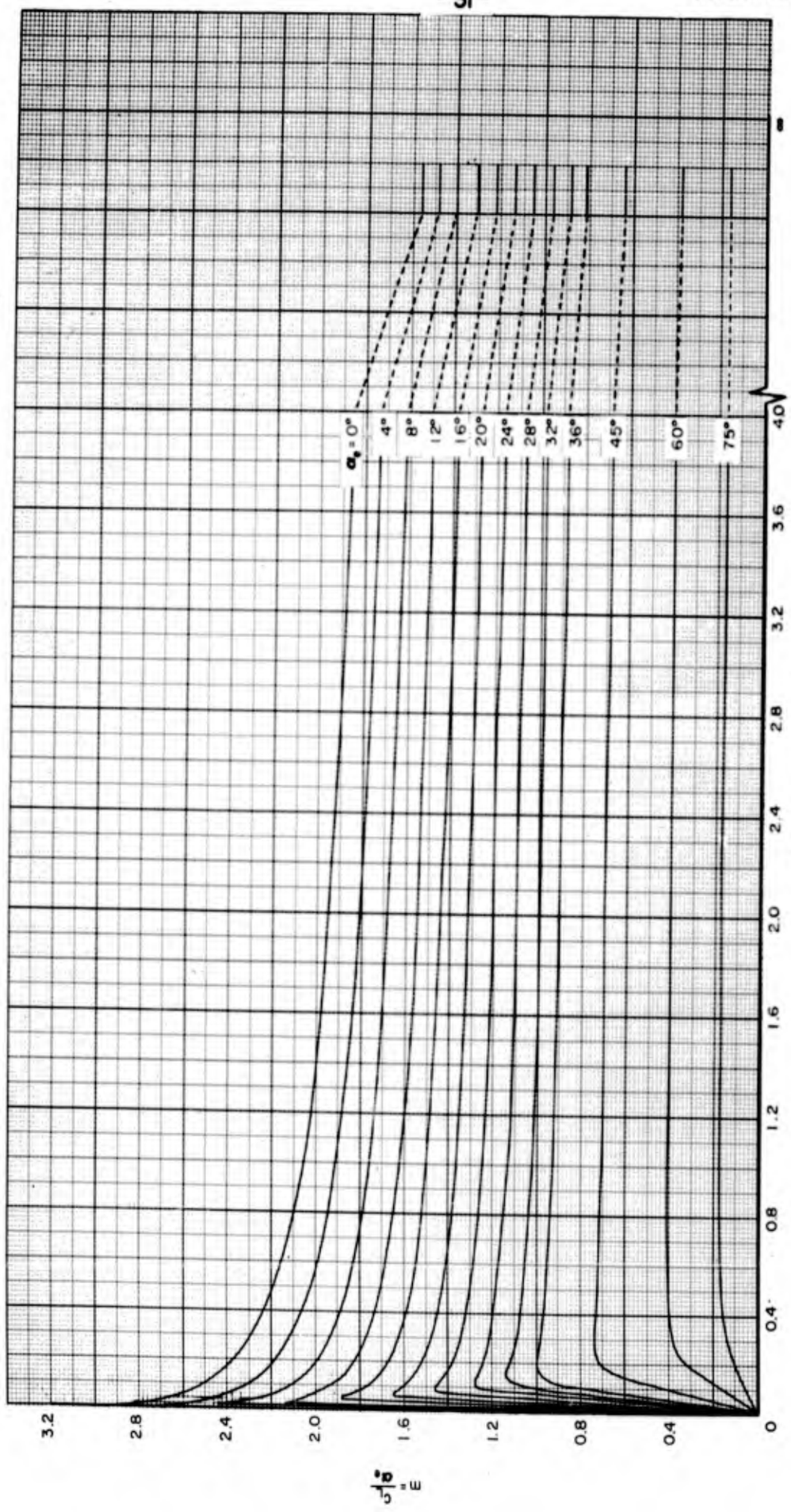

Figure 17- Green's Exact Solution for the Ratio $m = \frac{C_L}{\alpha_0}$ of a Two Dimensional Flat Plate

from Equation [8]. Since the result is, of course, smaller than the desired, initial value of c_L, the total effective angle of attack, α_e, must be increased to give a new value of the non-linear lift coefficient. The desired value of c_L is usually obtained after a very small number of such iterations. In order to decide whether the increase in α_e should be obtained by increasing k or δ, one must be aware of the following:

(a) A comparison between $y_c(h,x,0,\delta,0)$ as obtained from the linearized theory and that obtained by Johnson (16) from Green's exact solution shows that for small angles of attack and reasonable depth-chord ratios, the cavity ordinate values predicted by the linearized theory are approximately one percent too high (e.g., at h = 1 and $\delta = 4^o$, (linear value-exact value) ÷ exact value = 1.08 percent). The smallness of this error indicates that at practical angles of attack and operating depths the non-linear effects on cavity thickness may be neglected.

(b) A recent investigation of second order effects in supercavitating flow (22) showed that since non-linear effects on drag are approximately of the same relative magnitude as non-linear effects on lift, the lift drag ratio predicted by the linearized theory is very accurate.

(c) In a practical foil, the thickness contributed by camber is very small compared to that contributed by angle of attack and semi-parabolic thickness.

(d) An increase in δ (in order to obtain the desired lift coefficient) will result in increased section modulus and

increased drag. An increase in k, however, will, in practical cases, cause only a very small change in both L/D and $\overline{Z}$. Since for δ = constant, neither the $\overline{Z}$ vs c_ℓ nor the L/D vs c_ℓ curves are monotonic, the change in L/D and $\overline{Z}$ can be either positive or negative, but will, in any case, be very small. In practical designs it is almost always advisable to undercut the cavity to some degree (i.e., build the actual foil so that only part of the predicted cavity volume is filled with metal). The loss in $\overline{Z}$ that could ensue when the desired (non-linear) lift is achieved by an increase in k is, in all practical cases, small enough to be absorbed by undercutting.

We conclude that (a) in the process of correcting a foil that has been designed with linearized theory, the desired lift is to be achieved by an appropriate increase in the camber index rather than the design angle of attack; (b) the non-linear cavity drag is found from the non-linear lift and the linearized lift-drag ratio, that is

$$c_D = \frac{c_L}{(c_\ell / c_d)} \qquad [9]$$

For example, consider the design of a foil that is to operate at a depth of one chord and develop a lift coefficient of 0.189 and a $\overline{Z}$ of 3.35×10^{-4}. Assume that for the purpose of obtaining a rounded leading edge it has been decided to use $\tau = 0.004$. From Figure 13(e) we find that, according to the linearized theory, $\delta = 1.40^\circ$ and k = 0.15 will give the desired c_ℓ and $\overline{Z}$ and that the associated L/D = 38.0. From Figure 11 or Table IV we find that $c_\ell(h,k,0) = k \times 0.91642$ and $c_\ell(h,0,\delta) = \delta \times 2.0538$. Hence

$$\alpha_c = \frac{(0.15)(0.91642)}{2.0538} = 0.0669 = 3.83^\circ \text{ and } \alpha_e = 1.40 + 3.83 = 5.23^\circ.$$

From Figure 17, m = 1.854 so that, from Equation [8], the exact c_L = 0.170. We now increase the value of k and find, after a number of iterations, that the desired c_L of 0.189 is obtained with k = 0.176. With that value of k and with $\delta = 1.4^o$, we find, from Figure 13(e): $\bar{Z} = 3.42 \times 10^{-4}$ and L/D = 38.

OPERATION AT FINITE CAVITATION NUMBER

A free streamline theory, based on the Roshko Model, for the performance of supercavitating hydrofoils at infinite depth and finite cavitation number, was developed by Wu (23). Although the theory holds over a wide range of angle of attack and cavitation number, its application to practical foils is, of necessity very complex and time consuming. For the types of foils that are likely to be used in practical hydrofoil craft design, i.e., foils whose camber and angle of attack are small and whose design σ is of the order of 0.2 or smaller* it is quite adequate to use the much more easily evaluated expressions derived from linearized theory. The linearized expressions for finite σ derived by Wu (24) may be rewritten in the following form for the case of a two-term supercavitating hydrofoil designed for infinite depth:

$$c_{\ell_\sigma}(\infty,k,\delta) = \frac{\pi}{2}\left(\alpha+\delta+\frac{2}{\pi}k\right)(1+\sigma) + \frac{3\pi}{32}\sigma^2 \frac{\alpha+\delta+\frac{1}{15\pi}k}{\left(\alpha+\delta+\frac{4}{5\pi}k\right)^2}\left(1-\frac{\sigma}{2}\right) \quad [10]$$

$$c_{d_\sigma}(\infty,k,\delta,0) = \frac{\pi}{2}\left(\alpha+\delta+\frac{4}{5\pi}k\right)^2(1+\sigma) + \frac{3\pi}{32}\sigma^2 \frac{\alpha+\delta-\frac{4}{15\pi}k}{\alpha+\delta+\frac{4}{5\pi}k}\left(1-\frac{\sigma}{2}\right) \quad [11]$$

*Typical, conservative values of σ are 0.2 for vapor filled cavities and 0.03 for fully ventilated cavities.

$$\ell = \frac{4}{\sigma^2}\left(\alpha + \delta + \frac{4}{5\pi}k\right)^2\left(1 + \frac{3}{2}\sigma\right) \qquad [12]$$

where ℓ = the cavity length, measured from the trailing edge of the foil to the trailing edge of the cavity, normalized with respect to the foil chord.

The lift, drag and cavity length of circular arc supercavitating foils at infinite depth are given by

$$c_{\ell_\sigma}\,(\text{circ.arc}) = \frac{\pi}{2}\left(\alpha + \delta + \frac{9}{8}\gamma\right)(1+\sigma) + \frac{3\pi}{32}\sigma^2\,\frac{\alpha+\delta+\frac{3}{16}\gamma}{\left(\alpha+\delta+\frac{1}{2}\gamma\right)^2}\left(1-\frac{\sigma}{2}\right) \qquad [13]$$

$$c_{d_\sigma}(\text{circ.arc}) = \frac{\pi}{2}\left(\alpha+\delta+\frac{1}{2}\gamma\right)^2(1+\sigma) + \frac{3\pi}{32}\sigma^2\,\frac{\alpha+\delta-\frac{1}{8}\gamma}{\alpha+\delta+\frac{1}{2}\gamma}\left(1-\frac{\sigma}{2}\right) \qquad [14]$$

$$\ell = \frac{4}{\sigma^2}\left(\alpha + \delta + \frac{1}{2}\gamma\right)^2\left(1 + \frac{3}{2}\sigma\right) \qquad [15]$$

where γ is a measure of circular arc camber = 1/2 the angle subtended by the circular arc (see Figure 19).

It must be remembered that, according to the linearized theory (16) the angle between the foil reference line and the chord of a circular arc supercavitating hydrofoil is 1/4 γ. That is:

$$\text{Angle of attack measured from chord line} - (\alpha+\delta) = \frac{\gamma}{4}.$$

Equations [10] through [15] are considered adequately accurate for all cases in which $\ell \geq 4$.

The maximum thickness $\overline{T}$ of the cavity whose length is thus calculated from linearized theory may be found by methods given by Tulin (25) from the expression

$$\overline{T} = \frac{\sigma}{2}\,\ell \qquad [16]$$

The linearized theory tells us, in addition, (25) that the shape of the trailing half of the cavity very closely resembles an ellipse. Very little is known, however, about the exact shape of the cavity in the region of the foil itself, when the cavitation number is finite, even when the presence of the free surface is neglected ($h = \infty$). We can only make a qualitative statement of the obvious, namely, that cavity thicknesses will be smaller than those obtained when $\sigma = 0$. Thus, to prevent wetting of the upper surface foils operating at finite σ must be "undercut", i.e., their upper surface must be constructed so as to be <u>below</u> the cavity streamline predicted by the $\sigma = 0$ theory. Quantitative evaluations of the amount of such undercutting must await further studies, and, more importantly, much needed experimental measurements. Near surface, high speed hydrofoils which are fully vented to the atmosphere operate at cavitation numbers no larger than 0.03 or 0.04. For such foils it may be expected that the 10 percent - 20 percent undercutting used in practical cases to prevent upper surface wetting during operation in a seaway would also suffice to cover the finite σ complication.

The non-linear corrections to the lift and drag must, of course, be applied at finite as well as at zero cavitation number. It would seem logical that a good approximation to the non-linear lift at finite σ can be found from

$$c_{L_\sigma} = \frac{c_{\ell_\sigma}}{c_\ell}\, c_L \qquad (h = \infty) \qquad [17]$$

where c_{L_σ} = the non-linear lift coefficient at $\sigma \neq 0$,

c_{ℓ_σ} = the linearized lift coefficient at $\sigma \neq 0$

c_ℓ = the linearized lift coefficient at $\sigma = 0$

and c_L = the non-linear lift coefficient at $\sigma = 0$, found from Equation [8b].

Comparisons with tunnel experiments (26,27) in which wall effects were not taken into account show that at high incidence ($\delta + \alpha \approx 10^o$) and relatively large cavitation number ($\sigma \approx 0.3$) Equation [17] yields results which are approximately 8 percent above measured values. This apparent discrepancy does not seem very serious in view of the fact that the presence of walls tends to slightly reduce the lift developed (3). For lightly loaded foils and small cavitation numbers ($c_L < 0.25$ and $\sigma < 0.1$) Equation [17] is in very good agreement with experimental information now in existence.

In order to obtain - for current use - an expression that applies more accurately at larger foil loadings and cavitation numbers, several alternate methods of applying the non-linear correction at $\sigma \neq 0$ were tried. The expression that compares very well with existing experiments is

$$c_{L_\sigma} = c_L(1 + \sigma) + \frac{\sigma^2 \left(1 - \frac{1}{2}\sigma\right)}{4\, c_L} \qquad (h = \infty,\ \sigma < 0.4) \qquad [18]$$

in which the second term, while having the same σ dependence as the second term in Equations [10] and [13] (the linearized versions), is strictly empirical. It is recommended that Equation [18] be used until more experimental verification of one method or the other ([17] or [18]) can be obtained.

As in the case of zero cavitation number, the cavity drag for $\sigma \neq 0$, corrected for non-linear effects is found by dividing the corrected lift by the lift-drag ratio given by the linearized

theory (at $\sigma \neq 0$). Thus

$$c_{D_\sigma} = c_{L_\sigma} + \left[\frac{c_{\ell_\sigma}}{c_{d_\sigma}}\right] \qquad h = \infty \qquad [19]$$

Accurate information on the effect of finite cavitation number on the lift and drag of two dimensional foils designed for near surface operation must await further theoretical and experimental study, even for the linearized case. As mentioned previously, however, near surface fully ventilated foils operate at cavitation numbers of the order 0.04 or less. At such small values of σ it would seem reasonable to expect very good results from the approximations

$$\left.\begin{aligned} c_{L_\sigma} &\cong (1 + \sigma)\, c_L \qquad [20] \\ c_{D_\sigma} &\cong (1 + \sigma)\, c_D \qquad [21] \end{aligned}\right\} \quad h \neq \infty \ , \ \sigma \leq 0.04$$

THE LINEARIZED THEORY COMPARED WITH EXPERIMENTS

Many of the heretofore conducted experimental studies of the behavior of supercavitating hydrofoils were concerned primarily with foils of finite aspect ratio. Although most of these tests have shown excellent agreement between the linearized theory (as modified by the non-linear corrections and including three dimensional effects) and experiment (e.g. Johnson, 1961), the fact that the effects of finite aspect ratio were often large renders such tests far from ideal for purposes of checking the validity of a two-dimensional theory. The three

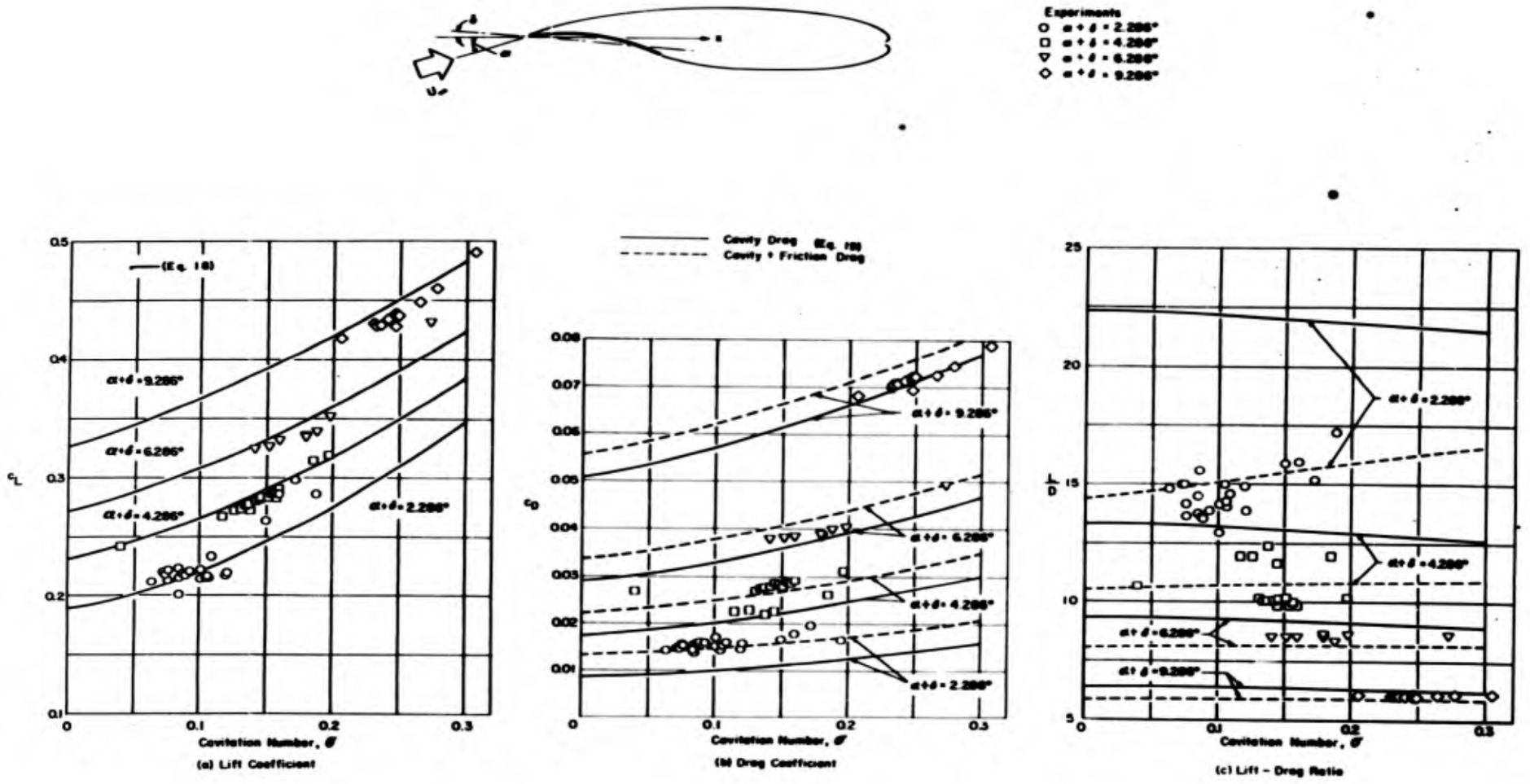

Figure 18- Comparison Between Theory and Experiment for a Two-Term Foil (k=0.1468) in Two-Dimensional Flow at Infinite Depth and Finite Cavitation Number. (Experiments by Waid and Lindberg)

comparisons made here between theory and experiment are restricted to tests made in two dimensional flow.

The first of these comparisons, shown in Figure 18, is between the present theory and tests conducted by Waid and Lindberg (26) on a two-term foil designed for infinite depth with a camber index of $k = 0.1468$. The experiments were conducted in CIT's High Speed Water Tunnel in which a two-dimensional channel had been installed. The foil whose chord length was 31 inches was located in the center of a 14 inch high section. It is assumed that this was a reasonably good simulation of infinite depth operation. The cavitation number, based on measured cavity pressure, varied between 0.04 and 0.30. In Figure 18 the lift coefficient, drag coefficient and lift-drag ratio are plotted vs. cavitation number for angles of attack of $\alpha + \delta = 2.286^\circ$, 4.486°, $6,486^\circ$ and 9.486° (these correspond to Waid and Lindberg's $\alpha = 3^\circ$, 5° and 10°, respectively). The solid and dotted lines represent the linearized theory for finite σ at $h = \infty$ (Equations [10] and [11]) corrected for non-linear effects (Equations [8b], [18] and [19]). Since the tests were conducted at Reynolds Numbers well in the transition region, the theoretical drag and lift-drag ratio are plotted both without friction (cavity drag alone) and with a turbulent friction coefficient of 0.00468. The experimental points in Figure 13 are taken directly from the test data tabulation (uncorrected for tunnel effects) in Reference (26).

The second and third comparisons are illustrated in Figures 19 and 20. They concern tests conducted by Parkin (27) on a circular arc ($\gamma = 8^\circ$, 2.380 inch chord) supercavitating foil and on a supercavitating flat plate (1.740 inch chord). These foils were tested in the same tunnel and test section as the previously mentioned two-term foils. The solid and dotted lines

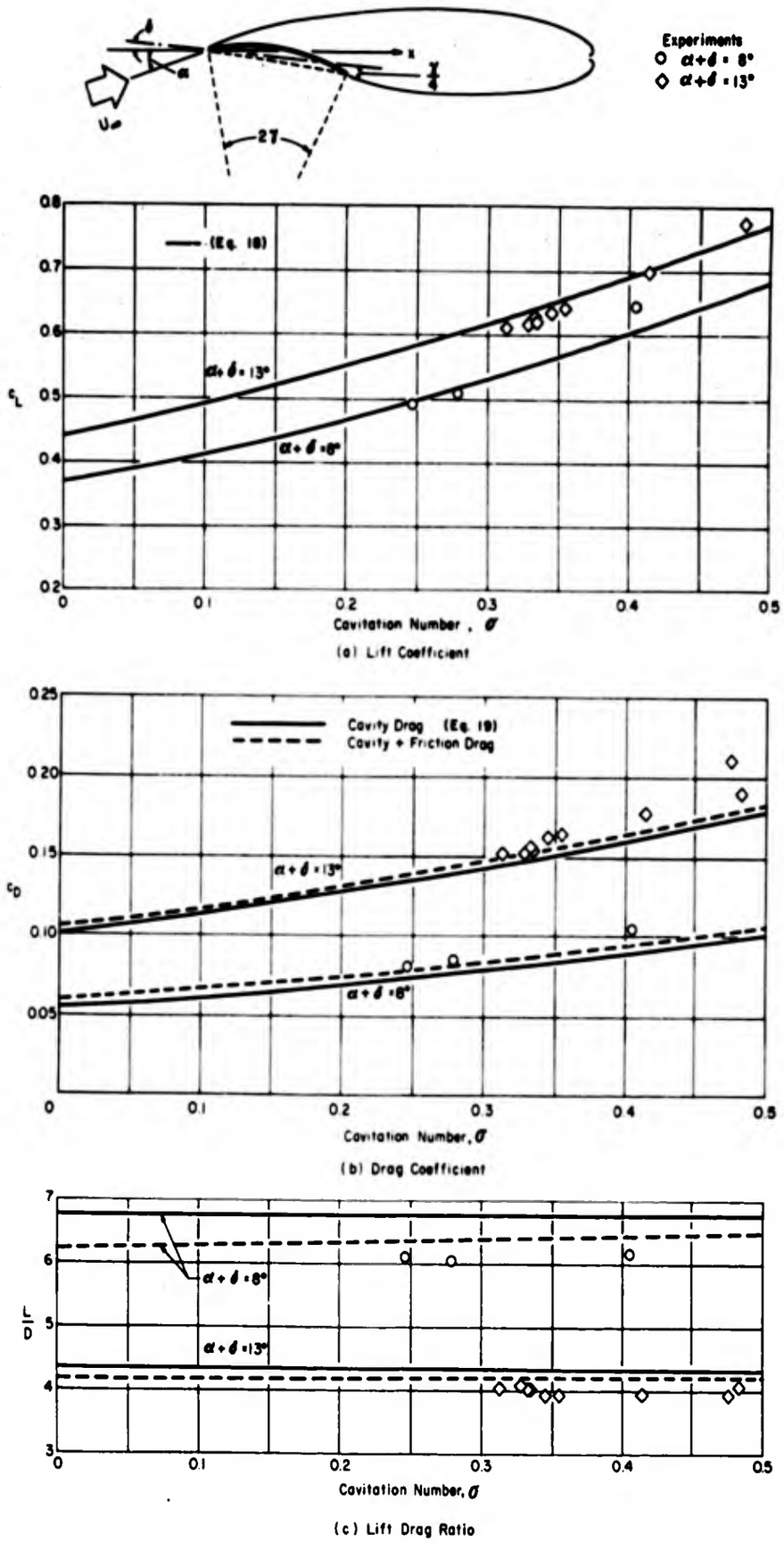

Figure 19- Comparison Between Theory and Experiment for a Circular Arc Foil ($\alpha = 8°$) in Two-Dimensional Flow at Infinite Depth and Finite Cavitation Number. (Experiments by Parkin)

represent the linearized theory for finite σ at $h = \infty$ (Equations [13] and [14], corrected for non-linear effects (Equations [8b], [18], and [19]). The experimental points were taken directly from the test data tabulation in Reference (27). Since the theory applies only to moderate values of σ only test points at $\sigma < 0.5$ are reproduced here. Similarly, only angles of attack ($\alpha + \delta$) of 8^o and 13^o for the circular arc and 8^o, 10^o and 15^o for the flat plate are shown in Figures 19 and 20, although Parkin's experiments were conducted over a much wider range of incidence. Comparisons between theory and experiment at low incidence are omitted because of the obvious upper surface wetting that occurred in that condition (the upper surfaces of the circular arc foil and of the wedge used for the flat plate experiments were not designed to remain within the cavity at low angles of attack). High angles of attack are omitted because the linearized theory cannot be expected to apply to that condition.

Figures 18, 19, and 20 show that the largest discrepancy in lift between the present theory and experiment is less than 3 percent, a value which is smaller than the scatter of experimental data. This discrepancy occurs at a large angle of attack and a large σ (Figure 13a). At smaller and hence more practical incidences and cavitation numbers the agreement is even better. The theoretical predictions of drag and lift drag ratio are in quite good agreement with measured values. As shown in Figures 18b, c, 19b, c, and 20 b, c, the pairs of c_D with and without friction and L/D with and without friction straddle the test points in most cases. The exceptions occur at small angles of attack where it is not known whether or not the upper foil surface (which was not designed to remain within

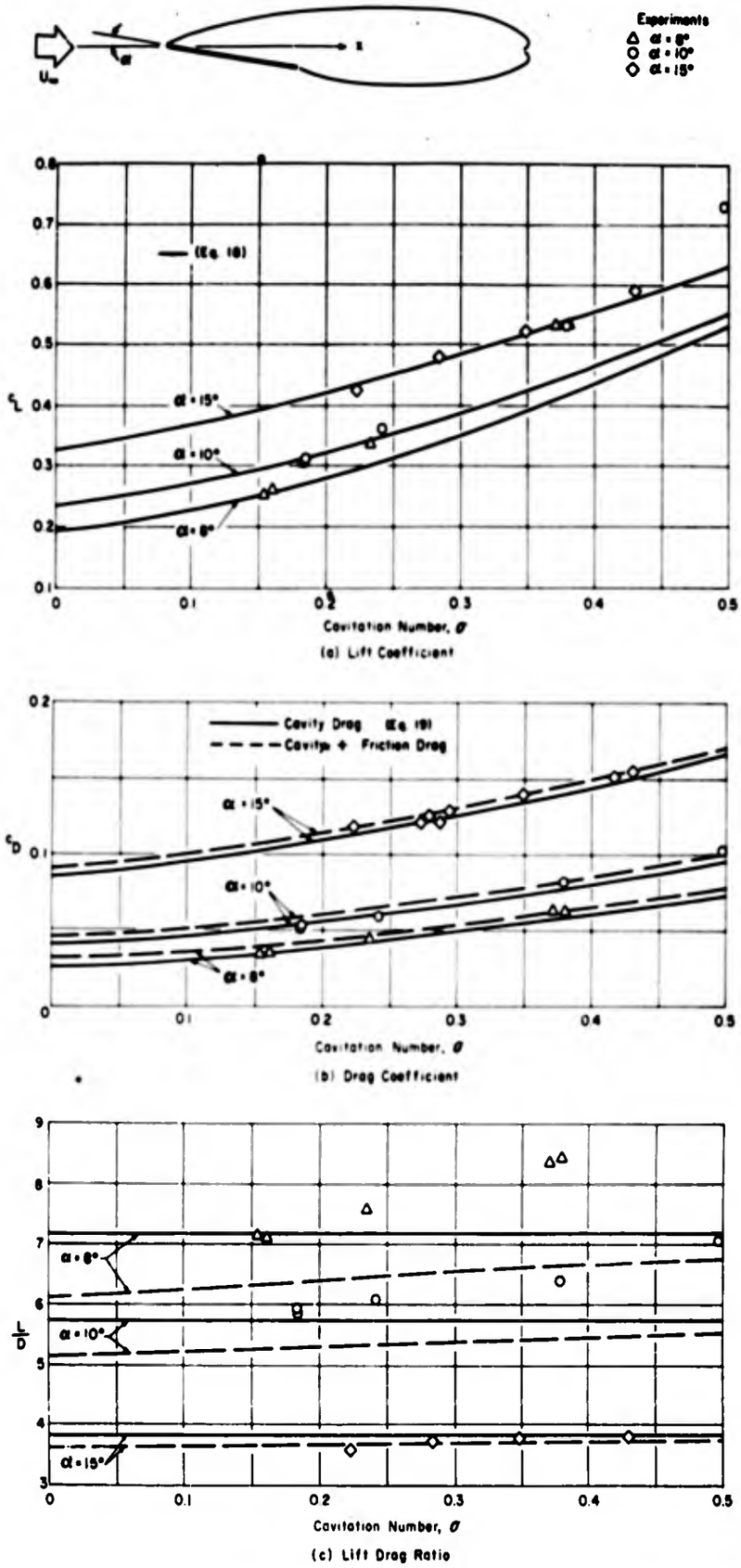

Figure 20 - Comparison Between Theory and Experiment for a Flat Plate in Two-Dimensional Flow at Infinite Depth and Finite Cavitation Number. (Experiments by Parkin)

the cavity) became wetted.

Further evidence of the usefulness of the linearized theory can be found in the lightly loaded, low blade-area-ratio supercavitating propellers that were constructed at the David Taylor Model Basin (14). These propellers which were designed on the basis of pure linearized theory (with 3 dimensional effects) performed very much according to expectations.

Unfortunately, no experimental information on two dimensional supercavitating hydrofoils at finite depth is available in the literature. However, the agreement between theory and experiment at infinite depth would seem to be a clear indication of the general validity of linearized theory (with non-linear corrections). Experimental information on the location of the upper cavity boundary in two dimensional flow is also not available at this time. In this connection it is only possible to make the qualitative statement that the wetting of the particular wedge tested by Parkin (27) (see above) at low angles of attack, is predicted by the linearized theory. It is very noteworthy, of course, that tests conducted by Johnson (16, 17, 19) on two, three and five term as well as flat plate foils in three dimensional flow at finite depth showed excellent agreement between theory and experiment with respect to the location of the cavity boundary as well as the forces experienced by the foils.

SUMMARY BIBLIOGRAPHY

A chronological listing of some of the work that has heretofore been accomplished in the field of supercavitating flows is to be found in Table IV. Generally the Table is intended to list contributions pertaining specifically only to supercavitating (or ventilated) lifting surfaces. In some cases, however, closely related subjects such as symmetric flows, air entrainment and ventilation inception have been included in order to emphasize their importance or to provide a measure of continuity. Where applicable, the Table denotes the types of profiles investigated, range of cavitation number, type of theory developed or used and - for reports on experimental work - the range of speeds, aspect ratio, the type of facility, etc. The contributions are listed in the Table only by author, origin and reference number and are identified more fully in the list of references.

REFERENCES

1. Johnson, V. E., Jr. and Tulin, M. P., The Hydrodynamic Characteristics of High Speed Hydrofoils, HYDRONAUTICS, Incorporated Technical Report 001-6, 1961.

2. Eisenberg, P., Mechanics of Cavitation, Section 12, Part I, Handbook of Fluid Dynamics, McGraw Hill Book Co., New York, 1961.

3. Tulin, M. P. Supercavitating Flows, Section 12, Part II, Handbook of Fluid Dynamics, McGraw Hill Book Co., New York, 1961.

4. Kirchhoff, G., Zur Theorie freier Flüssigkeitsstrahlen, Crelle's Journal für Mathematic, v. 70, 1869.

5. v. Helmholtz, Über discontinuierliche Flüssigkeitsbewegungen, Monatsbericht, Berliner Akademie der Wissenschaft, April 23, 1868.

6. Levi-Civita, T., Scie e leggi de resistentia, Rendiconti Circolo Mat. Palermo, v. 23, 1907.

7. Milne-Thomson, L. M., Theoretical Hydrodynamics, Third Edition, The Macmillan Co., New York, 1955.

8. Birkhoff, G., Hydrodynamics, Dover Publications, New York, 1950.

9. Rayleigh, Lord, On the Resistance of Fluids, Phil. Mag., 1876.

10. Green, A. E., Note on the Gliding of a Plate on the Surface of a Stream, Proc. Cambridge Phil. Soc. XXXII, 1936.

11. Chapligin, C. A., On the Lift Force and Resistance of a Long Flat Wing Assuming Separation From Its Upper Surface, Complete Works, Vol. III, 1935.

12. Tulin, M. P., Steady Two Dimensional Cavity Flows About Slender Bodies, DTMB Report 834, May, 1953.

13. Tulin, M. P. and Burkart, M. P., Linearized Theory for Flows About Lifting Foils at Zero Cavitation Number, DTMB Report C-638, February, 1955.

14. Tachmindji, Morgan, Miller and Hecker, The Design and Performance of Supercavitating Propellers, DTMB Report C-807, February, 1957.

15. Johnson, V. E., Jr., Theoretical Determination of Low-Drag Supercavitating Hydrofoils and their Two-dimensional Characteristics at Zero Cavitation Number, NACA Report 457G11a, September, 1957.

16. Johnson, V. E., Jr., Theoretical and Experimental Investigation of Arbitrary Aspect Ratio, Supercavitating Hydrofoils Operating Near the Free Water Surface, NACA Report RM L57116, December, 1957.

17. Johnson, V. E., Jr., The Influence of Depth of Submersion, Aspect Ratio, and Thickness on Supercavitating Hydrofoils Operating at Zero Cavitation Number, 2nd Symp. on Naval Hydrodynamics ONR, ACR-38, Washington, D.C., 1958.

18. Auslaender, J., The Behavior of Supercavitating Foils With Flaps Operating at High Speed Near a Free Surface, HYDRONAUTICS, Incorporated, Technical Report 001-2, July, 1960.

19. Johnson, V. E., Jr., Theoretical and Experimental Investigations of Supercavitating Hydrofoils Operating Near the Free Water Surface, NASA TR R-93, 1961.

20. Auslaender, J., Linearized Theory for Supercavitating Hydrofoils Operating at High Speeds Near a Free Surface, HYDRONAUTICS, Incorporated, Technical Report 001-5.

21. Christopher, K. W. and Johnson, V. E., Jr., Experimental Investigation of Aspect-Ratio-1 Supercavitating Hydrofoils at Speeds up to 185 Feet per Second, NASA Technical Note D-187, January, 1960.

22. Chen, C. F., Second-Order Supercavitating Hydrofoil Theory, HYDRONAUTICS, Incorporated, Technical Report 121-1, October, 1961.

23. Wu, T. Y., A Free Streamline Theory for Two-Dimensional Fully Cavitated Hydrofoils, J. of Math. and Phys., Vol. XXXV, No. 3, October 1956.

24. Wu, T. Y , A Note on the Linear and Non-Linear Theories for Fully Cavitated Hydrofoils, Cal. Inst. Tech., Report No. 21-22, August, 1956.

25. Tulin, M. P., Supercavitating Flow Past Foils and Struts, Cavitation in Hydrodynamics, Her Majesty's Stationery Office, London, 1956.

26. Waid, R. L. and Lindberg, Z. M., Experimental and Theoretical Investigation of a Supercavitating Hydrofoil, Cal. Inst. Tech., Report No. 47-8, April, 1957.

27. Parkin, B. R., Experiments on Circular Arc and Flat Plate Hydrofoils in Noncavitating and Full Cavity Flows, Cal. Inst. of Tech., Report No. 47-6, February, 1956.

28. Acosta, A. J., Note on Partial Cavitation of Flat Plate Hydrofoils, Cal. Inst. Tech., Report No. E-19.9, October, 1955.

29. Andrews, T. M., Pendulum Tests of Two Cruise Foils and Various Struts, Dynamic Developments, Inc., Oyster Bay, L. I., N.Y., October, 1961.

30. Armstrong, A. H , Abrupt and Smooth Separation in Plane and Axisymmetric Cavity Flow, Armament Research Establishment, Memo 22/53, Fort Halstead, Kent, U.K., 1953.

31. Auslaender, J., Design Charts for One-and Two Strut Supercavitating Hydrofoil Wings (Wing Series A), HYDRONAUTICS, Incorporated, Technical Report 001-8, October, 1961.

32. Bobyleff, D., Journal of The Russian Physico-Chemical Society, XIII, 1881 (See Lamb, H., Hydrodynamics, Section 78).

33. Brodetzky, S., Discontinuous Fluid Motion Past Circular and Elliptic Cylinders, Proc. Roy. Soc., Series A, Vol. 102, No. A 718, February, 1923.

34. Brown, P. W., Force Characteristics of Surface-Piercing Fully Ventilated Dihedral Hydrofoils, Stevens Inst. of Tech., Report No. 698, October, 1958.

35. Brown, P. W., Model Investigation of the Force Characteristics of a Hydrofoil With Various Flap Configurations, Stevens Inst of Tech., LR-757, July 1959.

36. Chen, C. F., Optimum Wing Strut Systems for High Speed Operation Near a Free Surface, HYDRONAUTICS, Incorporated, Tech. Report 001-1, June, 1960.

37. Chen, C. F., Linearized Theory for Thin, Supercavitating Hydrofoils with Spoiler Flaps Operating at High Speeds Beneath a Free Surface, HYDRONAUTICS, Incorporated, Tech. Report 119-1, June, 1961.

38. Christopher, K. W., Investigation of the Planing Lift of a Flat Plate at Speeds up to 170 Feet per Second, NACA TN 3951, March, 1957.

39. Christopher, K. W. and Johnson, V. E., Jr., Experimental Investigation of Two Low-Drag Supercavitating Hydrofoils at 200 Feet Per Second, NASA TN D-436, August, 1960.

40. Cohen, Hirsh and Gilbert, Robert, Two-Dimensional, Steady Cavity Flow About Slender Bodies in Channels of Finite Breadth, ASME Annual Meeting, Paper No. 56-A-29, 1956, (J. App. Mech., June, 1957).

41. Cohen, Hirsh and Southerland, C. D., Wall Effects in Cavitating Flow About a Hydrofoil (Finite Cavity Case), Rensselaer Polytechnic Inst., Math Report No. 7, Troy, N.Y., April, 1957.

42. Cumberbatch, E., Accelerating, Supercavitating Flow Past a Thin Two-Dimensional Wedge, Cal. Inst. Tech., Report No. 47-13, June, 1960.

43. Cumberbatch, E. and Wu, T. Y., Cavity Flow Past a Slender Pointed Hydrofoil, Cal. Inst. Tech., Report No. 47-11, March, 1960.

44. Cuthbert, J. W., An Analysis of Air Entrainment in Cavity Flows, HYDRONAUTICS, Incorporated, Report 003-1, October, 1960.

45. Efros, D. A., Construction of Free Streamline Flows by the Method of Electrical Simulation, Rensselaer Polytechnic Inst., Math. Trans. No. 1, Troy, N.Y., May, 1958, (Translated from Izvestia Akademie Nauk, USSR, O.T.N., No. 9, 1947).

46. Fabula, A. G., Theoretical Lift and Drag on Vented Hydrofoils for Zero Cavity Number and Steady Two-Dimensional Flow, NAVORD Report 7005, NOTS TP 2360, 4 November 1959.

47. Fabula, A. G., Application of Thin-Airfoil Theory to Hydrofoils with Cut-Off Trailing Edge, NAVWEPS, Report 7571, China Lake Cal., September, 1960.

48. Fabula, A. G., Linearized Theory of Vented Hydrofoils, U.S. Naval Ordnance Test Station, NAVWEPS Report 7637, China Lake, Cal., March, 1961.

49. Fedorov, E. A., The Motion of a Plate of Infinite Span Near the Free Surface of an Ideal Weightless Fluid, Proc. of the Central Aero-Hydrodynamical Inst., Report. No. 711, Moscow, 1958.

50. Fridsma, G., Force and Moment Characteristics of a Surface-Piercing, Fully Ventilated, Dihedral Hydrofoil, Davidson Laboratory Report No. 795, November, 1960.

51. Geurst, J. A., Linearized Two-Dimensional Cavity Flows About Symmetric Bodies, Technische Hogeschool, Instituut voor Toegepaste Wiskunde, Report 9, Delft, 1956.

52. Geurst, J. A. and Timman, R., Linearized Theory of Flow With Finite Cavities About a Wing, Technische Hogeschool, Instituut voor Toegepaste Wiskunde, Report No. 7, Delft, 1956.

53. Geurst, J. A., Linearized Theory for the Unsteady Motion of a Supercavitating Hydrofoil, Technische Hogeschool, Instituut voor Towgepaste Wiskunde, Report No. 22, Delft, April, 1960.

54. Gilbarg, D. and Rock, D. H., On Two Theories of Plane Potential Flows With Finite Cavities, NOL, Memorandum 8718, Washington, 1946.

55. Gilbarg, D. and Serrin, J., Free Boundaries and Jets in the Theory of Cavitation, J. of Math. and Phys., vol. 29, No. 1, April, 1950.

56. Gilbarg, D., Unsteady Flows With Free Boundaries, ZAMP, vol. III, 1952.

57. Hellsten, C. P. and Street, T. B.,Development of High Speed Hydrofoils, Grumman Preliminary Report No. M-Mar-78, August, 1961.

58. Ho, H. T., The Linearized Theory of a Supercavitating Hydrofoil With a Jet Flap., HYDRONAUTICS, Incorporated, Tech. Report 119-2, June, 1961.

59. Hug, M., Theoretical and Experimental Investigations of Forces on Cavitating Hydrofoils, Doctoral Dissertation, State University of Iowa, Iowa City, Iowa, February, 1956.

60. Johnson, V. E., Jr. and Rasnick, T. A., Investigation of a High-Speed Hydrofoil With Parabolic Thickness Distribution, NASA TN D-119, November, 1959.

61. Kaplan, P., Letter Report on Tests of Surface-Piercing Struts, Stevens Inst. of Tech., Letter Report No. 488, April, 1953.

62. Kaplan, P. and Henry, C. J., Study of the Hydroelastic Instability of Supercavitating Hydrofoils, Stevens Inst. of Tech., Report No. 838; also J. of Ship Research, Vol. 4, No. 3, 1961.

63. Kermeen, R. W., Water Tunnel Test of NACA 66-012 Hydrofoil in Noncavitating and cavitating Flows, Cal. Inst. Tech. Report No. 47-7, February, 1956.

64. Kermeen, R. W., Water Tunnel Tests of NACA 4412 and Walchner Profile 7 Hydrofoils in Noncavitating and Cavitating Flows, Cal. Inst. Tech., Report No. 47-5, February, 1956.

65. Kermeen, R. W., Experimental Investigations of Three-Dimensional Effects on Cavitating Hydrofoils, Cal. Inst. Tech., Report No. 47-14, September, 1960.

66. Kiceniuk, T., Preliminary Experimental Study of Vertical Hydrofoils of Low Aspect Ratio Piercing a Water Surface, Cal. Inst. Tech., Report No. E-55.2, December, 1954.

67. Kreisel, G., Admirality Research Laboratory, ARL Report No. R1/H/36, January, 1946.

68. Lang, T. G., Base-Vented Hydrofoils, NAVORD Report Report 6606 NOTS TP 2346, China Lake, Calif., NOTS, 19 October 1959.

69. Lang, T. G., Daybell, D. A. and Smith, K. E., Water-Tunnel Tests of Hydrofoils With Forced Ventilation, NAVORD Report 7008, NOTS TP 2363, China Lake, Calif. NOTS, 10 November 1959.

70. Lin, J. D., A Free Streamline Theory of Flows About a Flat Plate With Flap at Zero Cavitation Number, HYDRONAUTICS, Incorporated, Tech. Report 119-3, December, 1961.

71. Luu, T. S., Analytical Study and Rheoelectric Simulation of Supercavitating Flows Around Two- and Three-Dimensional Hydrofoils, Bureau D'Analyse et de Recherche Appliquées, Seine, December, 1961.

72. Martin, M., Unsteady Lift and Moment on Fully Cavitating Hydrofoils at Zero Cavitation Number, Stevenson Institute of Technology, Davidson Laboratory Report R-821, March, 1961.

73. McGehee, J. R. and Johnson, V. E., Jr., Hydrodynamic Characteristics of Two Low-Drag Supercavitating Hydrofoils, NASA Memorandum 5-9-59L, June, 1959.

74. Morgan, W. B., Optimum Supercavitating Sections, DTMB Report C-856, August, 1957.

75. Newman, J. N., Supercavitating Flow Past Bodies With Finite Leading Edge Thickness, DTMB Report 1081, September, 1956.

76. Parkin, B. R., A Note on the Cavity Flow Past a Hydrofoil in a Liquid With Gravity, Cal. Inst. Tech., Report No. 47-9, December, 1957.

77. Parkin, B. R., Linearized Theory of Cavity Flow in Two-Dimensions, Rand Corp., Report P-1745, Santa Monica, Cal., July, 1959.

78. Plesset, M. S. and Parkin, B. R., Hydrofoils in Noncavitating and Cavitating Flow, Cavitation in Hydrodynamics, Her Majesty's Stationery Office, London, 1956.

79. Plesset, M. S. and Shaffer, P. A., Jr., Cavity Drag in Two and Three Dimensions, U.S. NOTS, NAVORD Report 1014, October 1948.

80. Pykhteev, J. N., Solution of the Inverse Problem of Plane Cavitational Streamline Flow Along a Curvilinear Arc, Appl. Math and Mech. vol. XX, Inst. of Mechanics, Academy of Sciences, USSR, 1956.

81. Ramsen, J. A., An Experimental Hydrodynamic Investigation of the Inception of Vortex Ventilation, NACA TN 3903, April 1957.

82. Reichardt, H., The Laws of Cavitation Bubbles at Axially Symmetrical Bodies in a Flow, (M.A.P. Translation No. 766, August, 1946). Original published at Kaiser Wilhelm Institut für Stömungsforchung, Göttingen, October, 1945.

83. Riabouchinsky, D., Proc. London Math. Soc. (2), 19, pp. 206-215, 1921.

84. Ripken, J. F., Experimental Studies of a Hydrofoil Designed for Supercavitation, Univ. of Minn., St. Anthony Falls Hydraulic Lab Project Rept. No. 52, September, 1956.

85. Roshko, A., A new Hodograph for Free Streamline Theory, NACA TN 3168, July,1954.

86. Schiebe, F. R. and Wetzel, J. M., Ventilated Cavities on Submerged Hydrofoils of Finite Span, St. Anthony Falls Hydraulic Laboratory, Memorandum No. M-91, Minneapolis, Minn., July, 1961.

87. Schot, S. H., Surface Tension and Free Surface Effects in Steady Two-Dimensional Cavity Flow About Slender Bodies, DTMB Report 1566, January, 1962.

88. Shuford, C. L., Jr., A Review of Planing Theory and Experiment With a Theoretical Study of Pure-Planing Lift of Rectangular Flat Plates, NACA TN 3233, August, 1954.

89. Silberman, E., Experimental Studies of Supercavitating Flow About Simple Two-Dimensional Bodies in a Jet, Univ. of Minn., St. Anthony Falls Hydraulic Lab, Project Report No. 59, April, 1958.

90. Song, C. S., Pulsation of Ventilated Cavities, Univ. of Minn., St. Anthony Falls Hydraulic Laboratory, Tech. Paper No. 32, Series B, February, 1961.

91. Tulin, M. P., Supercavitating Flow Past Slender Delta Wings, J. of Ship Research, New York, December, 1959.

92. Tulin, M. P., The Hydrodynamics of High Speed Hydrofoil Craft, Third Symposium on Naval Hydrodynamics, H. Veeman and Zonen N. V., Wageningen, Netherlands, September, 1960.

93. Wadlin, K. L., Ventilated Flows With Hydrofoils, 12th General Meeting of the American Towing Tank Conference, Berkeley, Cal., August, 1959.

94. Wagner, H., Über das Gleiten von Wasserfahrzeugen, Jahrbuch der Schiffbautechnik v. 34, 1933. (Also published in English: Planing of Watercraft, NACA TM 1139, April, 1948).

95. Waid, R. L., Cavity Shapes for Circular Disks at Angles of Attack, Cal. Inst. Tech., Report No. E-73.4, September, 1957.

96. Woods, L. E., Aerodynamic Forces on an Oscillating Aerofoil Fitted With a Spoiler, Proc. of the Roy. Soc., vol. 239, 1957.

97. Wu, T., A Linearized Theory for Nonsteady Cavity Flows, Cal. Inst. Tech., Report No. 85-6.

TABLE I. THE PARAMETER a AND THE LINEARIZED TWO DIMENSIONAL LIFT AND DRAG COEFFICIENTS DUE TO TWO-TERM CAMBER, ANGLE OF ATTACK AND QUASI-PARABOLIC THICKNESS AT VARIOUS DEPTH-CHORD RATIOS

h	a	$\frac{c_\ell(h,k,0)}{k}$	$\frac{c_\ell(h,0,\delta)}{\delta}$	$\frac{c_d(h,0,0,\tau)}{\tau^2}$	$\frac{c_d(h,k,0,0)}{k^2}$
1/4	0.0650987	0.870617	2.31787	14.7481	0.0115161
1/2	0.117116	0.893448	2.18081	9.11330	0.0187619
3/4	0.162420	0.907018	2.10480	7.10755	0.0240946
1	0.203256	0.916397	2.05374	6.05140	0.0282996
2	0.339830	0.937169	1.94286	4.32959	0.0394117
3	0.451460	0.947693	1.88679	3.67979	0.0461863
4	0.548454	0.954335	1.85107	3.32445	0.0509484
5	0.635470	0.959012	1.82563	3.09543	0.0545603
6	0.715103	0.962530	1.80628	2.93329	0.0574349
8	0.858206	0.967551	1.77827	2.71548	0.0617954
10	0.985650	0.971021	1.75856	2.57333	0.0650067
100	3.67608	0.991280	1.63438	1.85000	0.0880871
∞	∞	1	$\pi/2$	$\pi/2$	$\delta/(25\pi)$

TABLE II. VALUES OF ξ VS x FOR THE TOP CAVITY BOUNDARY AND FOR THE FOIL BOTTOM SURFACE AT VARIOUS DEPTH-CHORD RATIOS.

	h = $\frac{1}{4}$		h = $\frac{1}{2}$		h = 1		h = 2		h = 5		h = ∞
x (%)	ξ_{bottom}	ξ_{top}	ξ_{bottom}	ξ_{top}	ξ_{bottom}	ξ_{top}	ξ_{bottom}	ξ_{top}	ξ_{bottom}	ξ_{top}	$-\xi_{top}$ / ξ_{bottom}
1	.0383015	-.0274247	.0465597	-.0367620	.0552914	-.0467834	.0638418	-.0567272	.0739202	-.0685976	.100000
2	.0576473	-.0359535	.0689077	-.0493394	.0808059	-.0638018	.0924427	-.0782182	.106134	-.0954901	.141421
3	.0739423	-.0414912	.0873196	-.0580078	.101452	-.0759640	.115264	-.0939348	.131494	-.115530	.173205
4	.0886825	-.0455319	.103710	-.0646826	.119590	-.0856294	.135101	-.106672	.153311	-.132028	.200000
5	.102441	-.0486494	.118821	-.0701025	.136132	-.0937102	.153036	-.117511	.172866	-.146266	.223606
6	.115512	-.0511354	.133027	-.0746454	.151544	-.100673	.169621	-.127006	.190814	-.158899	.244948
7	.128068	-.0531618	.146553	-.0785345	.166104	-.106795	.185187	-.135486	.207547	-.170318	.264575
8	.140220	-.0548392	.159545	-.0819149	.179991	-.112257	.199946	-.143166	.223319	-.180777	.282842
9	.152046	-.0562439	.172102	-.0848869	.193331	-.117183	.214049	-.150193	.238306	-.190452	.300000
10	.163602	-.0574305	.184298	-.0875234	.206214	-.121663	.227603	-.156677	.252636	-.199473	.316227
15	.218514	-.0612404	.241414	-.0972189	.265721	-.139328	.289450	-.183244	.317186	-.237498	.387298
20	.270343	-.0630982	.294330	-.103321	.319850	-.151897	.344777	-.203413	.373894	-.267716	.447213
25	.320280	-.0640469	.344632	-.107383	.370597	-.161359	.395977	-.219574	.425611	-.292980	.500000
30	.368920	-.0645418	.393120	-.110174	.418975	-.168723	.444269	-.232948	.473797	-.314750	.547722
35	.416610	-.0648028	.440263	-.112130	.465585	-.174581	.490377	-.244254	.519317	-.333892	.591607
40	.463568	-.0649411	.486362	-.113517	.510811	-.179313	.534769	-.253962	.562736	-.350967	.632455
45	.509945	-.0650146	.531626	-.114509	.554922	-.183179	.577770	-.262393	.604443	-.366367	.670820
50	.555847	-.0650539	.576202	-.115224	.598109	-.186364	.619614	-.269782	.644722	-.380375	.707106
55	.601354	-.0650748	.620201	-.115740	.640518	-.189006	.660478	-.276304	.683787	-.393206	.741619
60	.646526	-.0650859	.663709	-.116114	.682260	-.191209	.700500	-.282094	.721805	-.405025	.774596
65	.691410	-.0650919	.706792	-.116386	.723422	-.193053	.739787	-.287261	.758906	-.415963	.806225
70	.736044	-.0650950	.749504	-.116583	.764076	-.194602	.778427	-.291889	.795198	-.426127	.836660
75	.780460	-.0650967	.791890	-.116727	.804281	-.195907	.816493	-.296049	.830768	-.435604	.866025
80	.824681	-.0650976	.833985	-.116832	.844083	-.197009	.854043	-.299800	.865689	-.444469	.894427
85	.868729	-.0650981	.875819	-.116909	.883524	-.197942	.891129	-.303192	.900024	-.452781	.921954
90	.912622	-.0650984	.917419	-.116965	.922638	-.198732	.927793	-.306264	.933825	-.460595	.948683
95	.956375	-.0650984	.958806	-.117005	.961455	-.199402	.964073	-.309053	.967137	-.467955	.974679
100	1.000000	-.0650985	1.000000	-.117035	1.000000	-.199971	1.000000	-.311589	1.000000	-.474900	1.000000

TABLE III. FOIL BOTTOM SURFACE AND UPPER CAVITY BOUNDARY DUE TO TWO-TERM CAMBER, QUASI-PARABOLIC THICKNESS AND ANGLE OF ATTACK AT VARIOUS DEPTH-CHORD RATIOS.

(a) $h = \frac{1}{4}$

$\frac{x}{c}$ (%)	$\frac{y_0(\frac{1}{4},x,k,0,0)}{k}$	$\frac{y_c(\frac{1}{4},x,k,0,0)}{k}$	$\frac{y_c(\frac{1}{4},x,0,0,\tau)}{\tau}$	$\frac{y_0(\frac{1}{4},x,0,0,\tau)}{\tau}$	$\frac{y_c(\frac{1}{4},x,0,\delta,0)}{\delta}$
1	.00278256	.00240004	-.282806	.334289	.0684080
2	.00577334	.00471803	-.387634	.491173	.115269
3	.00890256	.00699686	-.463822	.619972	.156988
4	.0121429	.00924990	-.525408	.734714	.195920
5	.0154768	.0114842	-.577784	.840791	.233052
6	.0188914	.0137041	-.623700	.940936	.268908
7	.0223762	.0159129	-.664778	1.036774	.303817
8	.0259224	.0181121	-.702068	1.129325	.337986
9	.0295222	.0203040	-.736297	1.219324	.371575
10	.0331686	.0224892	-.767987	1.307263	.404687
15	.0518919	.0333509	-.899515	1.727071	.565585
20	.0709648	.0441479	-1.002099	2.128537	.722092
25	.0898321	.0549138	-1.086922	2.521490	.876532
30	.107997	.0656623	-1.159571	2.910134	1.029910
35	.124998	.0764041	-1.223289	3.296652	1.182774
40	.140395	.0871410	-1.280143	3.681999	1.335347
45	.153764	.0978561	-1.331538	4.066044	1.487494
50	.164691	.108599	-1.378477	4.450811	1.639976
55	.172771	.119336	-1.421704	4.835231	1.792346
60	.177607	.130068	-1.461788	5.219357	1.944613
65	.178807	.140806	-1.499172	5.603684	2.096967
70	.175983	.151549	-1.534210	5.988187	2.249394
75	.168751	.162201	-1.567189	6.369380	2.400512
80	.156730	.172930	-1.598346	6.753334	2.552725
85	.139542	.183229	-1.627879	7.121888	2.698834
90	.116813	.193386	-1.655953	7.485377	2.842935
95	.088169	.193746	-1.682709	7.498245	2.848036
100	.053239	.203857	-1.708271	7.860111	2.991493

TABLE III. (continued)

(b) $h = \frac{1}{2}$

x (%)	$\frac{y_0(\frac{1}{2},x,k,0,0)}{k}$	$\frac{y_c(\frac{1}{2},x,k,0,0)}{k}$	$\frac{y_0(\frac{1}{2},x,0,0,\tau)}{\tau}$	$\frac{y_c(\frac{1}{2},x,0,0,\tau)}{\tau}$	$\frac{y_c(\frac{1}{2},x,0,\delta,0)}{\delta}$
1	.00283272	.00236115	-.227434	.255973	.0586314
2	.00590234	.00461489	-.314398	.371636	.0977164
3	.00912112	.00681499	-.378526	.464620	.131973
4	.0124550	.00897831	-.430931	.546038	.163542
5	.0158827	.0111136	-.475903	.620175	.193324
6	.0193888	.0132267	-.515631	.689225	.221806
7	.0229610	.0153214	-.551414	.754481	.249290
8	.0265891	.0174005	-.584095	.816785	.275978
9	.0302643	.0194663	-.614255	.876718	.302015
10	.0339788	.0215207	-.642319	.934710	.327509
15	.0529128	.0316607	-.760228	1.204423	.449164
20	.0719540	.0416508	-.853767	1.453289	.564649
25	.0905372	.0515466	-.932139	1.690322	.676520
30	.108173	.0613800	-.999986	1.919974	.786097
35	.124419	.0711711	-1.060033	2.144787	.894152
40	.138861	.0809315	-1.114027	2.366281	1.001151
45	.151107	.0906721	-1.163170	2.585515	1.107433
50	.160777	.100397	-1.208324	2.803125	1.213192
55	.167506	.110107	-1.250131	3.019505	1.318543
60	.170937	.119816	-1.289087	3.235179	1.423687
65	.170721	.129517	-1.325581	3.450245	1.528632
70	.166513	.139215	-1.359923	3.664868	1.633432
75	.157977	.148908	-1.392368	3.879156	1.738119
80	.144779	.158600	-1.423127	4.093256	1.842753
85	.126589	.168291	-1.452375	4.307174	1.947324
90	.103082	.177945	-1.480262	4.520197	2.051478
95	.0739335	.187641	-1.506915	4.734095	2.156074
100	.0388235	.197338	-1.532444	4.947939	2.260654

TABLE III. (continued)

(c) h = 1

x (%)	$\frac{y_0(1,x,k,0,0)}{k}$	$\frac{y_c(1,x,k,0,0)}{k}$	$\frac{y_0(1,x,0,0,\tau)}{\tau}$	$\frac{y_c(1,x,0,0,\tau)}{\tau}$	$\frac{y_c(1,x,0,\delta,0)}{\delta}$
1	.00288430	.00232221	-.188407	.204829	.0514650
2	.00603293	.00451274	-.262100	.294991	.0850523
3	.00933949	.00663616	-.317040	.366445	.114145
4	.0127632	.00871246	-.362316	.428280	.140701
5	.0162791	.0107523	-.401442	.484010	.165549
6	.0198692	.0127627	-.436217	.535434	.189141
7	.0235194	.0147482	-.467708	.583620	.211754
8	.0272183	.0167123	-.496609	.629260	.233578
9	.0309561	.0186578	-.523401	.672835	.254747
10	.0347242	.0205867	-.548433	.714696	.275361
15	.0537744	.0300356	-.654683	.905747	.372326
20	.0726587	.0392455	-.740213	1.077166	.462467
25	.0908073	.0482897	-.812712	1.236616	.548276
30	.107745	.0572117	-.876090	1.387984	.631077
35	.123055	.0660403	-.932651	1.533550	.711677
40	.136351	.0747957	-.983885	1.674777	.790605
45	.147279	.0834925	-1.030821	1.812667	.868233
50	.155497	.0921423	-1.074200	1.947936	.944830
55	.160683	.100753	-1.114579	2.081112	1.020598
60	.162524	.109332	-1.152388	2.212594	1.095691
65	.160716	.117885	-1.187965	2.342696	1.170231
70	.154965	.126416	-1.221586	2.471663	1.244314
75	.144980	.134929	-1.253472	2.599688	1.318017
80	.130480	.143426	-1.283809	2.726932	1.391405
85	.111186	.151910	-1.312755	2.853522	1.464526
90	.0868243	.160383	-1.340442	2.979564	1.537426
95	.0571235	.168847	-1.366983	3.105143	1.610136
100	.0218173	.177303	-1.392477	3.230332	1.682687

TABLE III. (continued)

(d) h = 2

x (%)	$\frac{y_0(2,x,k,0,0)}{k}$	$\frac{y_c(2,x,k,0,0)}{k}$	$\frac{y_0(2,x,0,0,\tau)}{\tau}$	$\frac{y_c(2,x,0,0,\tau)}{\tau}$	$\frac{y_c(2,x,0,\delta,0)}{\delta}$
1	.00293311	.00228571	-.161254	.171070	.0462610
2	.00615472	.00441839	-.225374	.245019	.0759605
3	.00954037	.00647223	-.273564	.303052	.101455
4	.0130430	.00847031	-.313529	.352873	.124563
5	.0166341	.0104249	-.348248	.397461	.146053
6	.0202935	.0123439	-.379249	.438347	.166345
7	.0240057	.0142325	-.407439	.476435	.185700
8	.0277580	.0160951	-.433409	.512315	.204293
9	.0315398	.0179346	-.457567	.546398	.222251
10	.0353420	.0197535	-.480212	.578981	.239667
15	.0543995	.0285991	-.577114	.725774	.320712
20	.0730076	.0371323	-.656046	.854932	.394863
25	.0906013	.0454390	-.723602	.973045	.464488
30	.106724	.0535711	-.783145	1.083473	.530858
35	.120987	.0615634	-.836666	1.188203	.594756
40	.133039	.0694409	-.885458	1.288526	.656702
45	.142561	.0772223	-.930414	1.385331	.717067
50	.149254	.0849216	-.972182	1.479262	.776121
55	.152836	.0925509	-1.011251	1.570806	.834077
60	.153039	.100118	-1.047996	1.660333	.891095
65	.149604	.107633	-1.082717	1.748138	.947303
70	.142284	.115100	-1.115655	1.834462	1.002814
75	.130837	.122526	-1.147009	1.919496	1.057710
80	.115027	.129914	-1.176943	2.003400	1.112067
85	.0946282	.137270	-1.205597	2.086314	1.165949
90	.0694133	.144596	-1.233088	2.168348	1.219406
95	.0391637	.151895	-1.259519	2.249603	1.272486
100	.0036633	.159169	-1.284979	2.330156	1.325225

TABLE III. (continued)

(e) h = 5

x (%)	$\frac{y_0(5,x,k,0,0)}{k}$	$\frac{y_c(5,x,k,0,0)}{k}$	$\frac{y_0(5,x,0,0,\tau)}{\tau}$	$\frac{y_c(5,x,0,0,\tau)}{\tau}$	$\frac{y_c(5,x,0,\delta,0)}{\delta}$
1	.00298867	.00224486	-.137800	.143046	.0415628
2	.00629085	.00431376	-.193412	.203909	.0678221
3	.00976101	.00629157	-.235520	.251269	.0901726
4	.0133449	.00820529	-.270644	.291649	.110294
5	.0170108	.0100679	-.301310	.327574	.128901
6	.0207357	.0118892	-.328812	.360337	.146381
7	.0245024	.0136753	-.353918	.390707	.162978
8	.0282975	.0154299	-.377130	.419186	.178853
9	.0321094	.0171578	-.398794	.446121	.194125
10	.0359283	.0188610	-.419165	.471766	.208881
15	.0548615	.0270792	-.507028	.586038	.276870
20	.0729933	.0349158	-.579436	.684928	.338165
25	.0897746	.0424707	-.642009	.774055	.394991
30	.104781	.0498030	-.697623	.856296	.448544
35	.117660	.0569530	-.747985	.933357	.499568
40	.128106	.0639486	-.794205	1.006346	.548555
45	.135846	.0708134	-.837052	1.076035	.595863
50	.140630	.0775630	-.877085	1.142981	.641750
55	.142228	.0842116	-.914727	1.207607	.686420
60	.140423	.0907721	-.950304	1.270237	.730033
65	.135011	.0972497	-.984075	1.331133	.772712
70	.125797	.103653	-1.016251	1.390503	.814565
75	.112594	.109993	-1.047005	1.448521	.855679
80	.0952231	.116270	-1.076480	1.505330	.896128
85	.0735103	.122491	-1.104800	1.561051	.935971
90	.0472874	.128661	-1.132067	1.615791	.975268
95	.0163916	.134785	-1.158371	1.669635	1.014062
100	-.0193369	.140863	-1.183790	1.722662	1.052395

TABLE III. (concluded)

(f) $h = \infty$

x (%)	$\frac{y_0(\infty,x,k,0,0)}{k}$	$\frac{y_c(\infty,x,k,0,0)}{k}$	$\frac{y_0(\infty,x,0,0,\tau)}{\tau}$	$\frac{y_c(\infty,x,0,0,\tau)}{\tau}$	$\frac{y_c(\infty,x,0,\delta,0)}{\delta}$
1	.00312368	.00214773	-.100000	.100000	.0334068
2	.00660619	.00406930	-.141421	.141421	.0538470
3	.0102512	.00587558	-.173205	.173205	.0709617
4	.0139886	.00760024	-.200000	.200000	.0861749
5	.0177780	.00926102	-.223606	.223606	.100092
6	.0215920	.0108692	-.244948	.244948	.113043
7	.0254106	.0124327	-.264575	.264575	.125235
8	.0292182	.0139572	-.282842	.282842	.136807
9	.0330023	.0154472	-.300000	.300000	.147857
10	.0367526	.0169061	-.316227	.316227	.158462
15	.0547287	.0238215	-.387298	.387298	.206454
20	.0709229	.0302502	-.447213	.447213	.248594
25	.0848826	.0363143	-.500000	.500000	.286785
30	.0963022	.0420882	-.547722	.547722	.322060
35	.104957	.0476217	-.591607	.591607	.355055
40	.110674	.0529509	-.632455	.632455	.386200
45	.113314	.0581025	-.670820	.670820	.415801
50	.112760	.0630980	-.707106	.707106	.444086
55	.108915	.0679540	-.741619	.741619	.471230
60	.101694	.0726844	-.774596	.774596	.497372
65	.0910259	.0773007	-.806225	.806225	.522624
70	.0768439	.0818127	-.836660	.836660	.547078
75	.0590912	.0862286	-.866025	.866025	.570810
80	.0377162	.0905552	-.894427	.894427	.593887
85	.0126721	.0947996	-.921954	.921954	.616362
90	-.0160835	.0989665	-.948683	.948683	.638285
95	-.0485898	.103061	-.974679	.974679	.659696
100	-.0848826	.107088	-1.000000	1.000000	.680633

REFERENCE NO.	FIRST AUTHOR	YEAR	ORIGIN (1)	δ	PROFILE (2)	FLAPS (3)	STEADY FLOW	UNSTEADY FLOW (3)	meas. (4)	AIR ENTRAINMENT	theory	VENTILATION INCEPTION DISCUSSION	finite depth	infinite depth	3-D effects	gravity	strength	cavity shape (6)	linearized	non-linear	lift	drag	moment	speed (fps)	chord (in.)	aspect ratio
												THEORY (3)														
5	Helmholtz	'68		0			x						x						x		x					
4	Kirchoff	'69		0	Fn		x						x						x		x					
9	Rayleigh	'76		0	F		x						x			x			x	x	x	x				
32	Bobyleff	'81		0	W		x						x						x		x					
83	Riabouchinsky	'21		finite	Fn		x						x			x			x		x					
33	Brodetsky	'23	PRS	0	cyl		x						x			x			x							
94	Wagner	'33	KWIS	0	F		x					0			•				x	x	x		13-31	2-30	.39-6	
10	Green	'36		0	F		x					x	x			x			x	x	x	x				
82	Reichardt	'45	VL	.01-.12	d,cones		x						x			+			x		x					
67	Kreisel	'46	ARL	finite	wedge		x					•	x			x										
54	Gilbarg	'46	NOL	finite	Fn		x						x			x			x		x					
45	Efros	'47	IAN	finite	Asp,Sp		x						x	x		•			x	•	x					
79	Plesset	'48	NOTS	finite	W,cone		x						x			+			x		x					
59	Gilbarg	'50	IU	finite	F,W		x						x			x			x	x	x					
56	Gilbarg	'52	IU	finite	Fn			x					x			x										
30	Armstrong	'53	ARE	finite	Sp,Sa		x						x			x			x							
61	Kaplan	'53	SIT		sn		x																	2.6-35	10	
12	Tulin	'53	DTMB	finite	Sp,W		x						x			x	x				x					
85	Roshko	'54	CIT	finite	Fn,cyl,W		x						x			x			x							
88	Shuford	'54	NACA	0	F		x					0		x			x				x					
66	Kiceniuk	'54	CIT		L		x				x														1.277	2-4
13	Tulin	'55	DTMB	0	F,2	x	x						x			x	x				x	x	x			
28	Acosta	'55	CIT	finite	F		x						x			4	x				x					
52	Geurst	'56	ITW	finite	F		x						x				x				x	x				
51	Geurst	'56	ITW	finite	Sp		x						x			x	x					x				
78	Plesset	'56	CIT	finite	C		x						x				x				x	x				
80	Pykhteev	'56					x						x			x	x				x					
25	Tulin	'56	ONR	finite	F,Fn,Sp,Sa		x						x	•		•	x				x	x	x			
59	Hug	'56	SUR	finite	F		x						x				x				x	x	x		5	∞
64	Kermeen	'56	CIT	.41-4.8	NACA 4412		x																	20-35	3,3.3	∞
63	Kermeen	'56	CIT	.04-5.4	NACA 66-012		x																	30-60	3.3	∞
27	Parkin	'56	CIT	.12-2.3	F,C		x						•						•	•	•	•		25,30	1.74,2.38	∞
24	Wu	'56	CIT	finite	C		x						x					x	x	x	x					
75	Newman	'56	DTMB	0	W		x						x					x			x					
84	Ripken	'56	Minn	.07-.49	2		x						•					•			•	•		25-50	2.5	∞
23	Wu	'56	CIT	finite	C,F		x						x				x		x	x	x	x	x			∞
40	Cohen	'56	RPI	finite	Sa,F		x						x			x	x					x				
96	Woods	'57	NSWUT	0	F			x					x				x				x		x			
38	Christopher	'57	NACA	0	F		x																	80-170	4,8	.111
41	Cohen	'57	RPI	finite			x						x			4	x				x					
81	Ramsen	'57	NACA		F		x				x													15-18	14.14,36	.25
26	Waid	'57	CIT	finite	2		x						•								•	•		20-45	3	∞
15	Johnson	'57	NACA	0	F,2,3,5		x						x			x	x				x	x				
74	Morgan	'57	DTMB	0	F,2,3,5		x						x			x	x				x	x				
95	Waid	'57	CIT	.04-.17	d		x					x				x								12-24		
97	Wu	'57	CIT	finite	W			x					x			8	x				x	x	x			
16	Johnson	'57	NACA	0	F,Fn,2,3,5,C		x				x	x	x	x		x	x		x		x	x	x	20-80	7.07	1
76	Parkin	'57	CIT	finite	F		x						x		x	x	x				x	x	x			
49	Fedorov	'58	CAHI	0	F		x					x				x			x		x	x	x			
89	Silberman	'58	Minn	.05-.30	cyl,F,W		x																	20-45	1,2	
34	Brown	'58	SIT		C		x						•	•			•				x	x		10-40	2	var.

*See end of table for explanation of ( ) numbered notes.

TABLE IV - SUMMARY BI

EXPERIMENT (4)													REMARKS
	chord (in.)	aspect ratio	depth (chords)	vapor cavity	vented cavity	cavity meas.	lift	drag	moment	tunnel	tank	planform	
													Discovery of free streamline (Helmholtz) motion
													Exact solutions for wedges Introduction of Riabouchinsky Model for finite cavities
	2-30	.39-6	0 ∞		• x		•	• x		x		rect.	Planing The only exact finite depth solution Re-entrant jet observed; Empirical expressions derived
													Introduction of Re-entrant Jet Model in formal literature Comparison between Re-entrant Jet and Riabouchinsky Models Electrical simulation; discussion of cascade flow included
								•					
	10		.5,1,2		x			x			x		Abrupt-and smooth-(shock-free) entry discussed Surface piercing struts; side force also measured Introduction of linearized theory of supercavitating flow
	1.277	2-4	0		• x		• x					rect. rect.	Introduction of the Roshko Dissipation Model Planing Surface piercing
													Introduction of low drag supercavitating foils Partial cavitation
							•	•					Finite depth effects included for fully wetted foils Inverse problem
	5 3,3.3	∞ ∞	∞ ∞	x x			x x	x	x	x x		rect. rect.	Min. drag struts & Sa bodies at σ = 0; P at σ ≠ 0 NACA 66-012 tested under supercavitating conditions Welchner profile also tested
	3.3 1.74,2.38	∞ ∞	∞ ∞	x x			x x	x x	x x	x x		rect. rect.	Wu's theory used (Reference 23)
	2.5	∞ ∞	∞ ∞	x •		+	• x •	• x •	• •	•		rect. rect.	Partial wetting of top surface Exp. lift and drag calculated from pressure measurements
	4,8	.111	0		x		x	x	x		x	rect.	Wall effects discussed Cavity separation from arbitrary point on upper surface Planing
	14.14,36 3	.25 ∞	.02-.10 ∞	x	x x	+ +	x x	x	x	x	x	rect. rect.	Wall effects discussed Vortex ventilation investigation; scaling investigated Wu's theory used (Reference 23)
				x					x				Friction drag included to obtain optimum lift coefficients Experiments on disks at incidence in free surface tunnel
	7.07	1	0-.85	x	x	x	x	x	x		x	square	Experiments also at finite σ
	1,2 2	var.	.25-2	x	x x	x +	x x	x x		x	x	rect. rect.	Separation from arbitrary point on upper surface Free Jet tunnel Surface piercing foils; dihedral

HYDRONAUTICS, Incorporated

REFERENCE NO.	FIRST AUTHOR	YEAR	ORIGIN (1)	σ	PROFILE (2)	FLAPS (3)	STEADY FLOW	UNSTEADY FLOW (3) meas. (4)	AIR ENTRAINMENT theory	THEORY (3) VENTILATION INCEPTION DISCUSSION finite depth (5)	infinite depth	3-D effects	gravity	strength	cavity shape (6)	linearized	non-linear	lift	drag	moment	speed (fps)	chord (in.)	aspect ratio
73	McGehee	'59	NASA	.00-5.5	S		x			x	•	•	•			•		•	•	•	20-80	4.08-7.07	1,3
77	Parkin	'59	CIT	finite			x				•	•		•		•		•	•	•			
35	Brown	'59	SIT	finite	P,C	x	x														1.9-35	3.48	3.2
93	Wadlin	'59	NASA	0			x			x											12-250	7.07	1
68	Lang	'59	NOTS	finite	P,p,NACA 16		x				•	x		x			x		x	x			
46	Fabula	'59	NOTS	0	F,C		x					x			•		x		x	x	x		
60	Johnson	'59	NASA		P,p		x										•		•		130-190	7.07	1
69	Lang	'59	NOTS	.04-.30	NACA		x		x		x	•	•				•		•	•		4	1.44,∞
91	Tulin	'59	HYD	0,∞	F		x					x	x		9	x			x	x			
21	Christopher	'60	NASA	.07-.53	S,F		x										•		•		60-185	7.07	1
43	Cumberbatch	'60	CIT	finite	F		x					x	x			x	•		x				
53	Geurst	'60	ITW	finite	F		x					x				x	•		x	x			
38	Chen	'60	HYD	0			x				x	•	x	•	x	x	•		x	x			
42	Cumberbatch	'60	CIT	finite	W			x				x				x			x				
18	Auslaender	'60	HYD	0	F	x	x				x	•				x			x	x			
39	Christopher	'60	NASA	.00-.05	S		x			x											110-200	4.08,7.07	1,3
47	Fabula	'60	NOTS	finite	Sp,C		x									x	•		•	x			
65	Kermeen	'60	CIT	.01-.07	W		x														20,25,30	1.50-4.50	0.5-4
92	Tulin	'60	HYD		•	•	•	•			•	•	•	•	•	•			•	•			
44	Cuthbert	'60	HYD	finite			x		•	x													
50	Fridsma	'60	SIT	≈0	F		x		•			•	•			•			•	•			
19	Johnson	'61	NASA	0	F,2,3,5,C		x			x	x	x	x	•	x	x	x	x	x	x	20	1	3.43-10.4
1	Johnson	'61	HYD	0	2,3,5, τ,F		x			x	•	•	•		•	•	•		•	•	20-80	7.07	1
3	Tulin	'61	HYD	.00-1.0	W,cyl,Sp,F,2		x	•			•	•			4	•			•	•			1,3
90	Song	'61	Minn	.04-.20				x	•	x	x	x		•	•	4	x						∞
62	Kaplan	'61	SIT	finite	sn			x							x								
48	Fabula	'61	NOTS	finite	W,F,C	x	x					x				x			x	x	x		
26	Auslaender	'61	HYD	0	F,P,2,3,5,τ		x				x	x			x	x	x		x	x	x		∞
37	Chen	'61	HYD	0	F	x	x				x	x				x	x		x	x			
58	Ho	'61	HYD	0	F	x	x					x				x	x		x	x	x		
86	Schiebe	'61	Minn	.07-.33	F		x		x	x		•	•	•					•	•	12-18	3	2.5,4
57	Hellsten	'61	Grun	.17-.54	2,2+τ		x														67-135	6.34-8	3
29	Andrews	'61	Grun	finite	F,p,C	x															30	2.4,4	2,3.2
31	Auslaender	'61	HYD	0	F,2,τ		x					•	•		•	•	•		•	•			
22	Chen	'61	HYD	0	C,F		x					x				x		x	x	x	x		
71	Luu	'61	BARA	finite	F,2	x	x					x	x			x		x	x	x	x		
70	Lin	'61	HYD	0	F	x	x				x	x						x	x	x			
72	Martin	'61	SIT	0	F			x				x							x	•	x		
87	Schot	'62	DTMB	0	Sp,F		x				x	x			x	x			x				
	Auslaender	'62	HYD	finite	F,2,τ		x			x	•	•		•	•	•	•		•	•			∞

*See end of table for explanation of ( ) numbered notes.

TABLE IV - CONTINUED

	EXPERIMENT (4)												REMARKS
	chord (in.)	aspect ratio	depth (chords)	vapor cavity	vented cavity	cavity meas.(7)	lift	drag	moment	tunnel	tank	planform	
	4.08-7.07	1,3	0-.85		x	x	x •	x •	x		x	rect.	Foils tested with and without end plates Review
5	3.48	3.2	.48-2.87	x	x	+	x	x			x	tapered	Base vented; flaps; sweep
	7.07	1	.5-1.5		x	+					x	square	Comprehensive discussion of ventilation & its inception Base vented foils Fully or partially vented
0	7.07 4	1 1.44,∞	0.5 ∞		x x	+ +	x x	x x	x x	x	x	square	Base vented foils NACA a = 1 m.l. with 0010 thickness & NACA 65-015 Slender delta wing
	7.07	1	0-1	x	x	x	x	x	x		x	square	
													3-D effects near free surface
0	4.08,7.07	1,3	0-1	x	x	x	x •	x	x		x	rect.	
30	1.56-4.50	0.5-4	∞	x			x	x	x	x		rect.	Base vented foils
	1	3.43-10.4	1-3		x		x	x	x		x	rect.	Survey; comparisons between hydrofoil and aircraft environm't Study of air entrainment
	7.07	1 1,3 ∞	.07-.85 .07,.14 ∞	x •	x •	x + +	x •	x •	x		x •	square rect. rect.	Dihedral; fully vented Experiments also at finite σ Survey; comparisons between hydrofoil and airfoil design
		∞	∞	•			•			•			Survey; wall- & free jet- boundary effects also discussed Free jet tunnel; theory for pulsating cavities Hydroelastic effects
													Base vented foils Foils designed for depth Spoiler flaps
	3 6.34-8 2.4,4	2.5,4 3 2,3.2	1-3 .75-1.25 .3-2.8	x	x x x	+ +	x x x	x x x	x x		x x	rect. rect. tapered	Jet flaps Whirling tank Delta wing also tested; pendulum facility
													Hydrofoil wing series; design charts Second order theory; arbitrary profile Also annular foil with flaps; rheoelectric simulation
		∞	∞	•	•		•	•					Non-linear theory for flaps;cambered foil with flap discussed Unsteady forces due to sinusoidal gust Effect of surface tension discussed for Sp case Design charts and methods

ABLE IV - CONTINUED

TABLE IV. (Continued)

Explanation of Notes

(1)

Origin usually denotes where the work was done, not necessarily where it was published

Abbreviations:

ARE	Armament Research Establishment
ARL	Admiralty Research Laboratory
BARA	Bureau D'Analyse et de Recherche Appliques
CAHI	Central Aero-Hydrodynamical Institute, USSR
CIT	California Institute of Technology
DTMB	David Taylor Model Basin
Grum	Grumman Aircraft Engineering Corporation
HYD	HYDRONAUTICS, Incorporated
IAN	Izvestia Akademie Nauk
ITW	Instituut Voor Toegepaste Wiskunde
IU	Indiana University
KWIS	Kaiser Wilhelm Institut für Strömungsforschung
Minn	University of Minnesota
NACA	National Advisory Committee for Aeronautics
NASA	National Aeronautics and Space Administration
NOL	Naval Ordnance Laboratory
NOTS	Naval Ordnance Test Station
NSWUT	New South Wales University of Technology, Sydney
PRS	Proceedings of the Royal Society
RPI	Rennselaer Polytechnic Institute
SIT	Stevens Institute of Technology
SUI	State University of Iowa
VL	Volkenrode (Guided Missile) Laboratory, Germany

TABLE IV. (Continued)

(2) Types of Profile

F	flat plate at incidence (assymmetric flow)
Fn	flat plate normal to the stream (symmetric flow)
2	two term camber
3	three term camber
5	five term camber
C	circular arc camber
P	constant pressure camber
τ	quasi-parabolic thickness
p	parabolic thickness
A	NACA "a = 1" mean line
Sp	plane symmetric flow
Sa	axially symmetric flow
L	Lenticular
sn	sharp nosed
W	wedge
cyl	cylinder
Asp	plane assymmetric flow
d	disk

(3) x Theory developed
* Theory discussed

(4) x Tests performed
* Tests quoted

(5) "finite" depth means "finite or zero depth".- an x or * in this column does not necessarily mean that the zero depth (planing case) is treated specifically. If only the planing case is treated, a zero appears in the column.

(6) ℓ = length only; w = max thickness only; + = w and ℓ only

(7) x = measurements of cavity location
+ = visual observations recorded to indicate whether or not cavity was developed as intended.

(8) cavity area

(9) cavity width

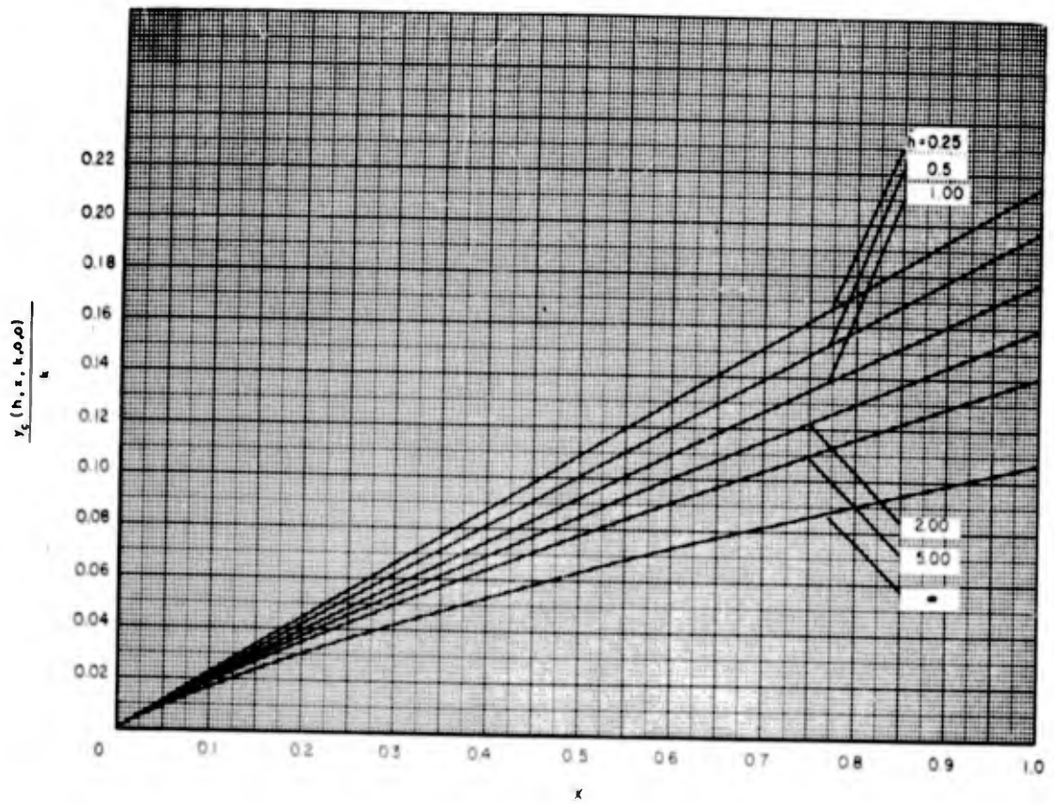

(a)- Top Cavity Shape

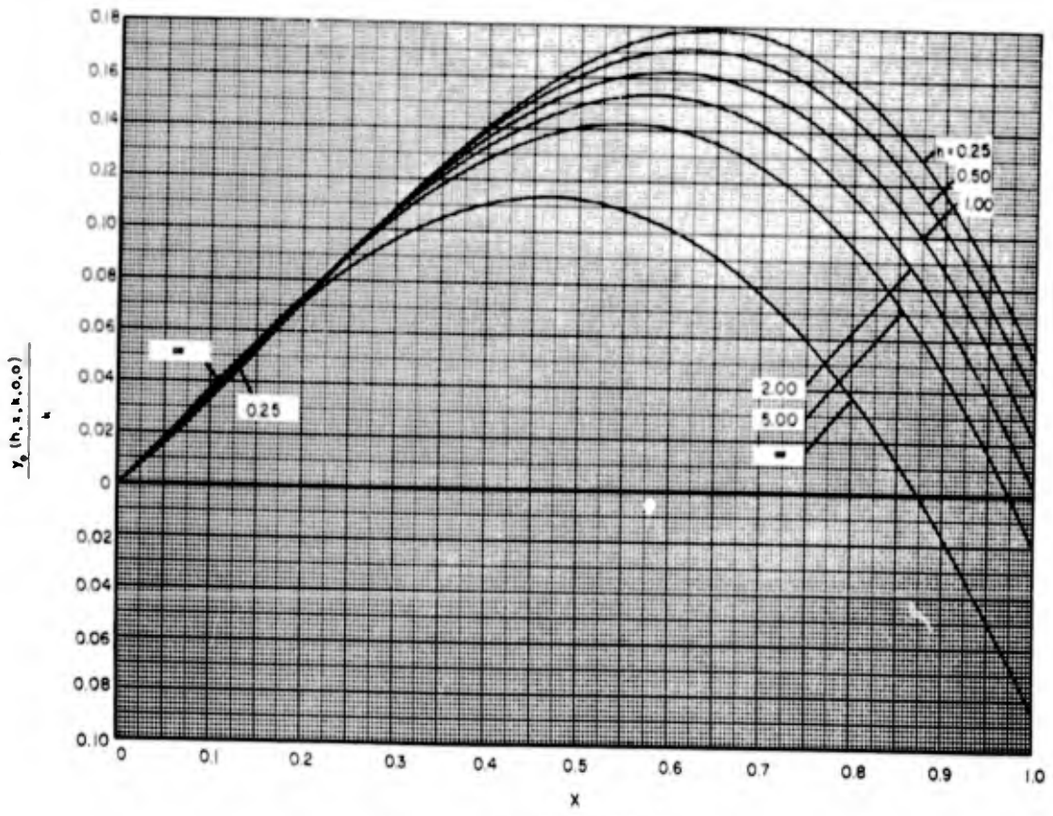

(b)- Bottom Surface Shape

Figure 9 - Bottom Surface and Top Cavity Shape Due to Two-Term Camber at Various Depth-Chord Ratios

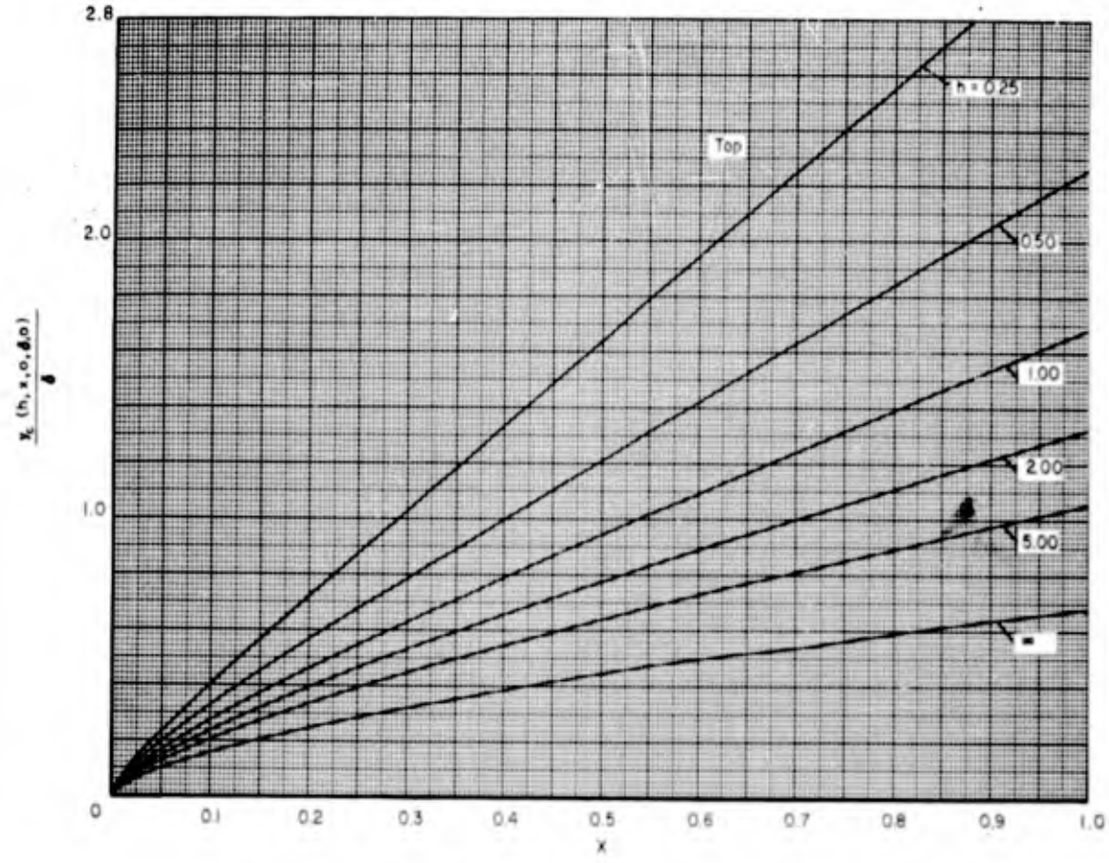

Figure 10a - Top Cavity Shape Due to Design Angle of Attack at Various Depth-Chord Ratios

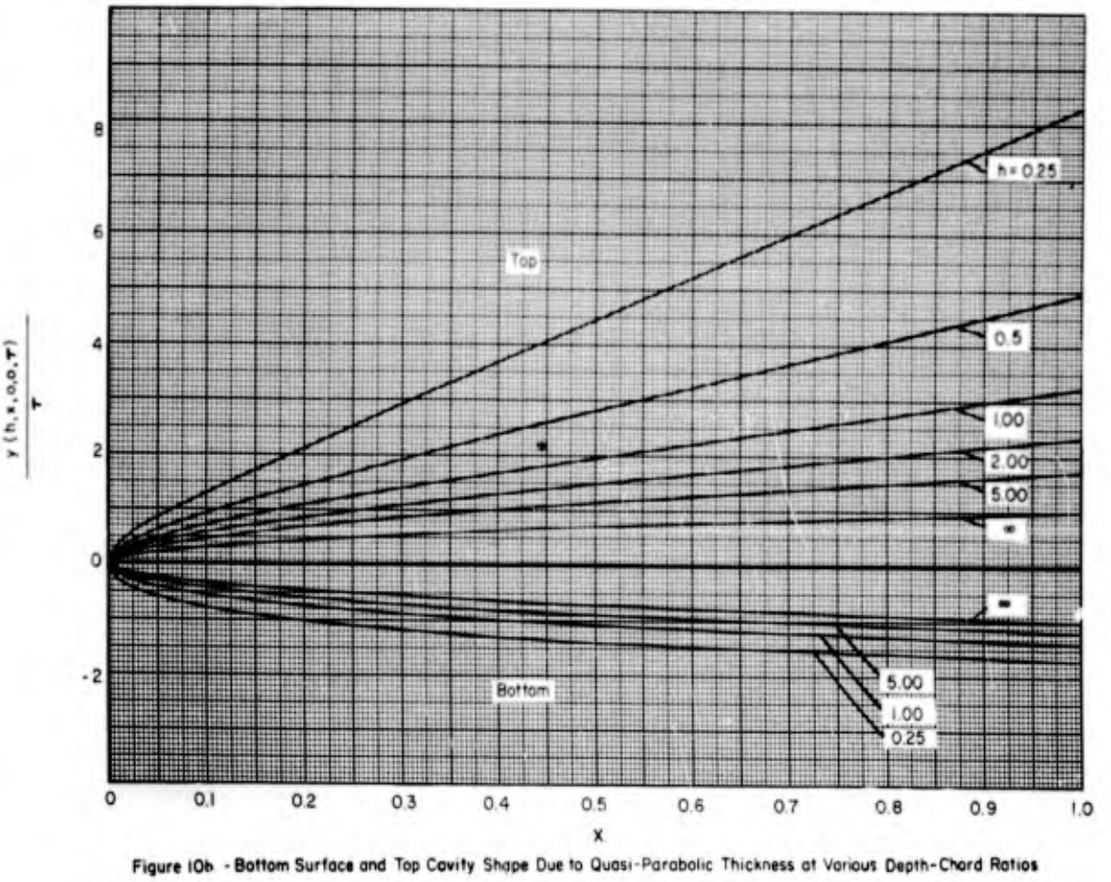

Figure 10b - Bottom Surface and Top Cavity Shape Due to Quasi-Parabolic Thickness at Various Depth-Chord Ratios

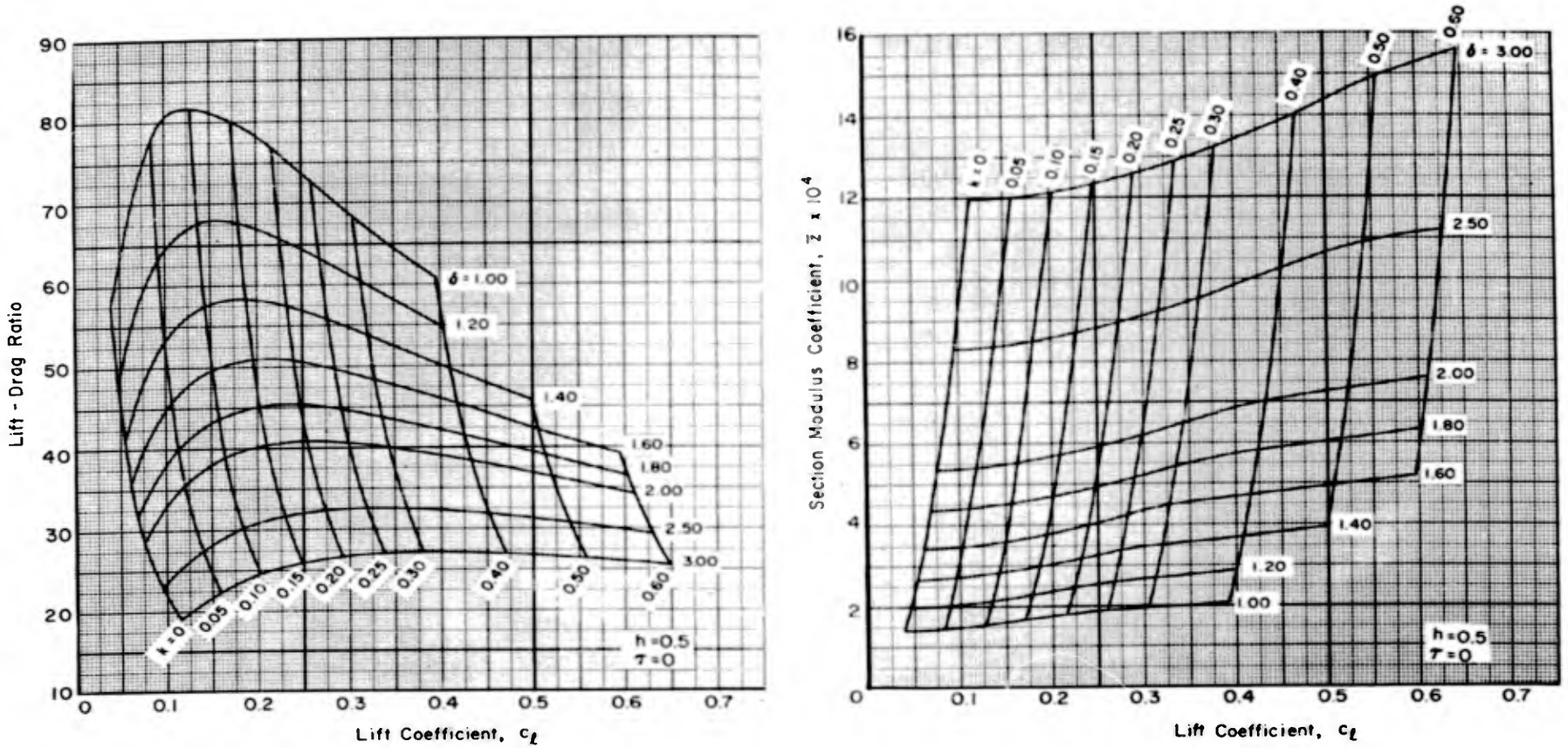

(a) $\tau = 0$

FIGURE 12. - LIFT-DRAG RATIO AND SECTION MODULUS VS. LIFT COEFFICIENT OF TWO-TERM FOILS DESIGNED FOR OPERATION AT A DEPTH OF 1/2 CHORD. CONTOURS OF CONSTANT CAMBER INDEX AND ANGLE OF ATTACK.

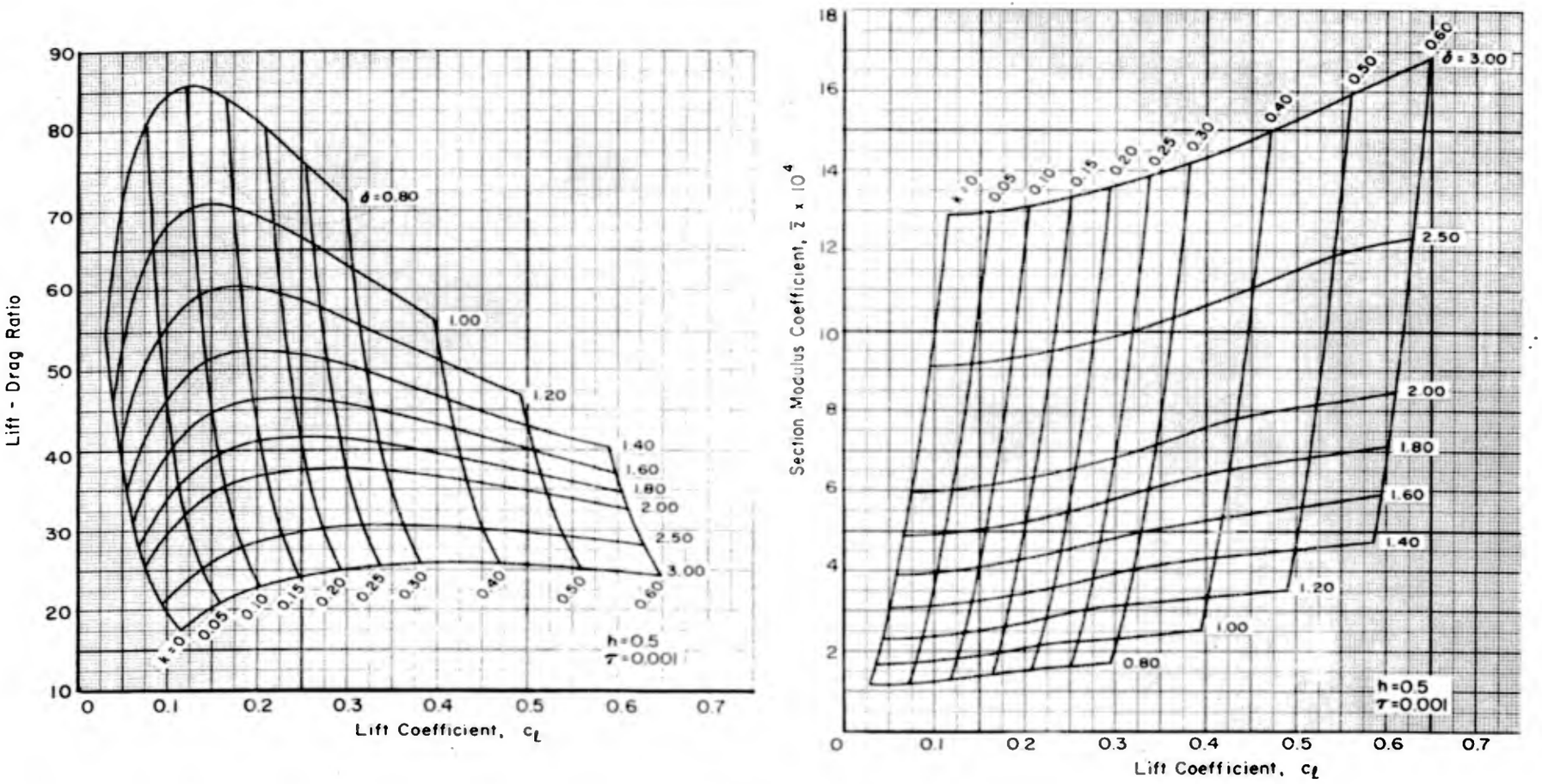

(b) τ = 0.001

FIGURE 12. - (continued)

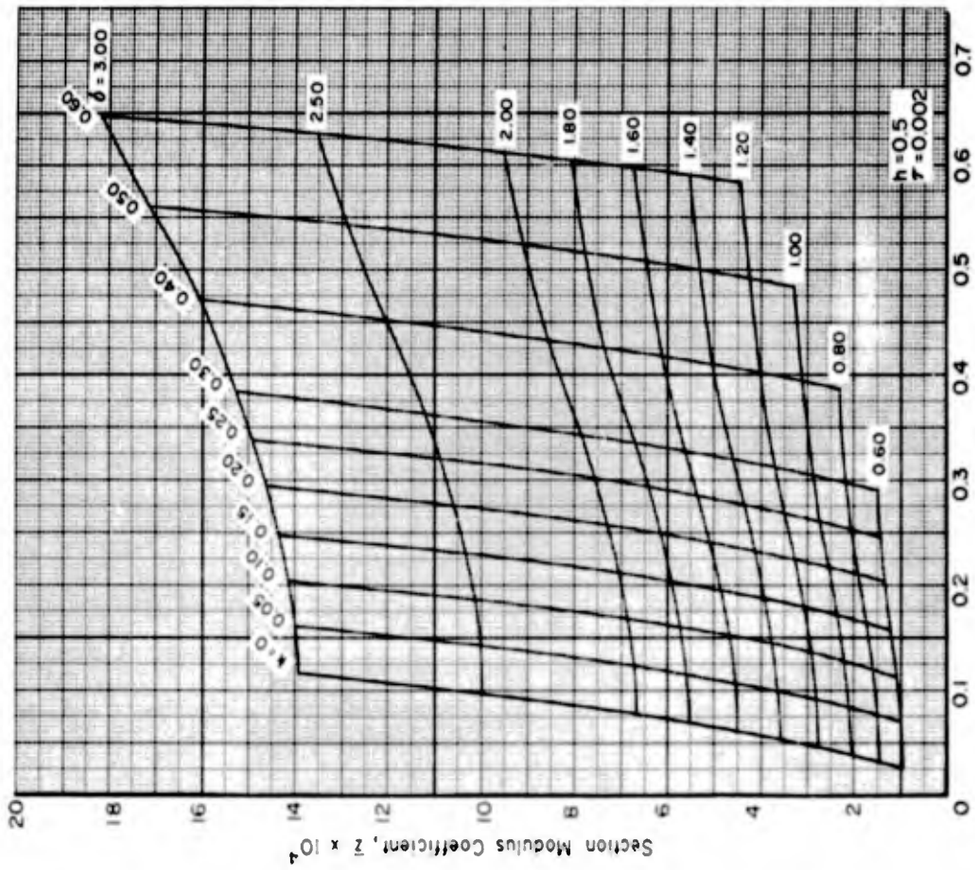

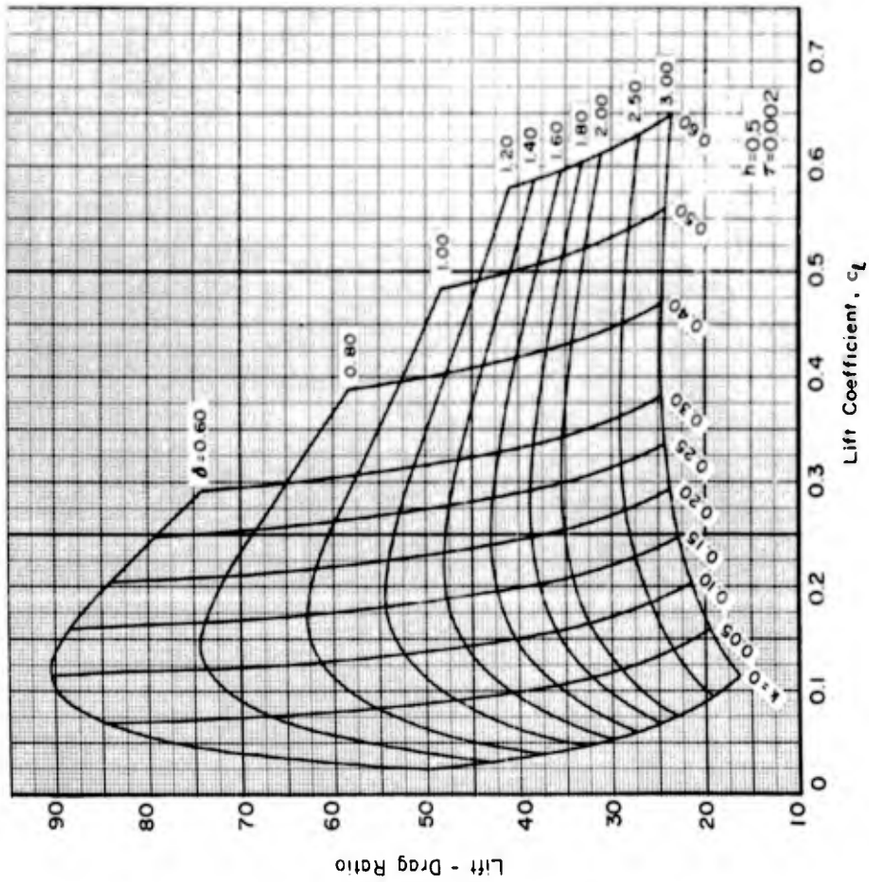

(c) τ = 0.002

FIGURE 12. - (continued)

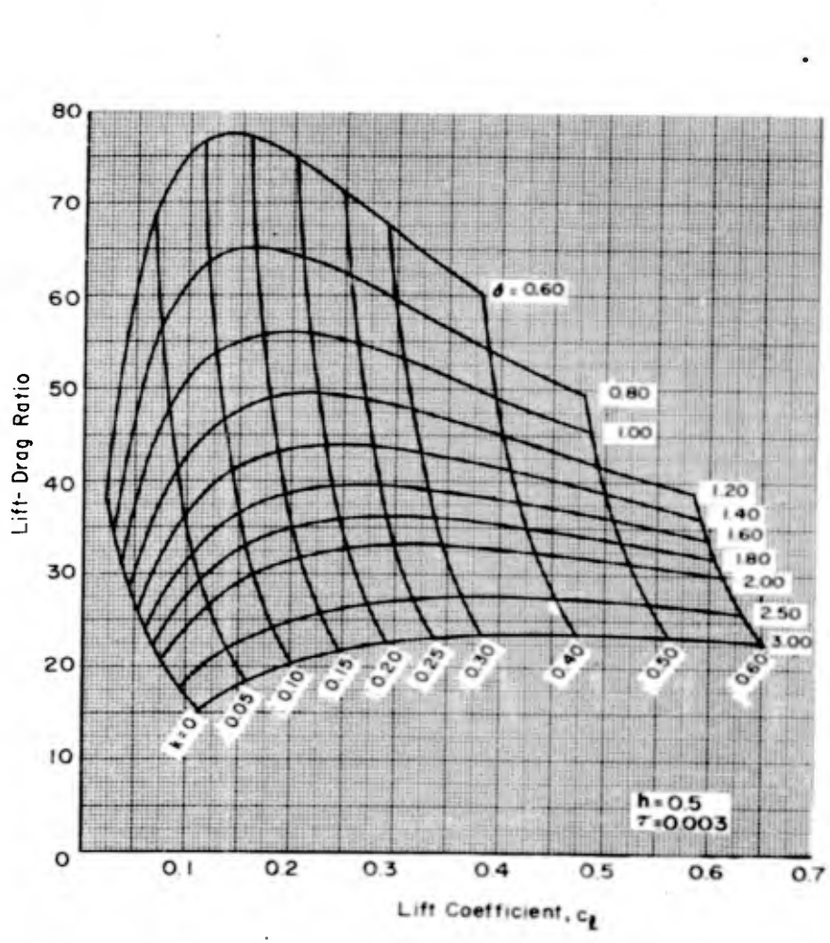

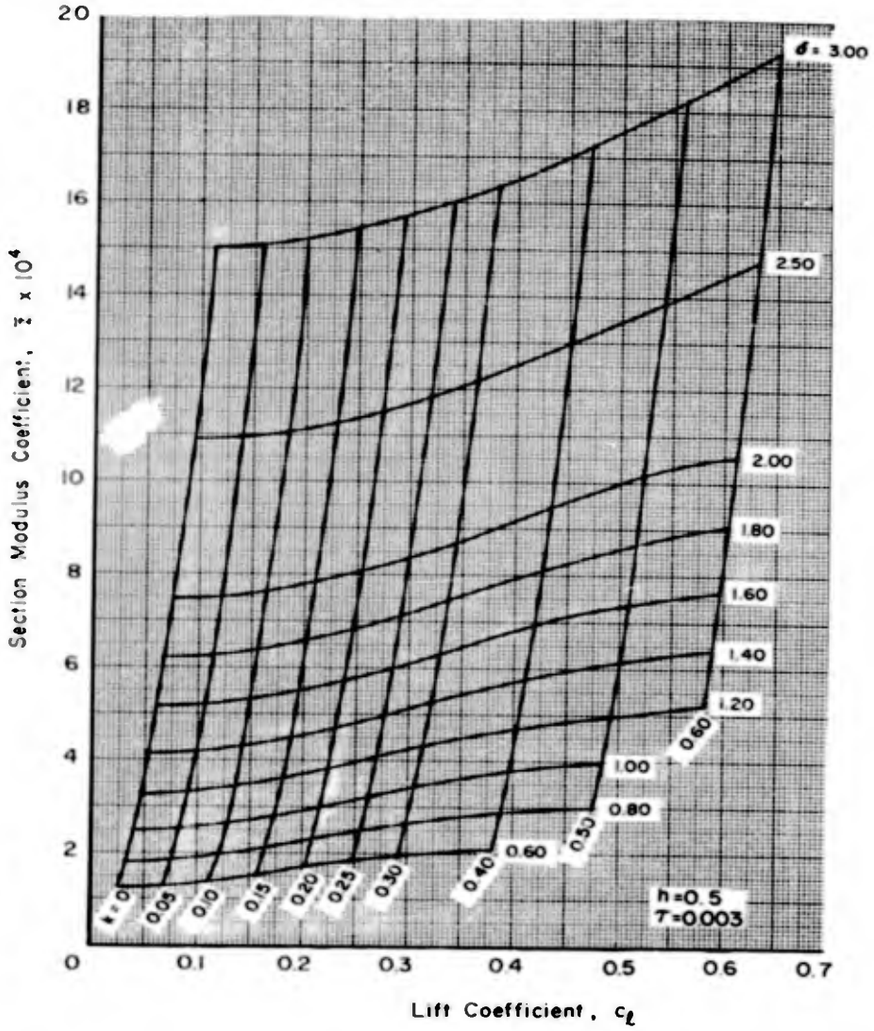

(d) τ = 0.003

FIGURE 12. - (continued)

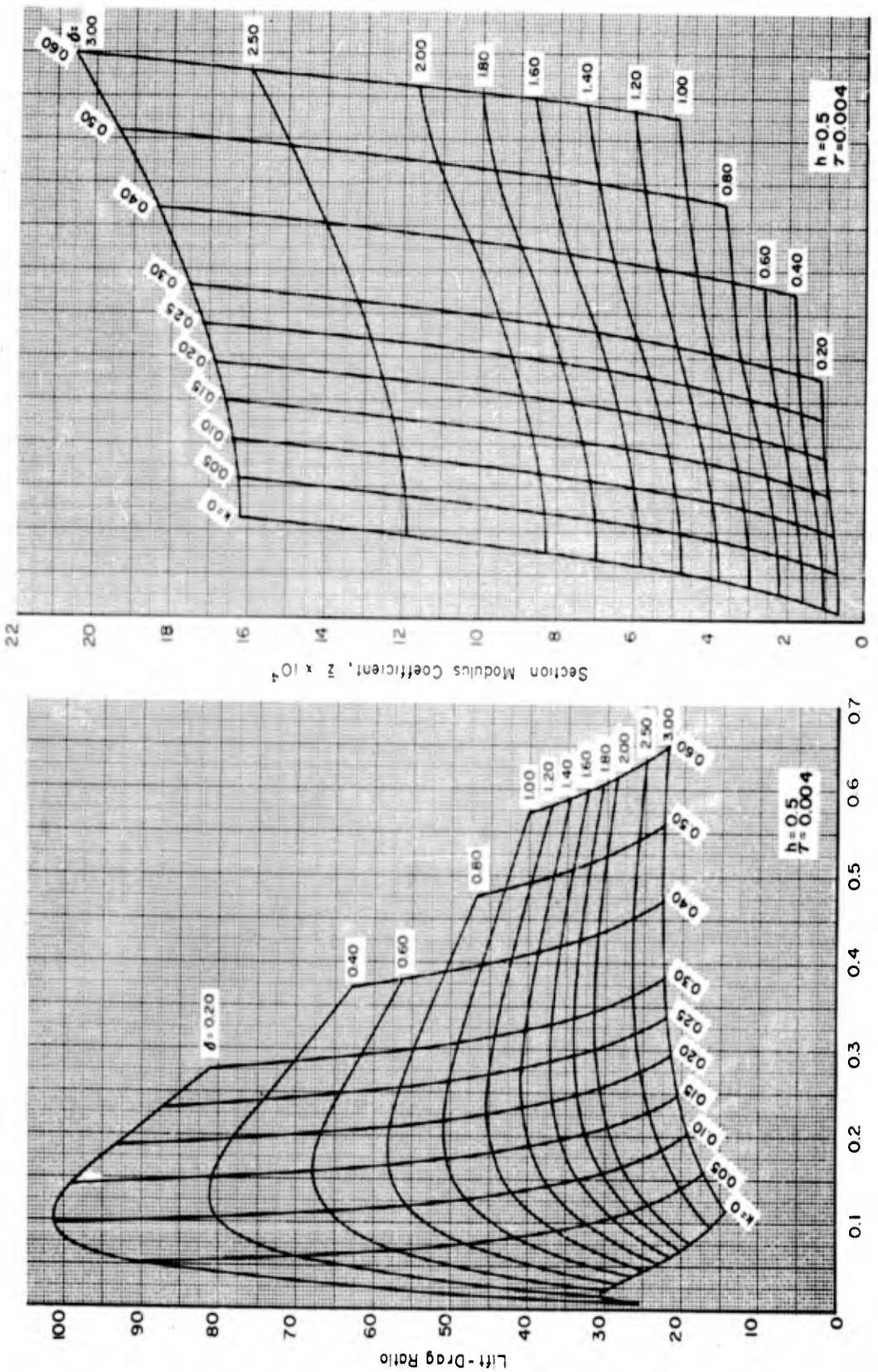

(e) τ = 0.004

FIGURE 12. - (continued)

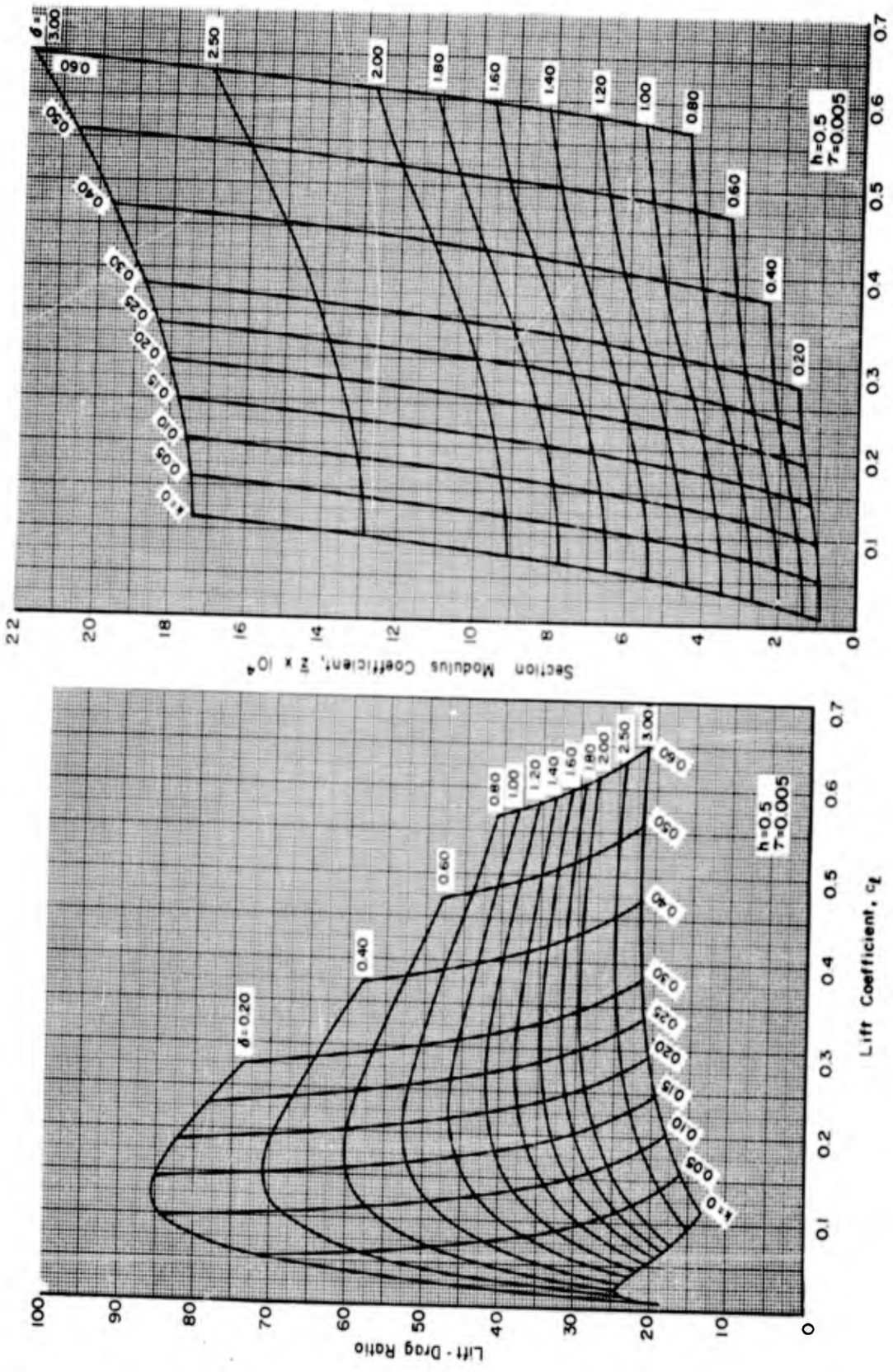

(f) τ = 0.005

FIGURE 12. - (continued)

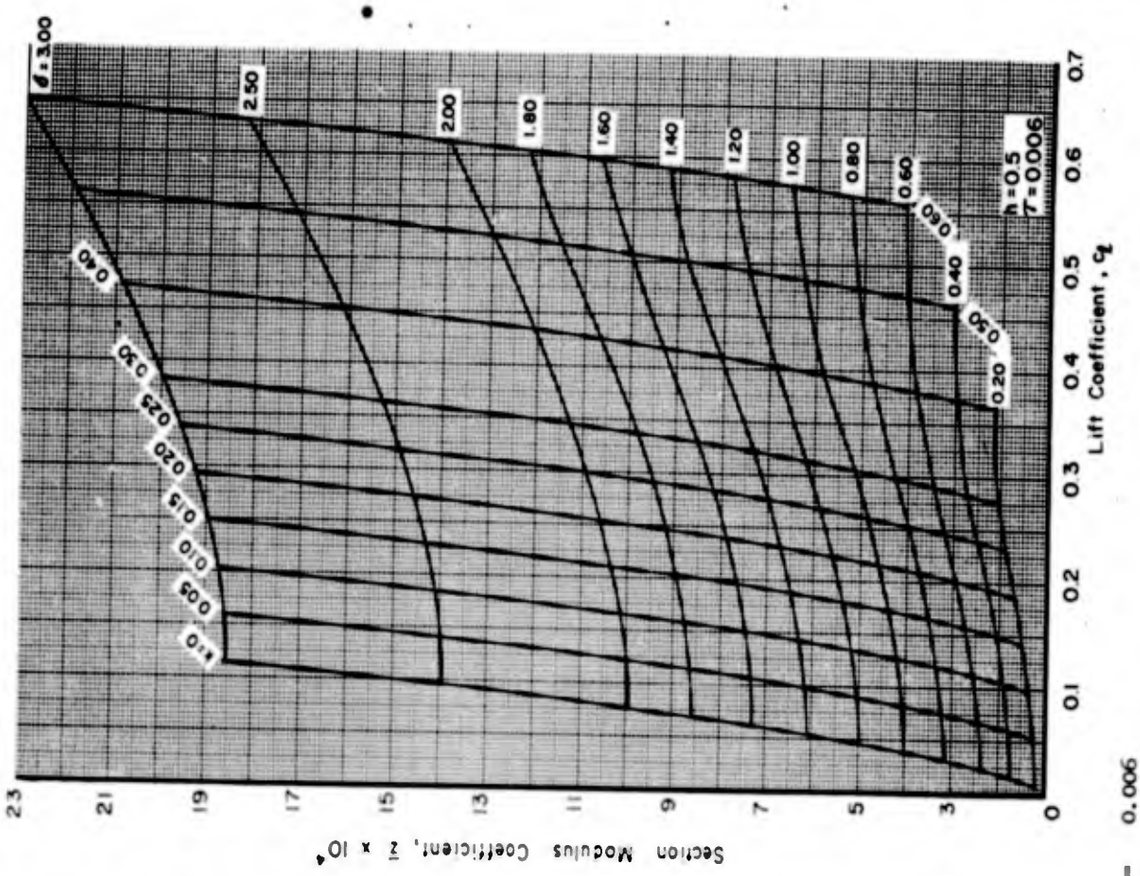

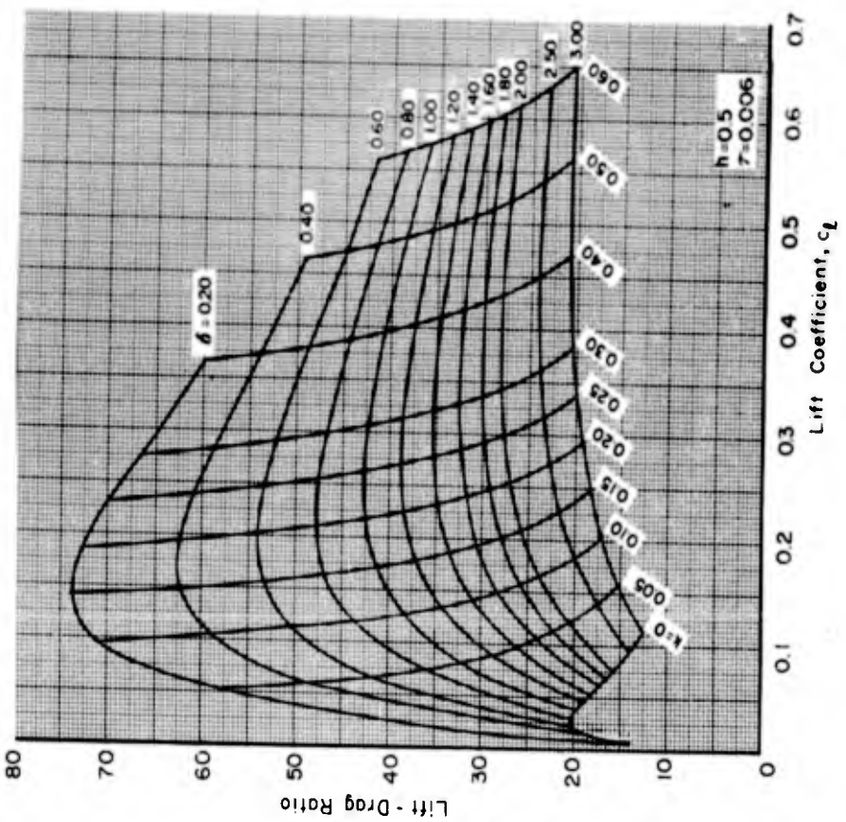

(g) τ = 0.006

FIGURE 12. - (continued)

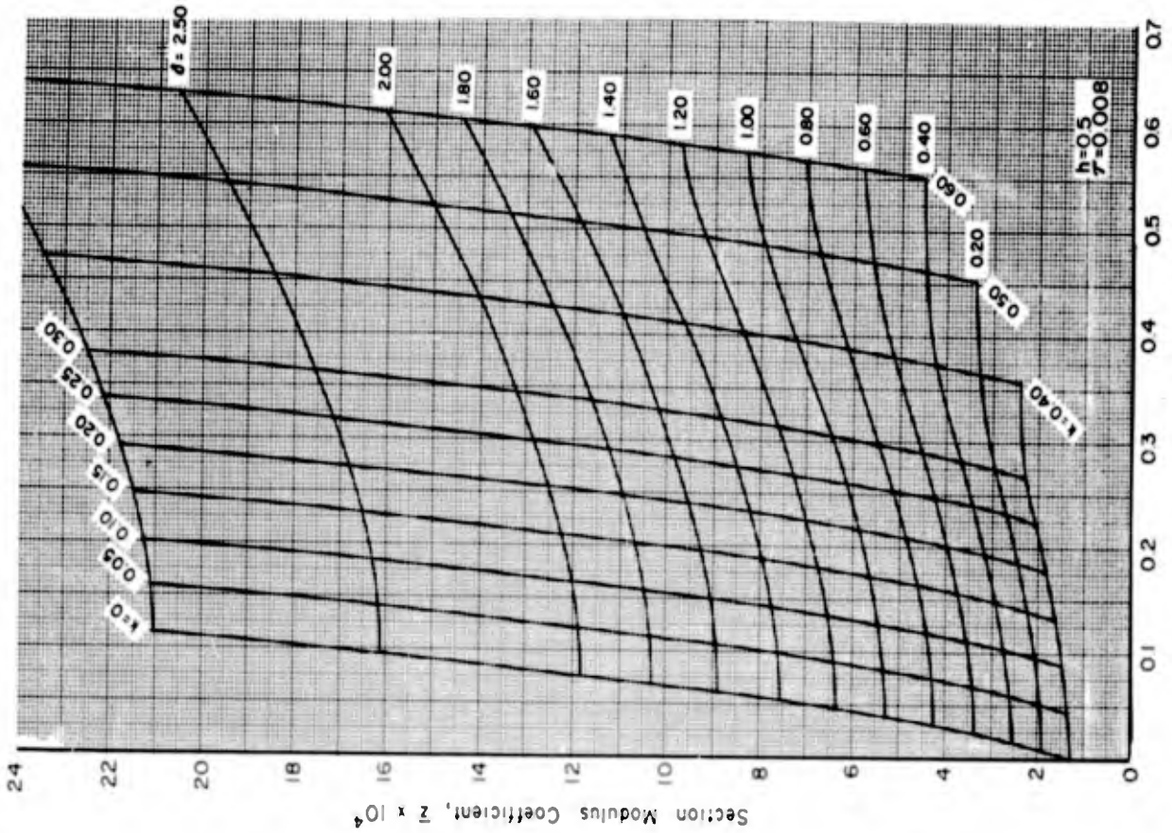

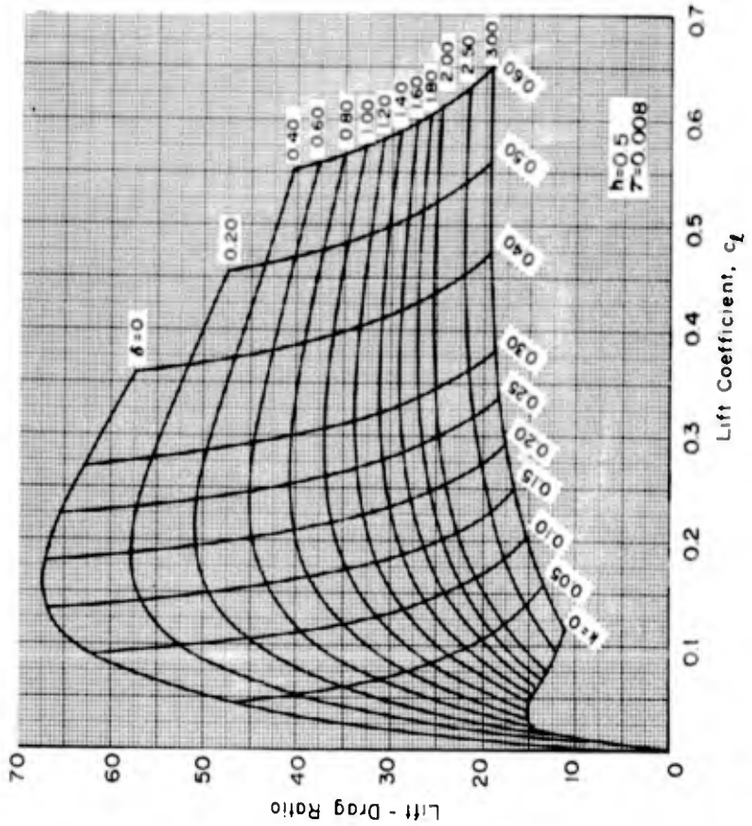

(h) τ = 0.008

FIGURE 12. - (continued)

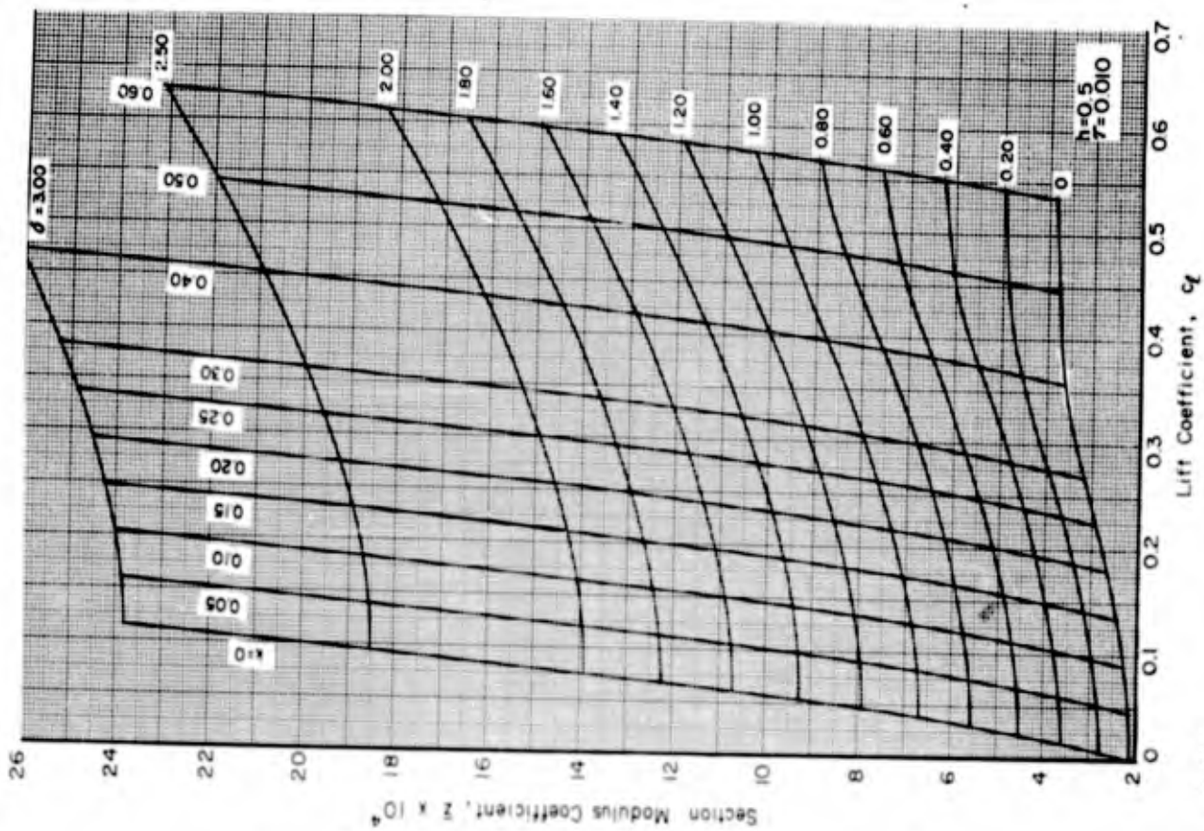

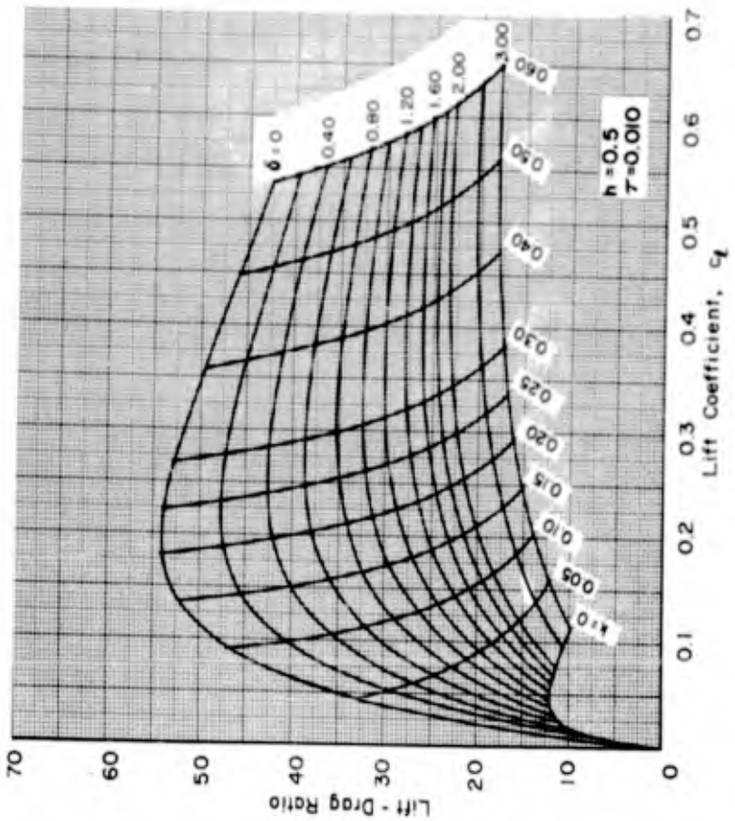

(1) τ = 0.010

FIGURE 12. - (concluded)

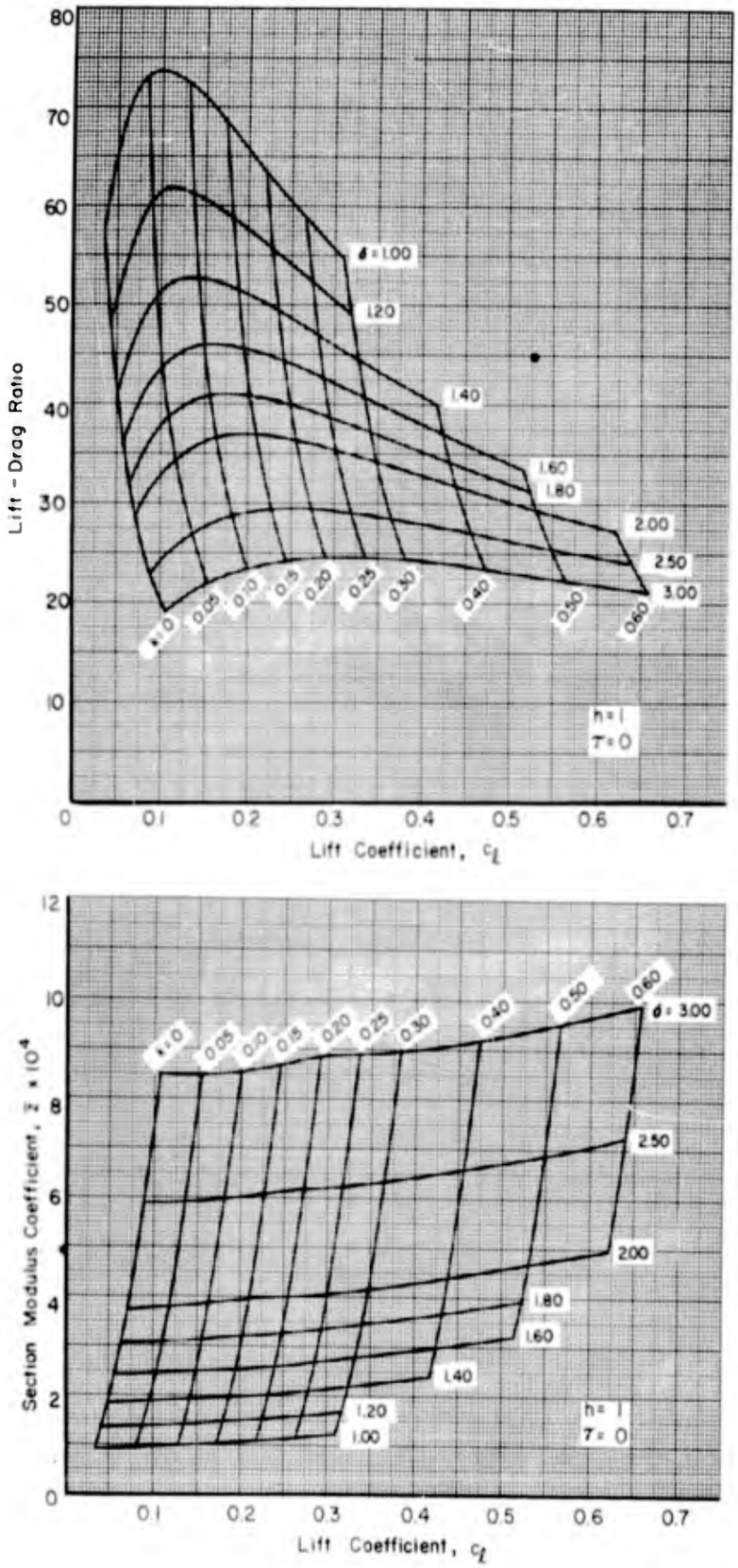

(a) $\tau = 0$

FIGURE 13. - LIFT-DRAG RATIO AND SECTION MODULUS VS. LIFT COEFFICIENT OF TWO-TERM FOILS DESIGNED FOR OPERATION AT A DEPTH OF 1 CHORD. CONTOURS OF CONSTANT CAMBER INDEX AND ANGLE OF ATTACK.

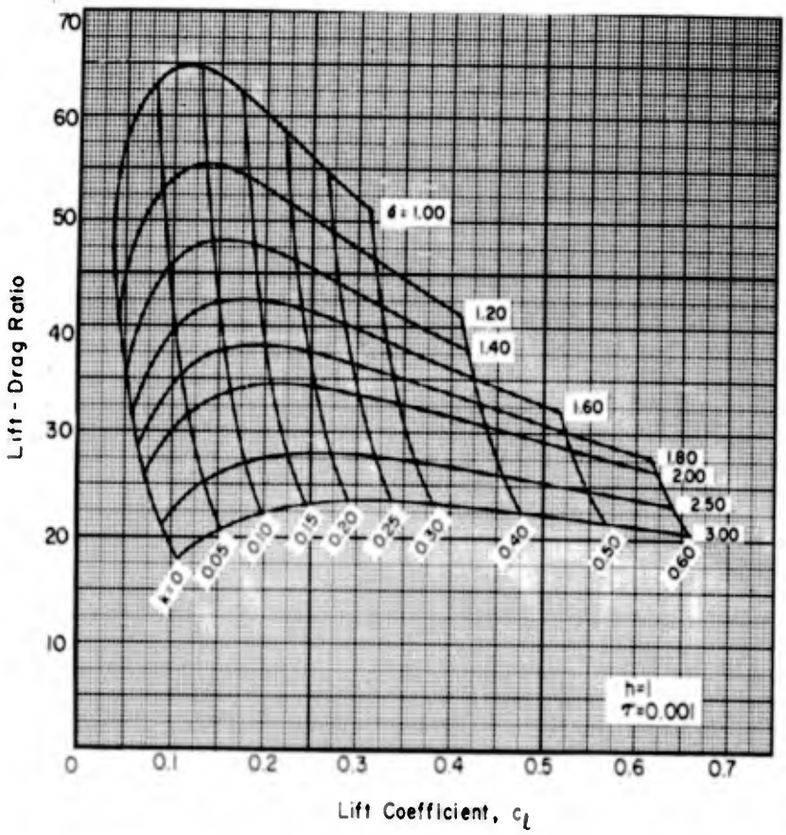

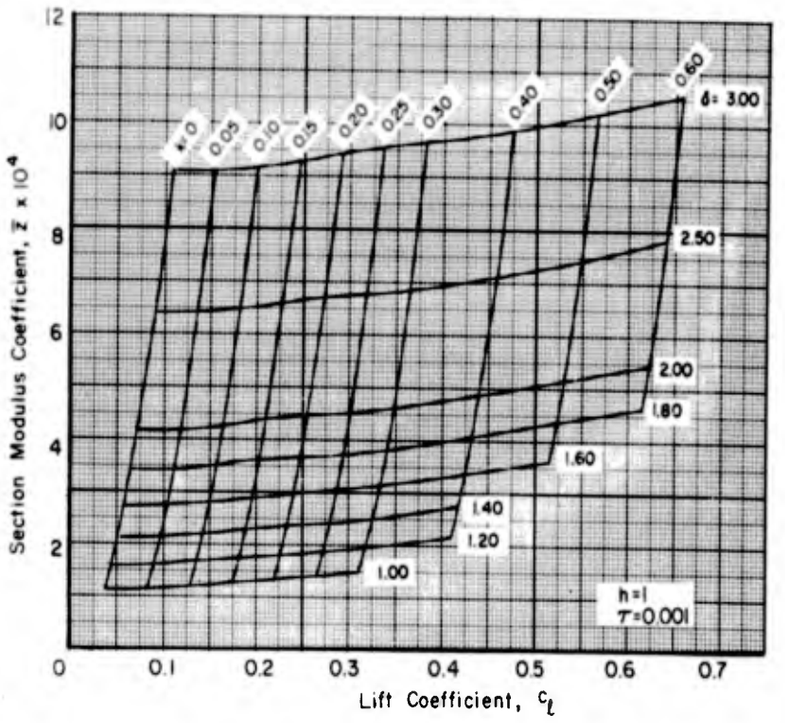

(b) τ = 0.001

FIGURE 13. - (continued)

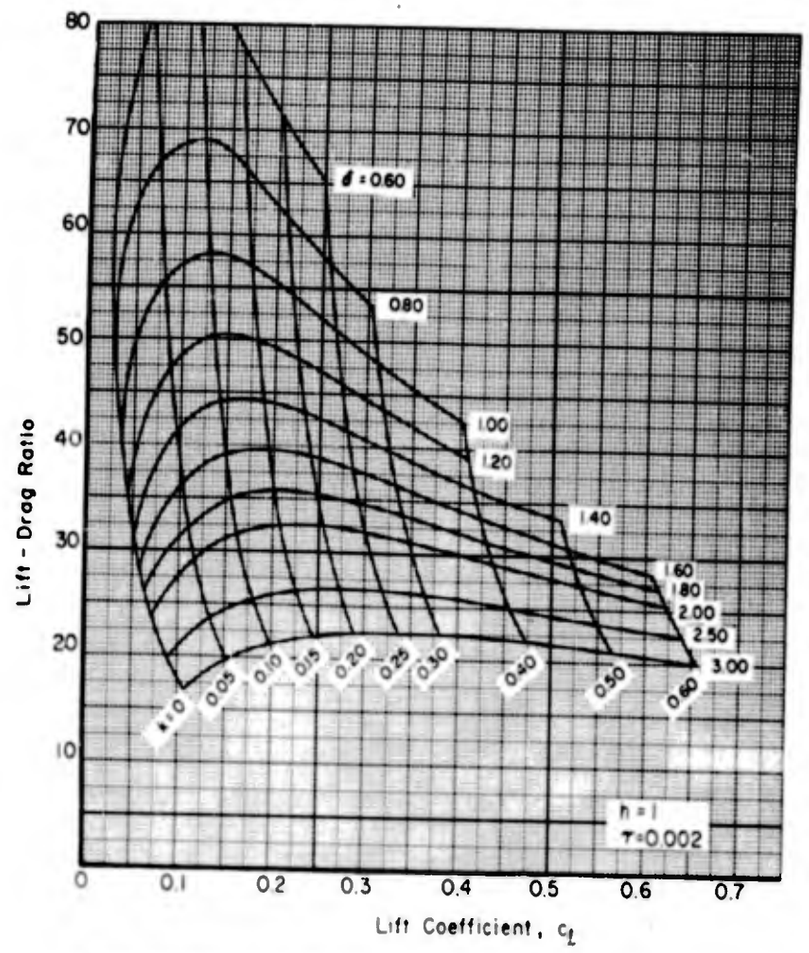

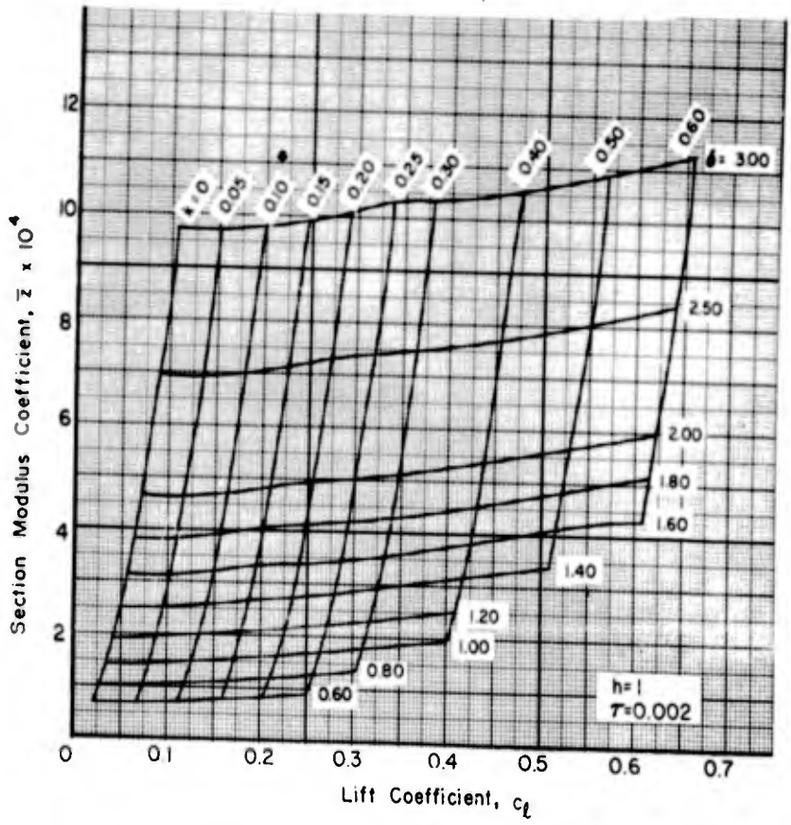

(c) $\tau = 0.002$

FIGURE 13. - (continued)

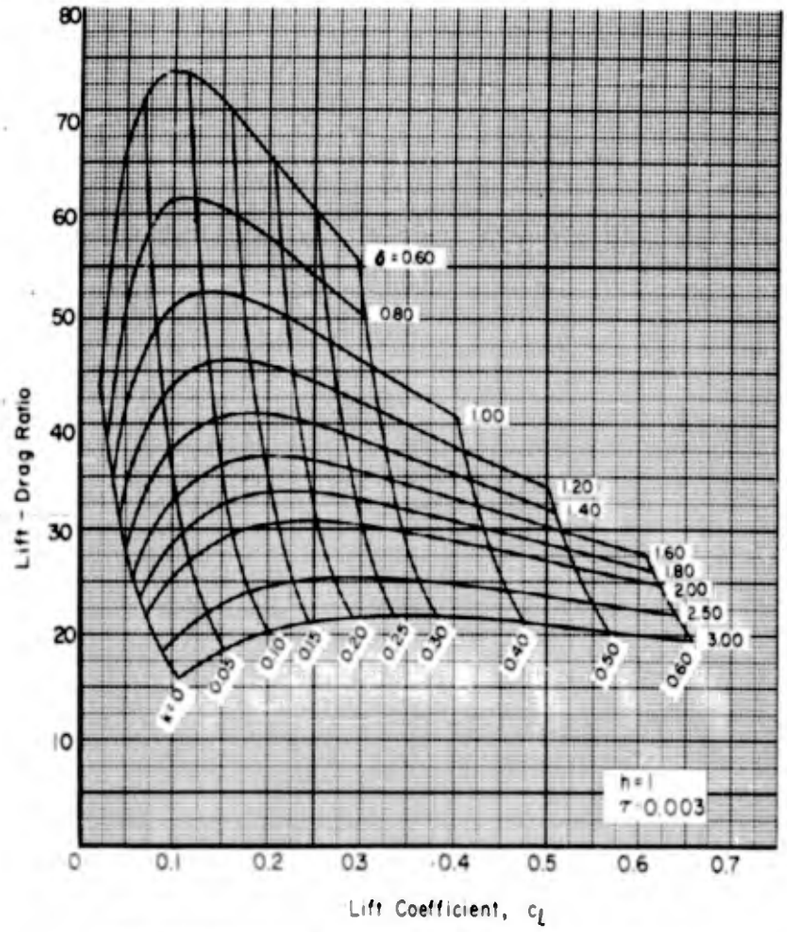

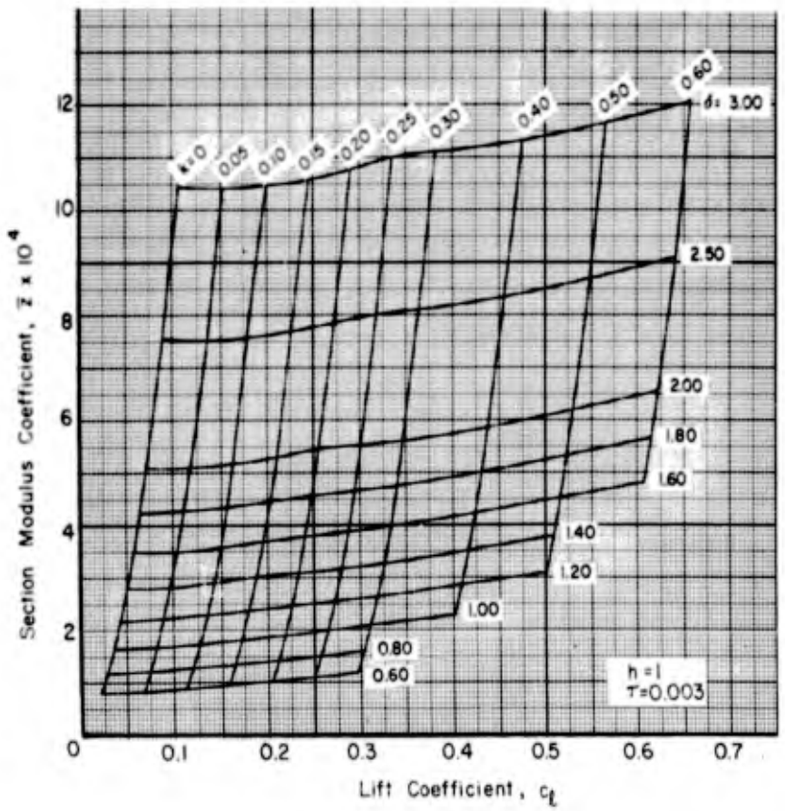

(d) τ = 0.003

FIGURE 13. - (continued)

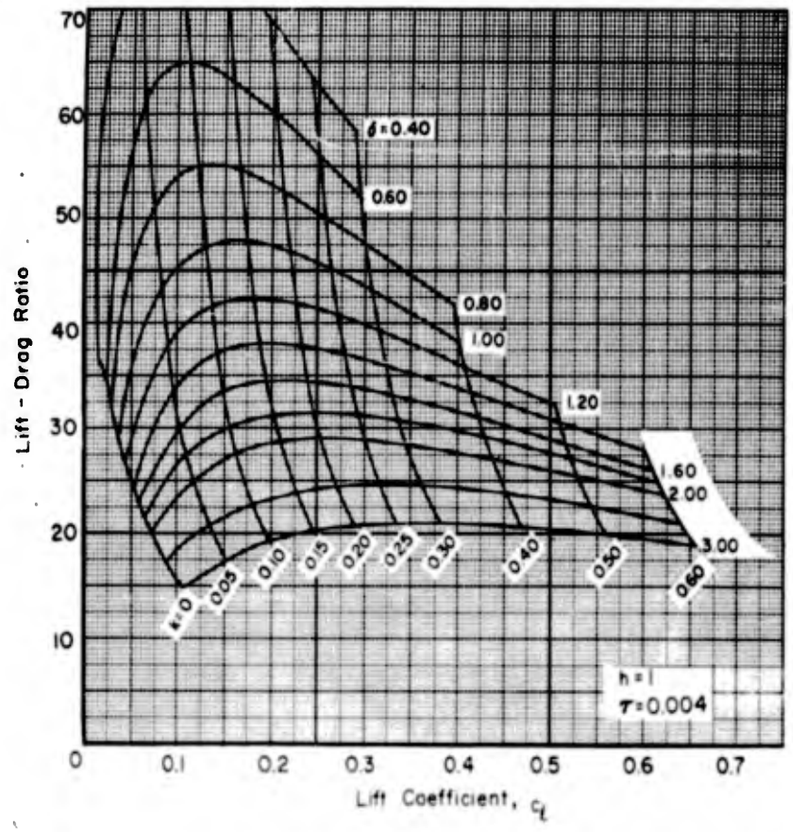

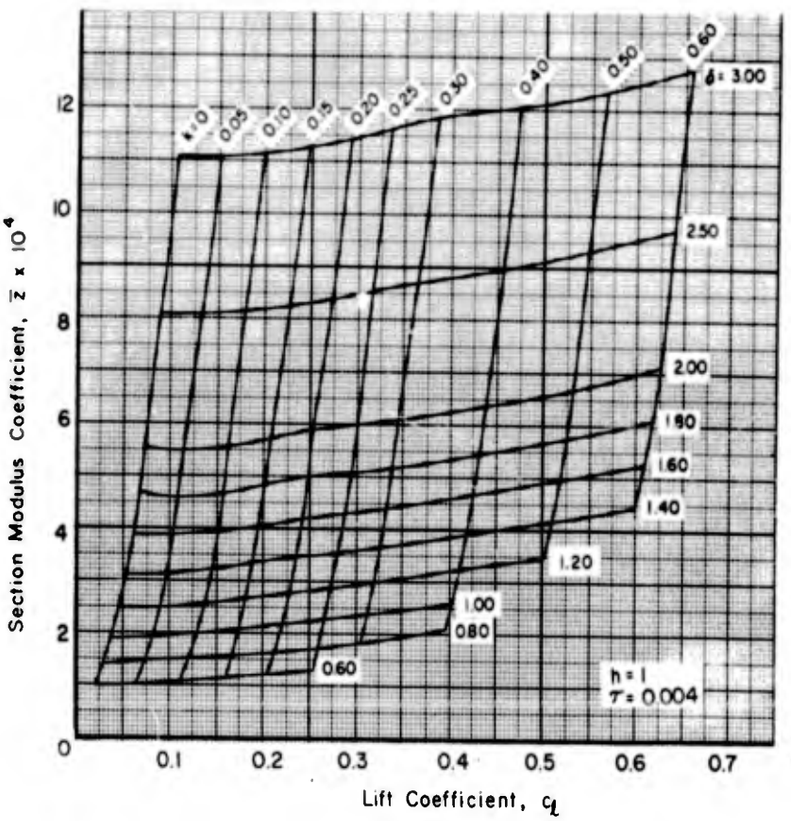

(e) τ = 0.004

FIGURE 13. - (continued)

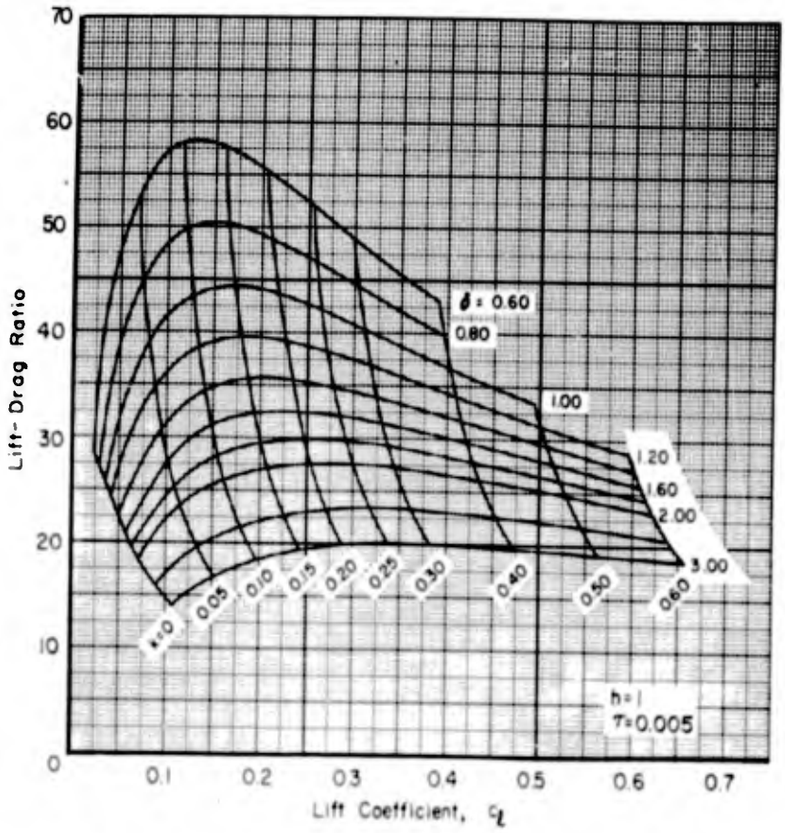

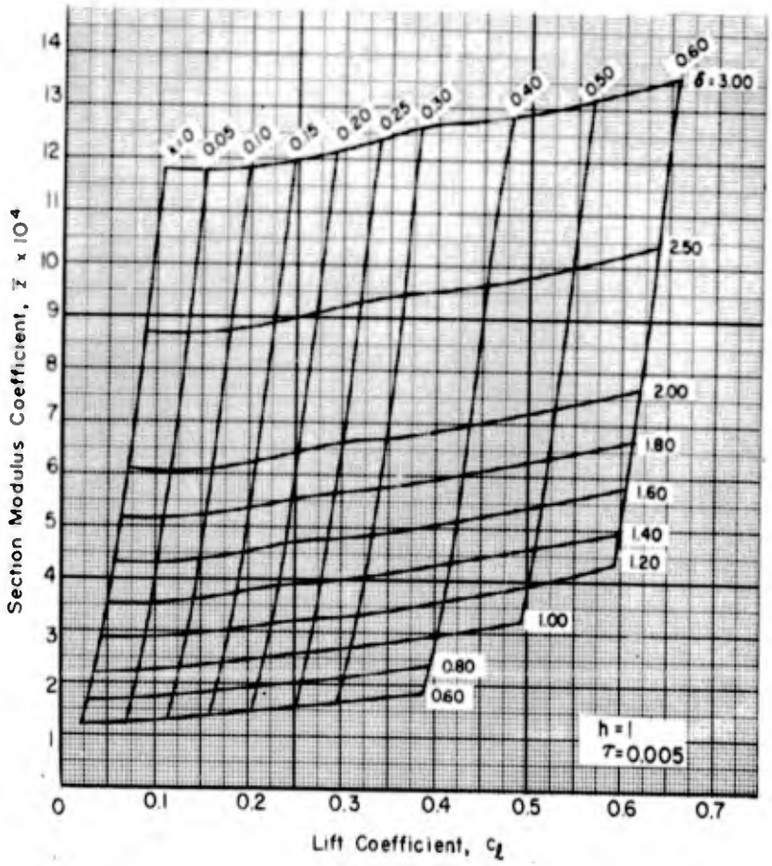

(f) τ = 0.005

FIGURE 13. - (continued)

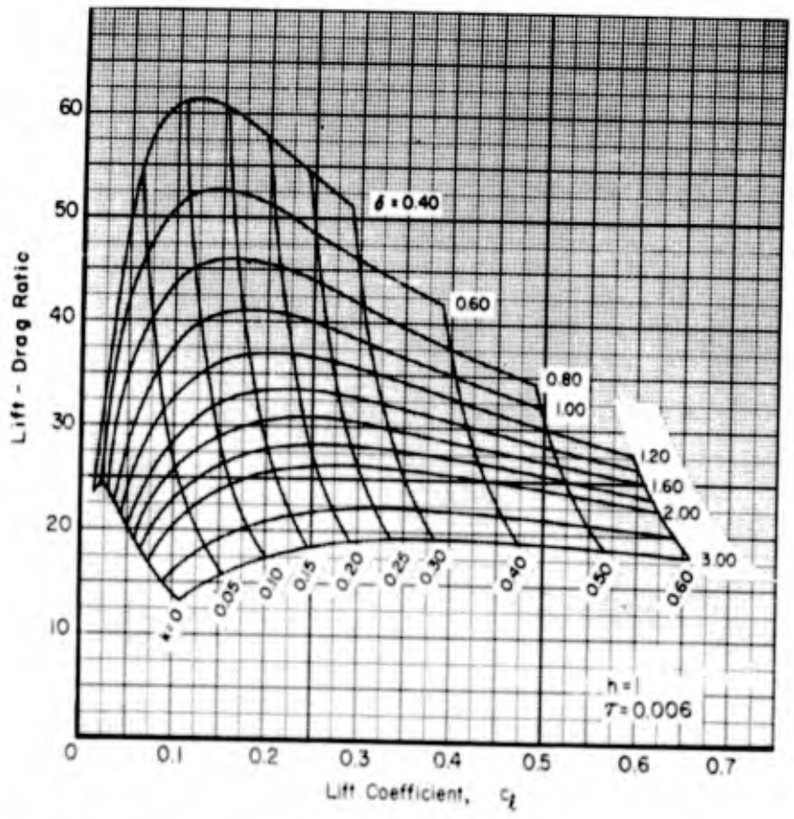

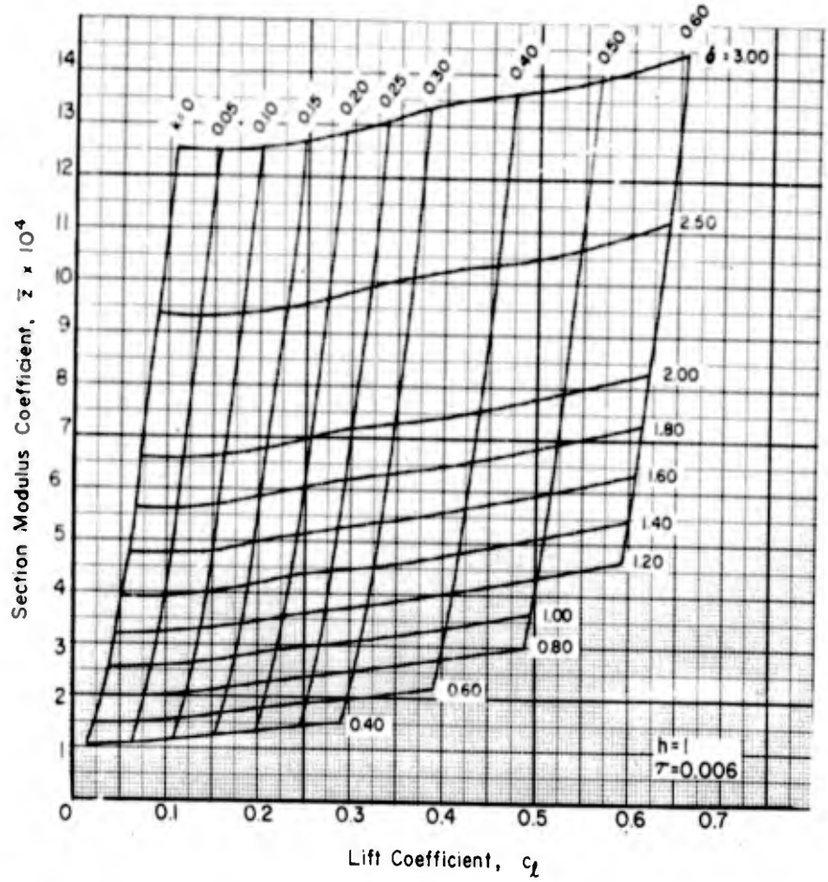

(g) τ = 0.006

FIGURE 13. - (continued)

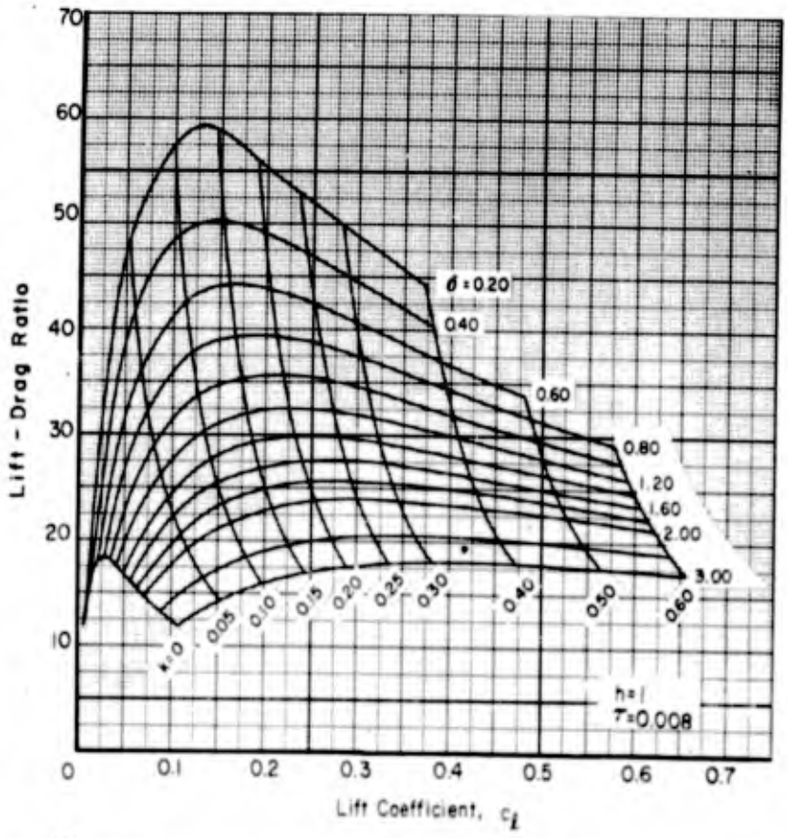

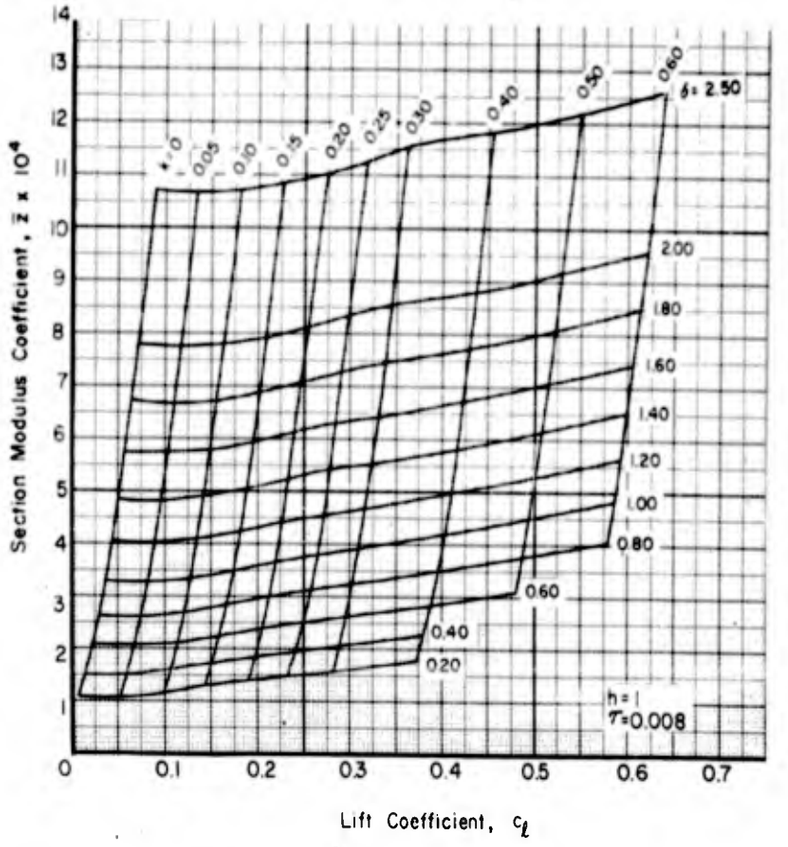

(h) τ = 0.008

FIGURE 13. - (continued)

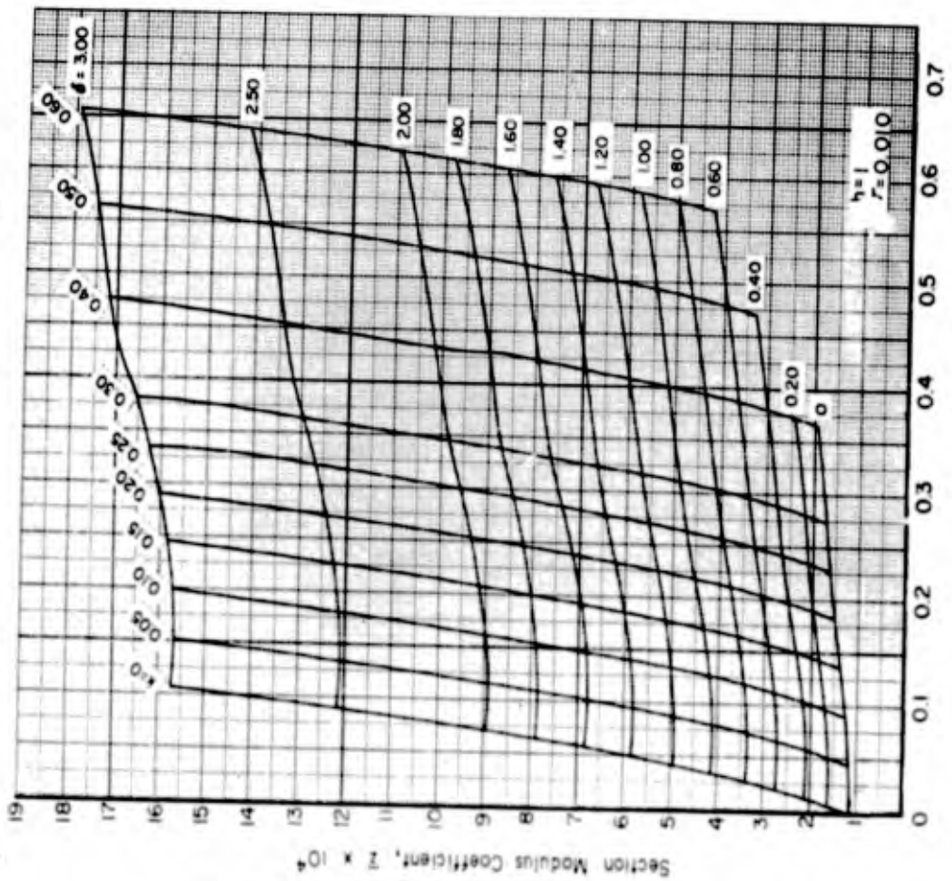

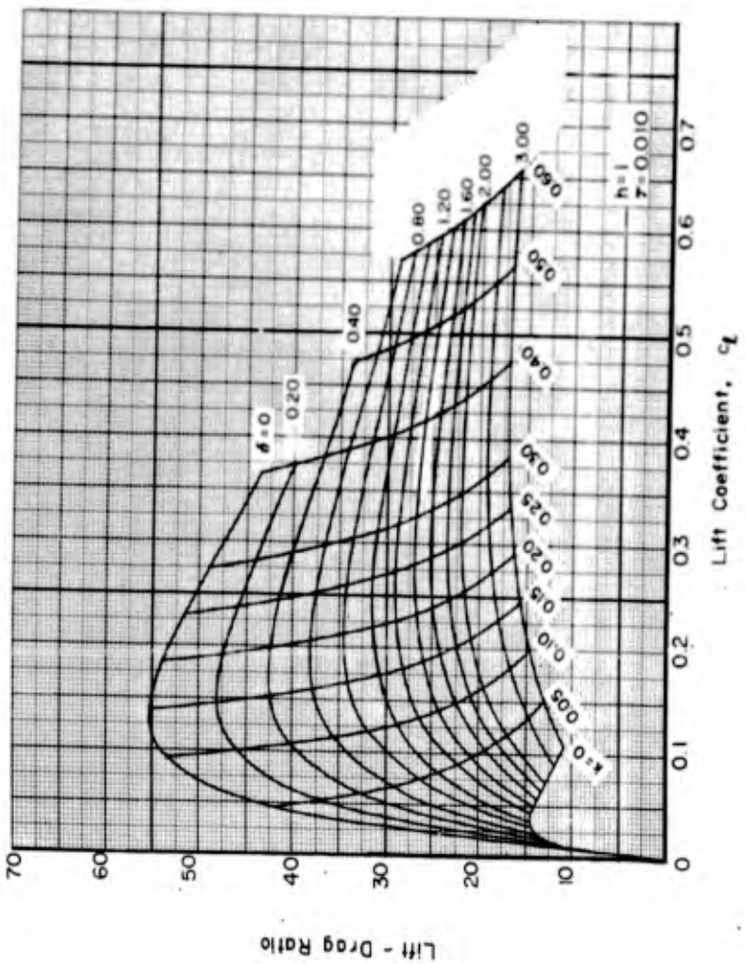

(1) τ = 0.010

FIGURE 13. - (concluded)

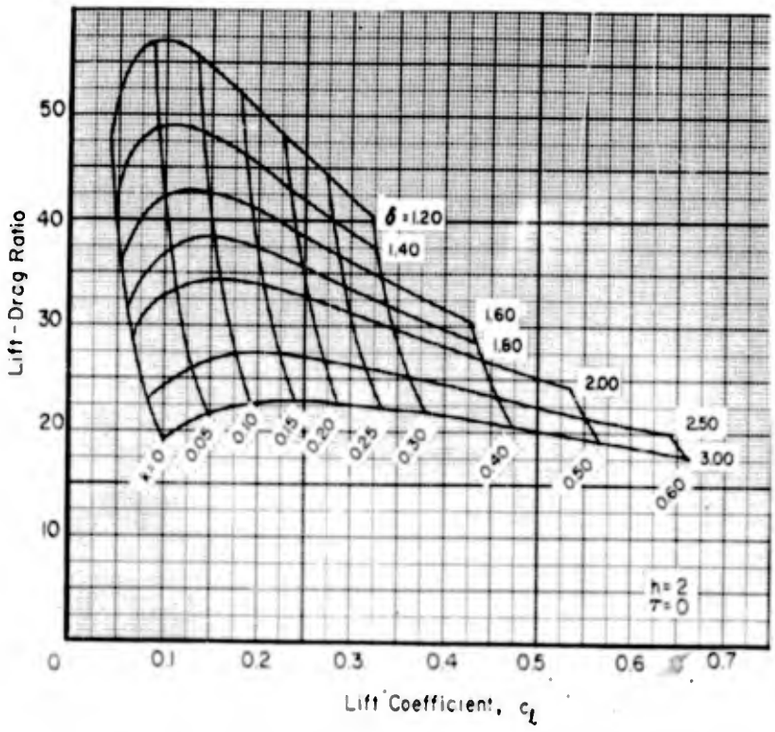

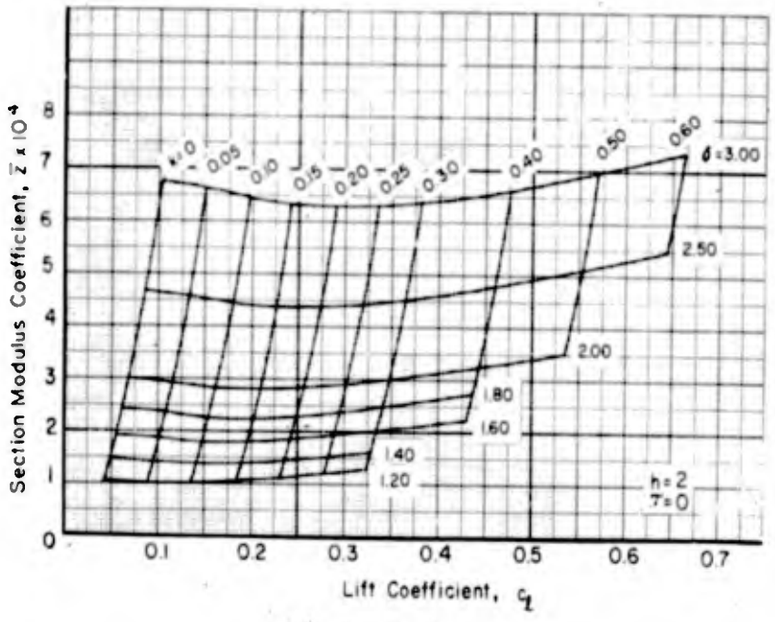

(a) $\tau = 0$

FIGURE 14. - LIFT-DRAG RATIO AND SECTION MODULUS VS. LIFT COEFFICIENT OF TWO-TERM FOILS DESIGNED FOR OPERATION AT A DEPTH OF 2 CHORDS. CONTOURS OF CONSTANT CAMBER INDEX AND ANGLE OF ATTACK.

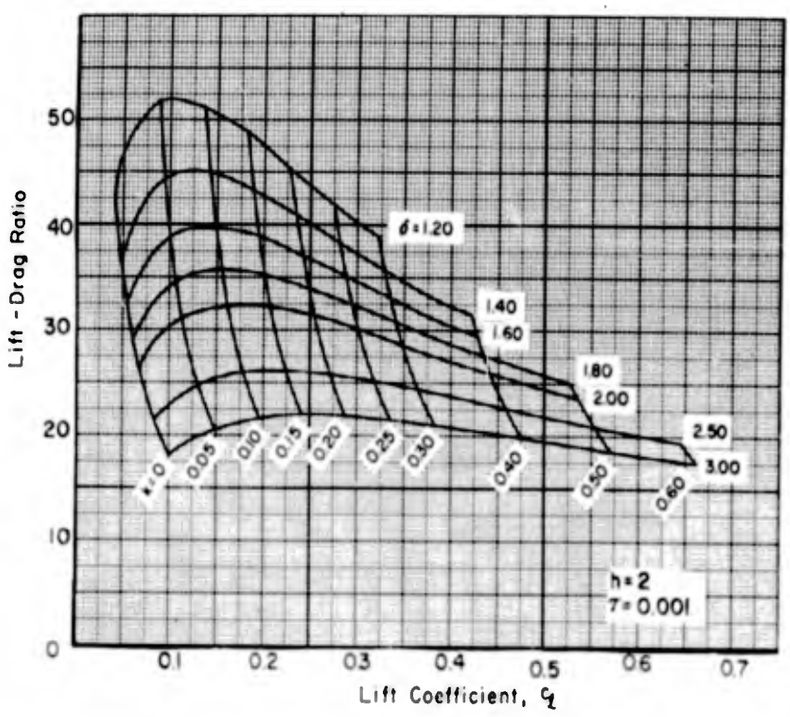

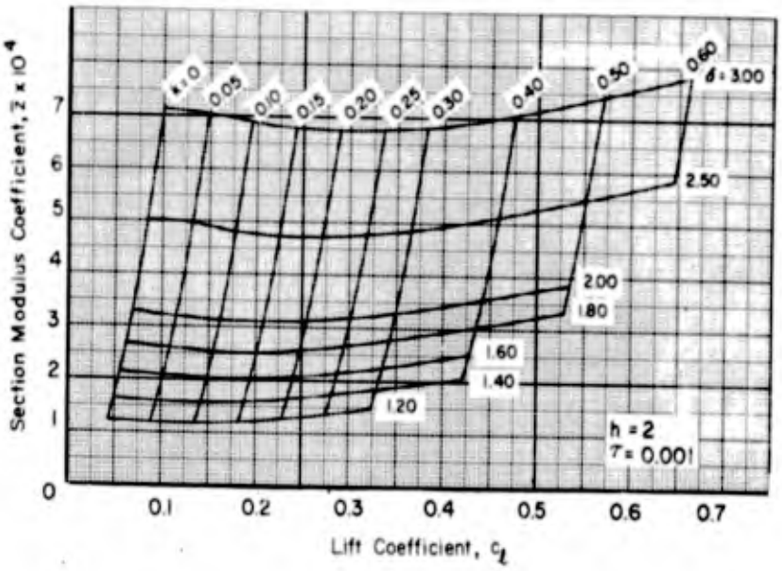

(b) τ = 0.001

FIGURE 14. - (continued)

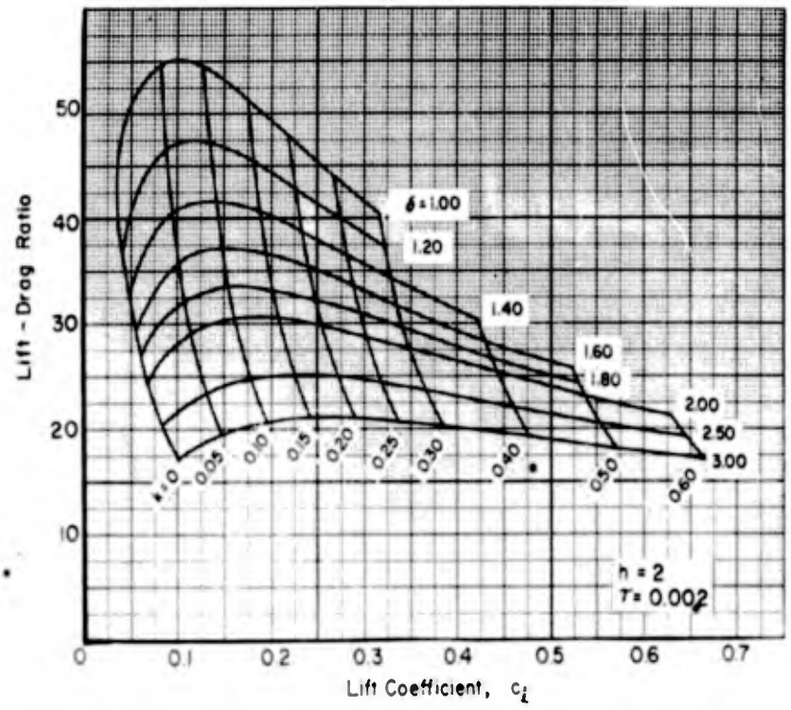

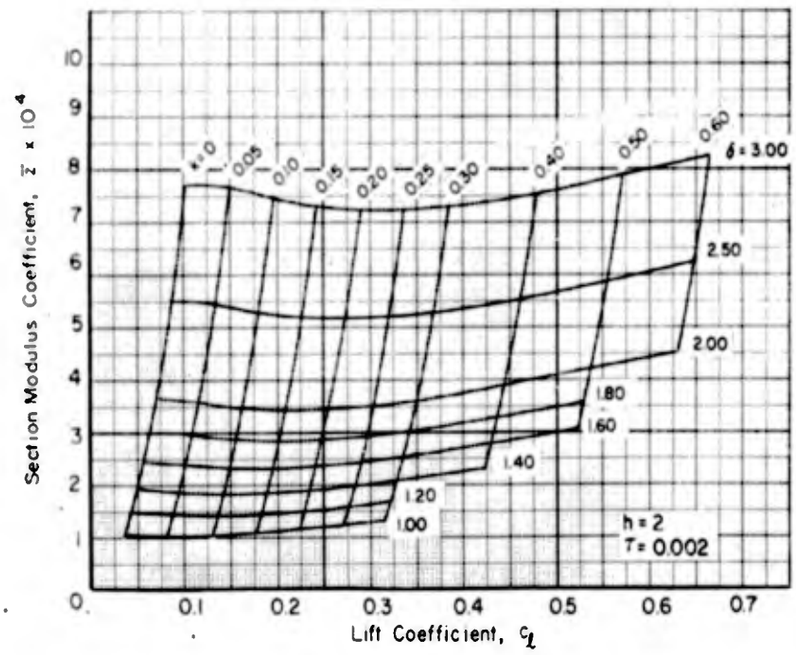

(c) τ = 0.002

FIGURE 14. - (continued)

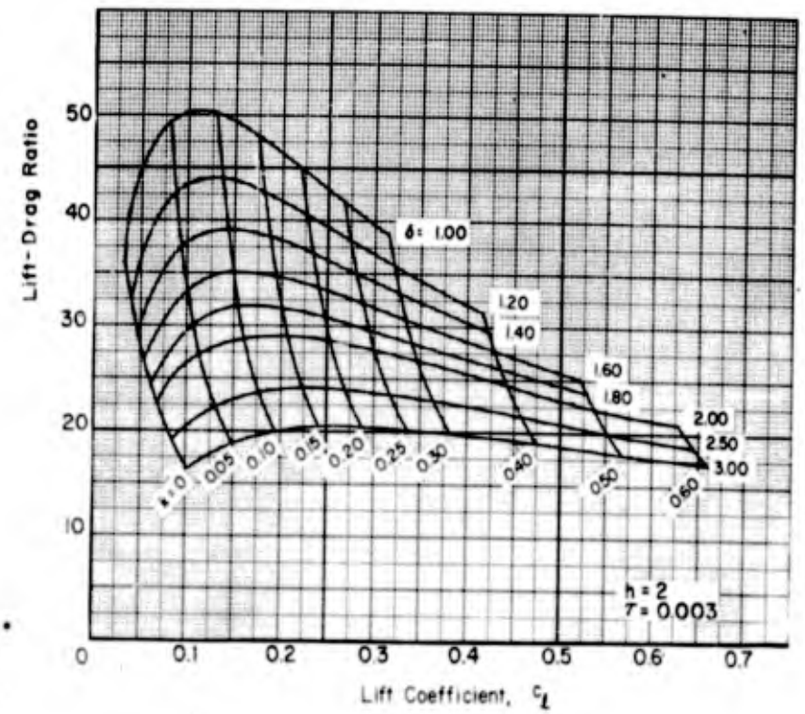

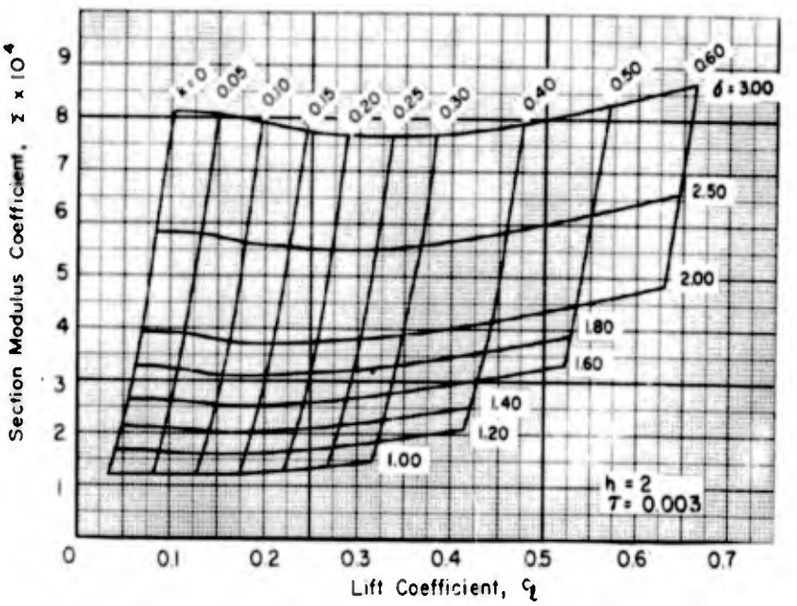

(d) τ = 0.003

FIGURE 14. - (continued)

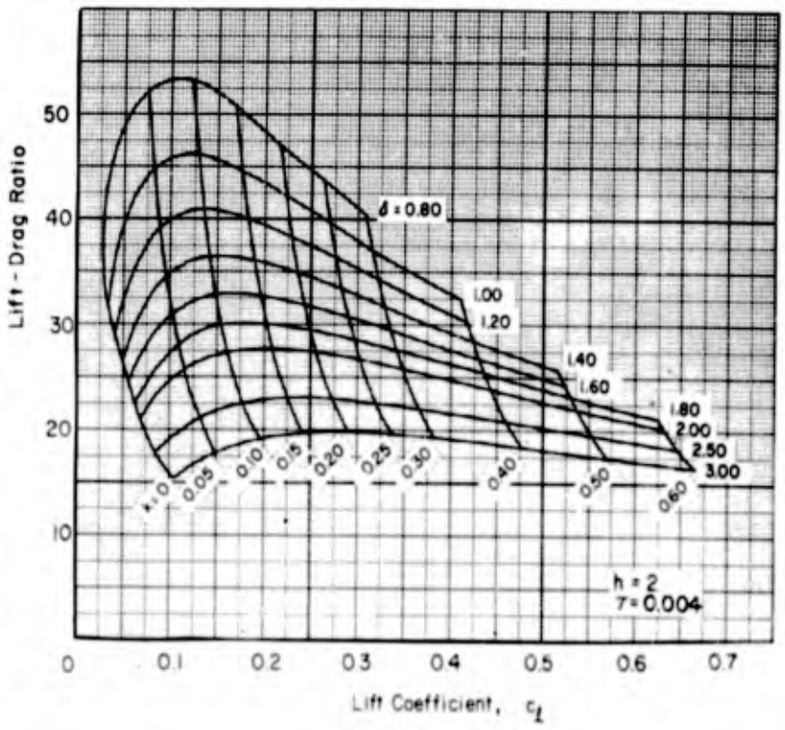

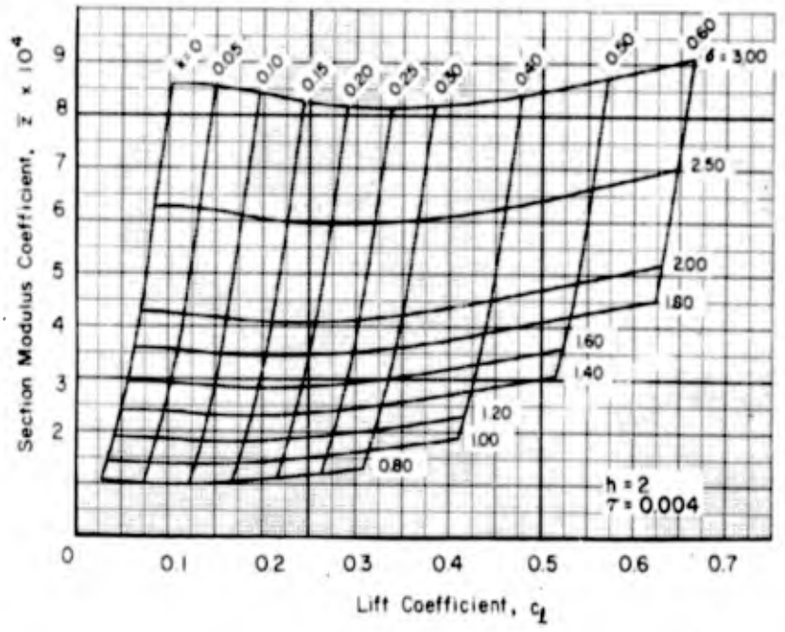

(e) τ = 0.004

FIGURE 14. - (continued)

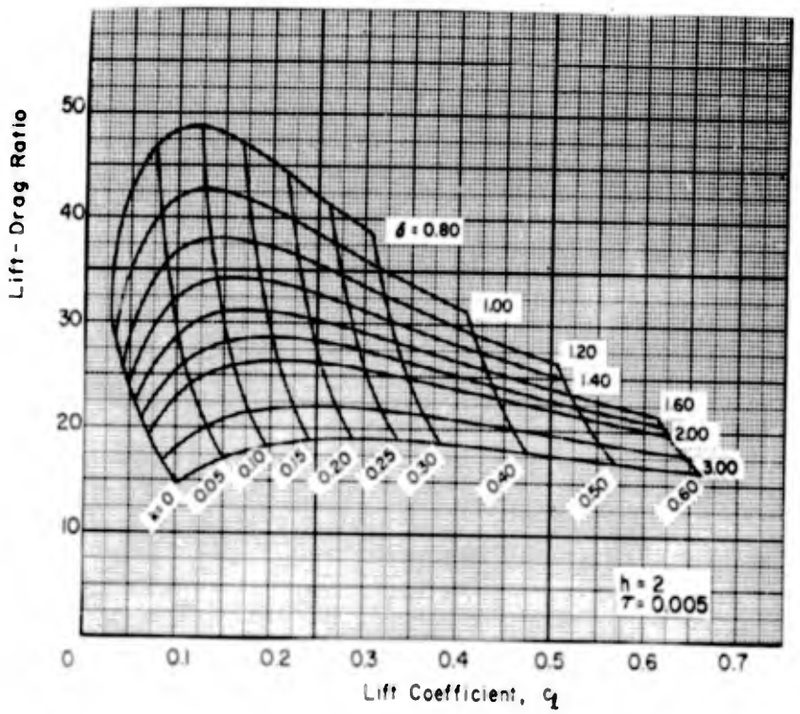

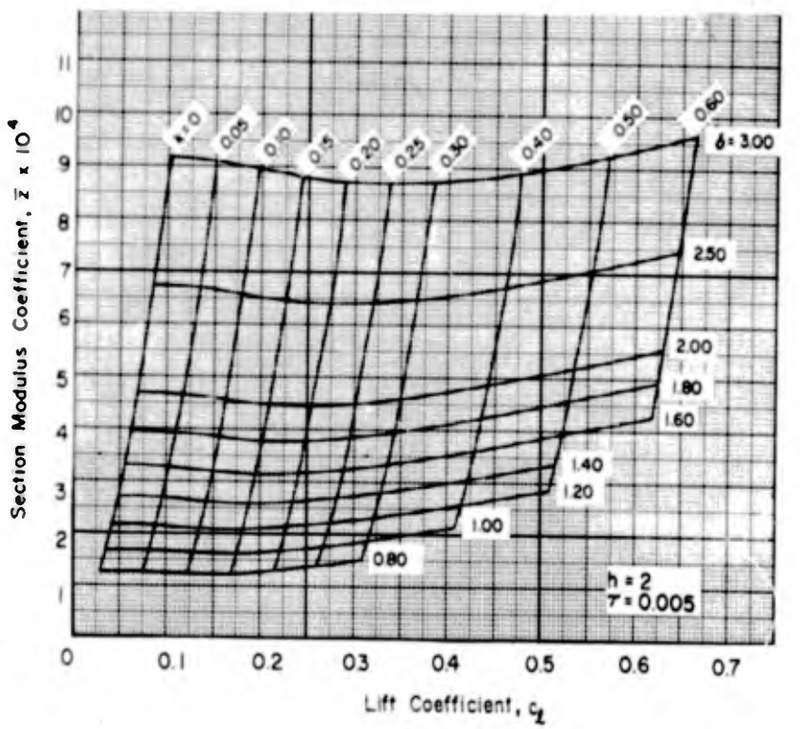

(f) τ = 0.005

FIGURE 14. - (continued)

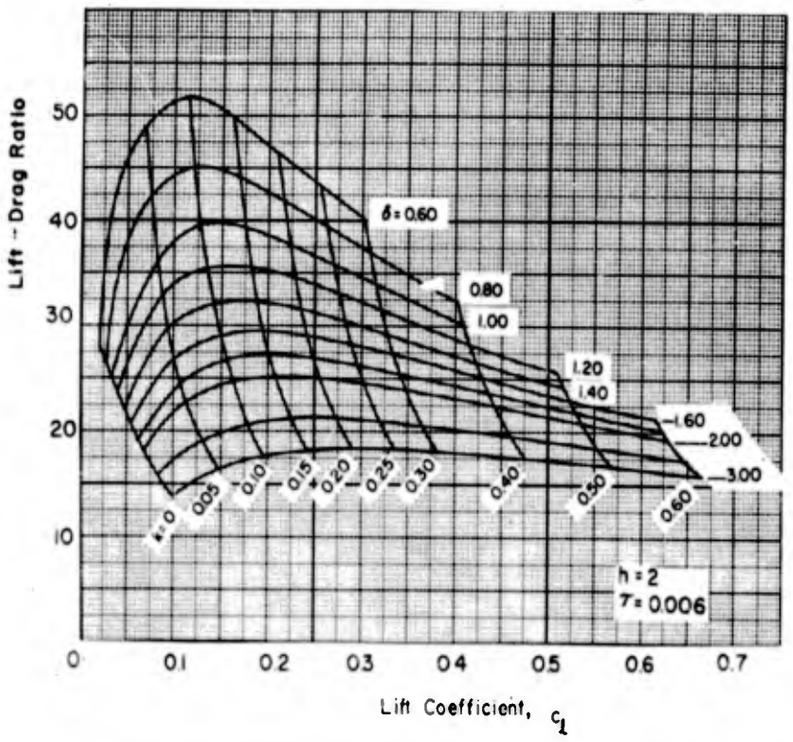

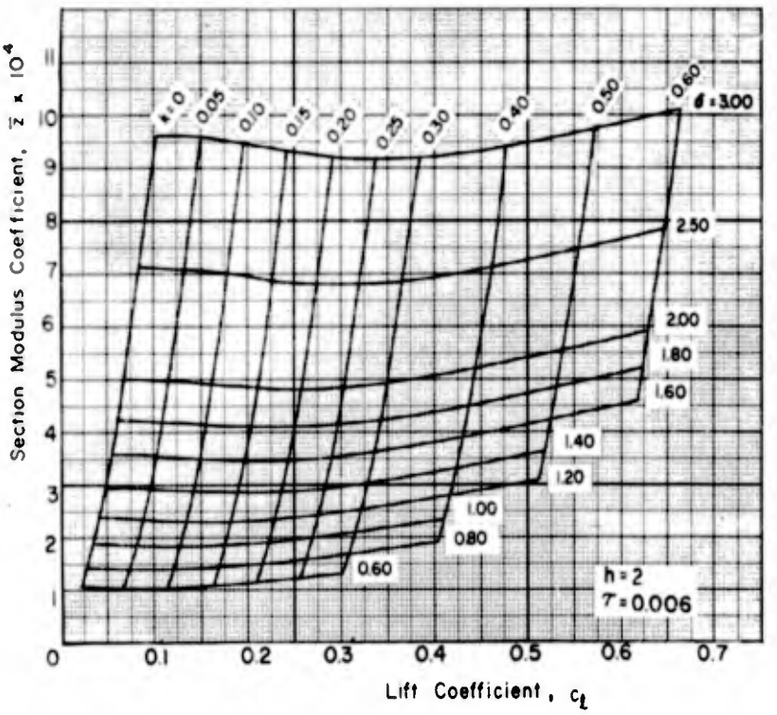

(g) τ = 0.006

FIGURE 14. - (continued)

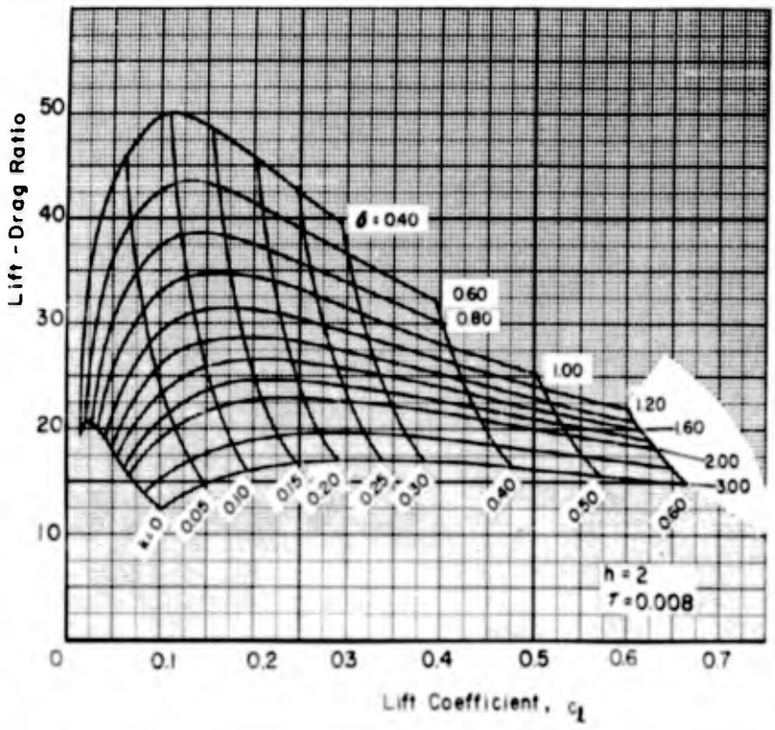

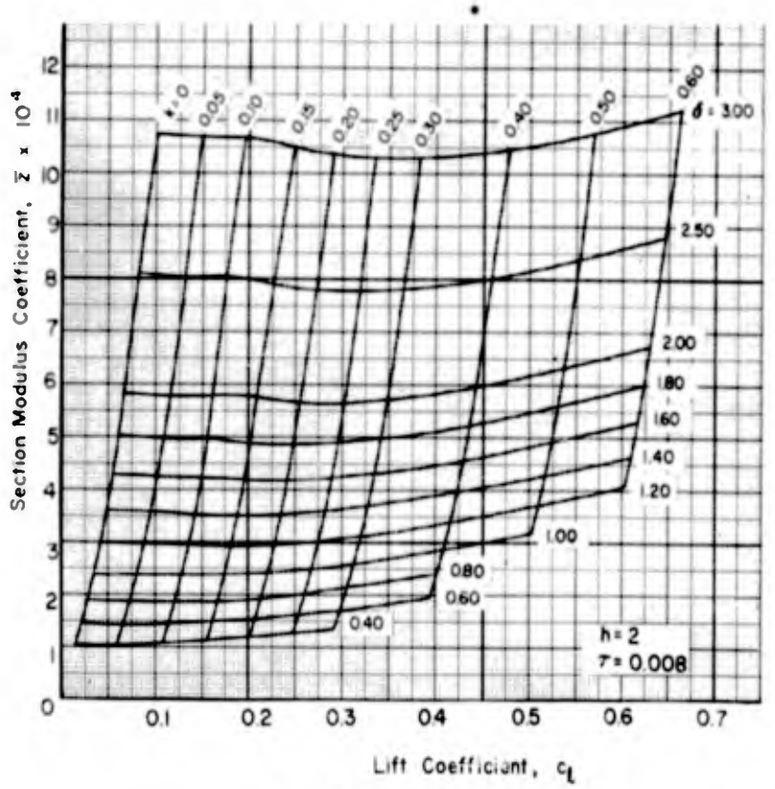

(h) τ = 0.008

FIGURE 14. - (continued)

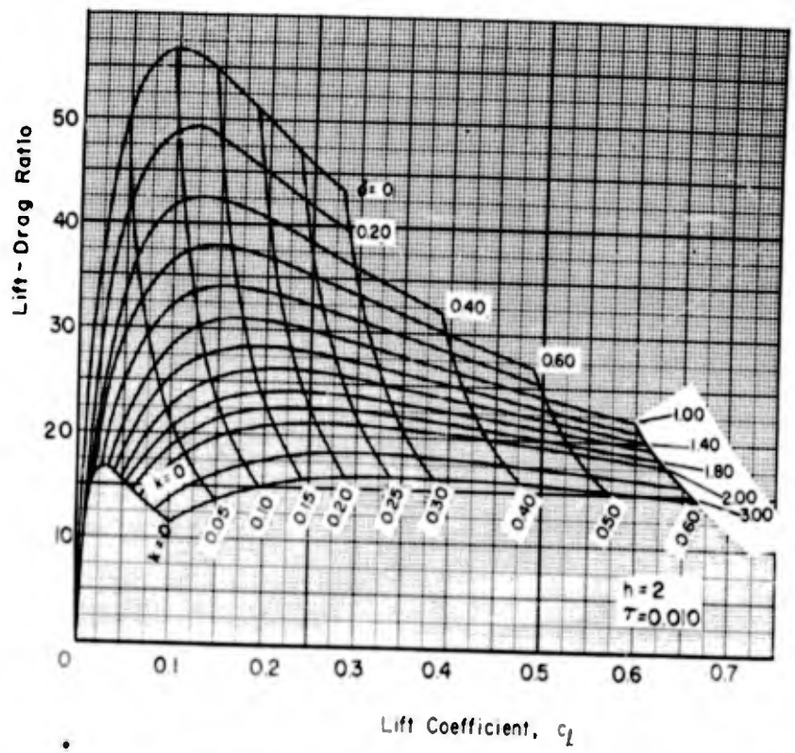

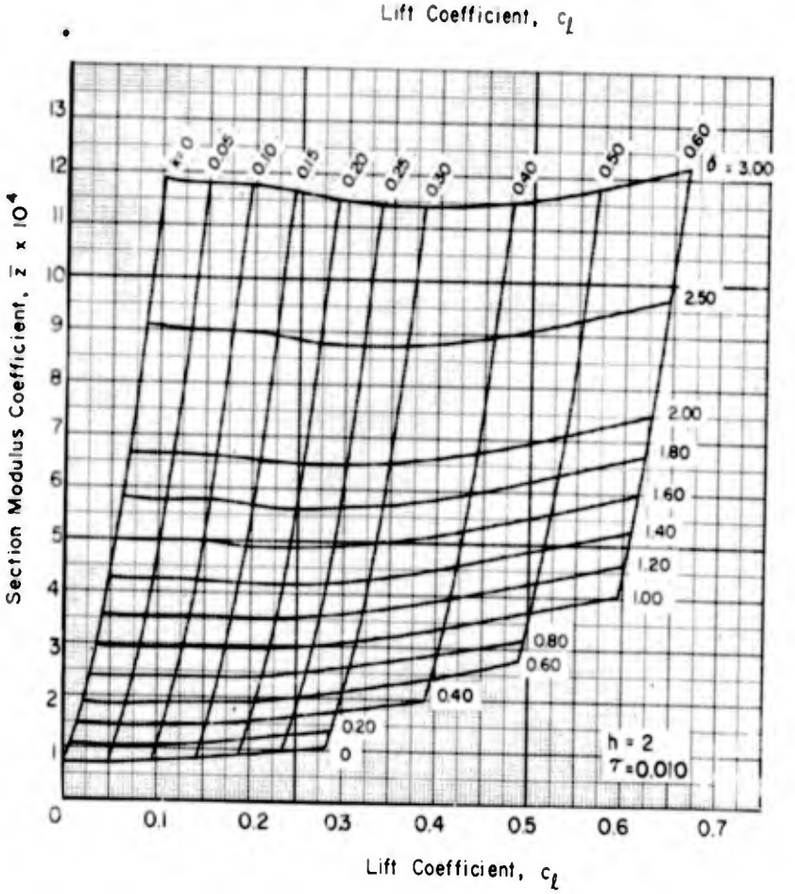

(1) τ = 0.010

FIGURE 14. - (concluded)

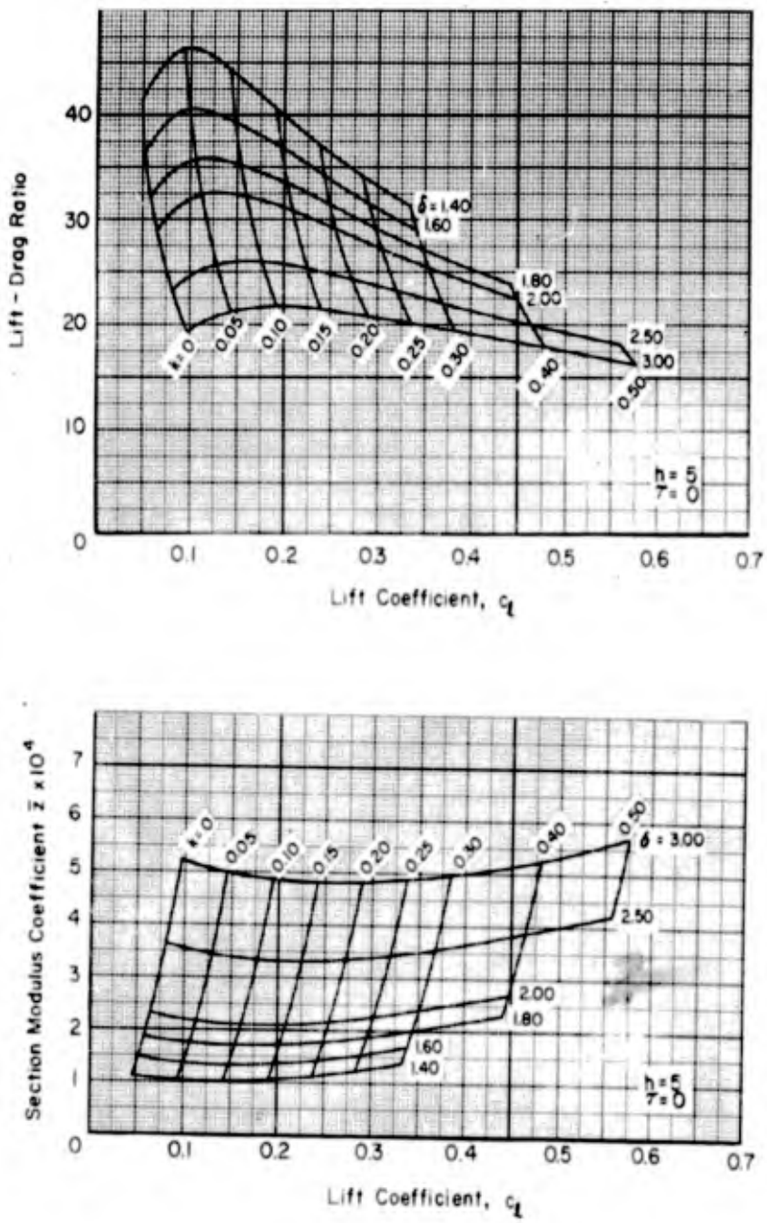

(a) $\tau = 0$

FIGURE 15. - LIFT-DRAG RATIO AND SECTION MODULUS VS. LIFT COEFFICIENT OF TWO-TERM FOILS DESIGNED FOR OPERATION AT A DEPTH OF 5 CHORDS. CONTOURS OF CONSTANT CAMBER INDEX AND ANGLE OF ATTACK.

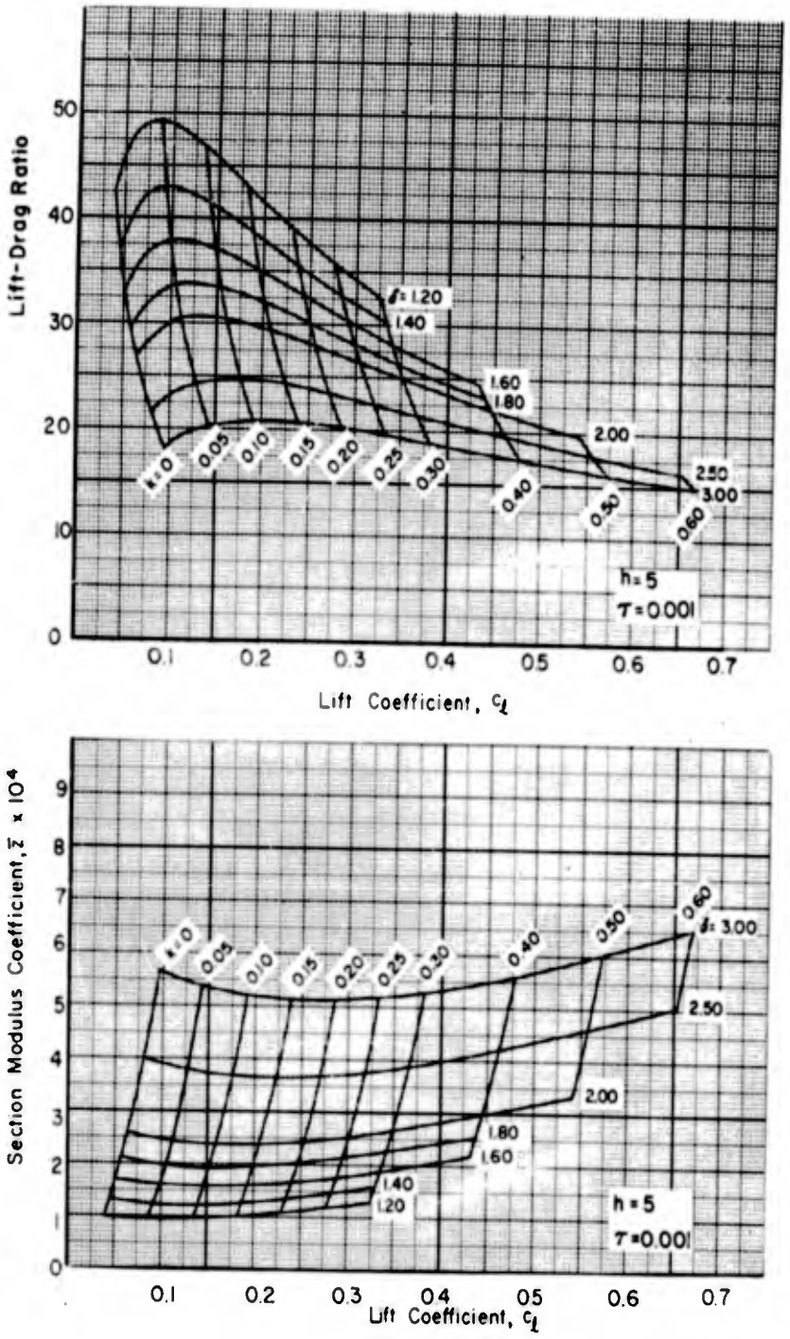

(b) τ = 0.001

FIGURE 15. - (continued)

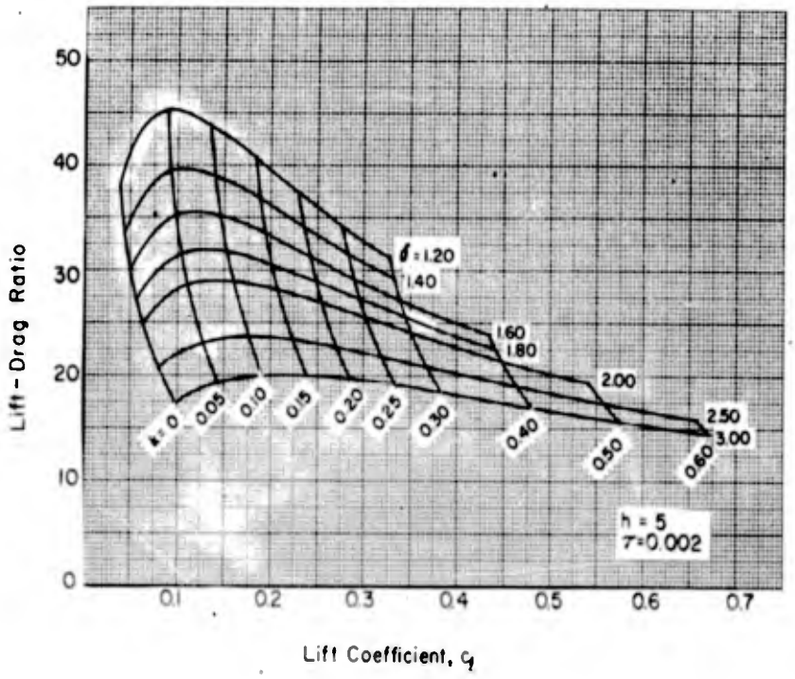

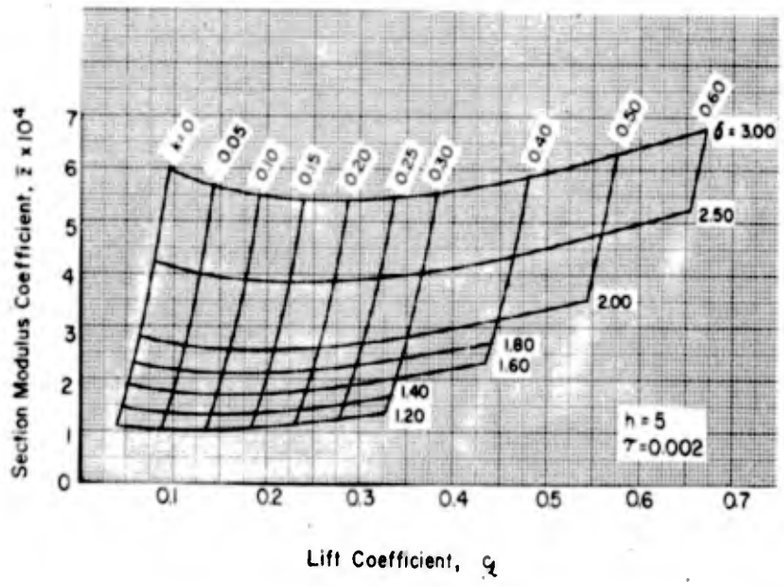

(c) τ = 0.002

FIGURE 15. - (continued)

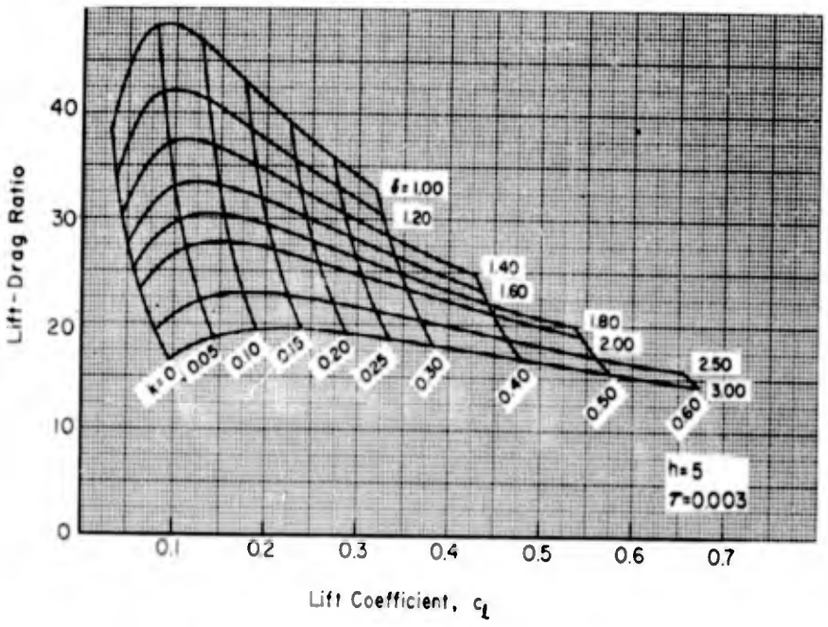

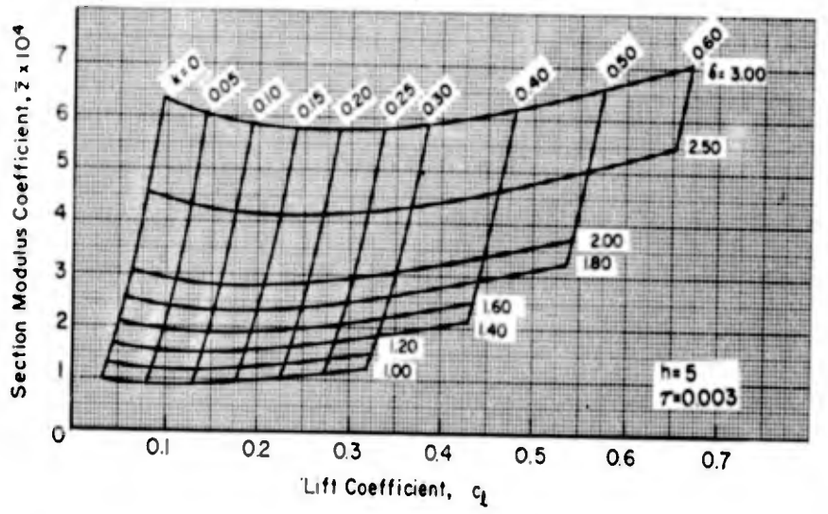

(d) τ = 0.003

FIGURE 15. - (continued)

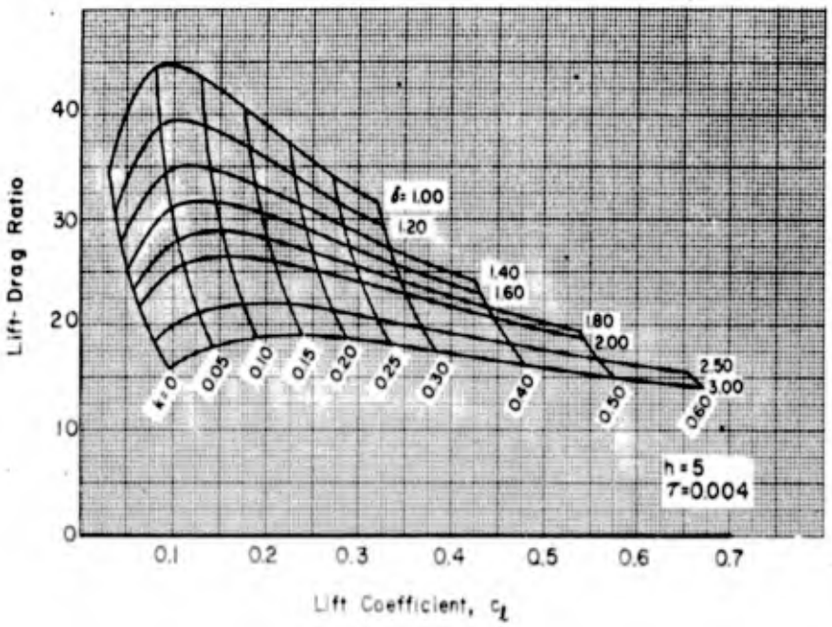

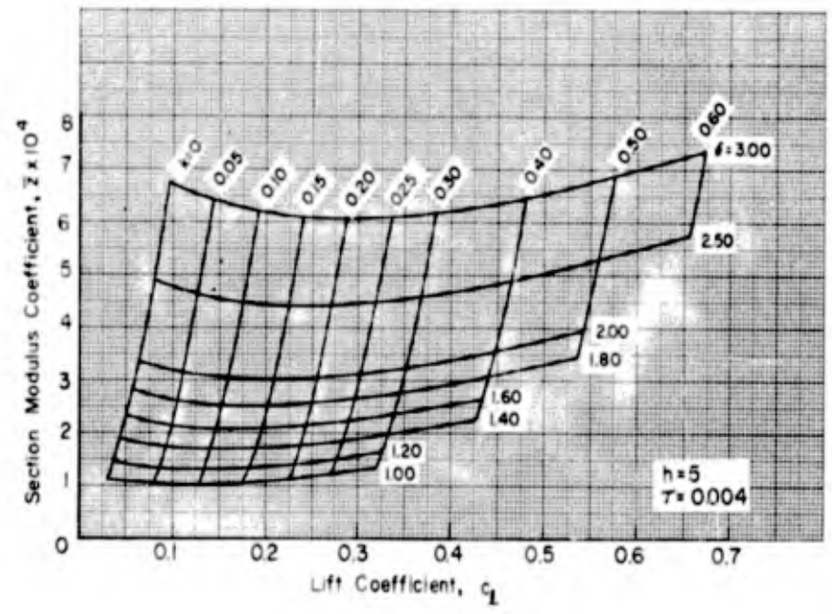

(e) τ = 0.004

FIGURE 15. - (continued)

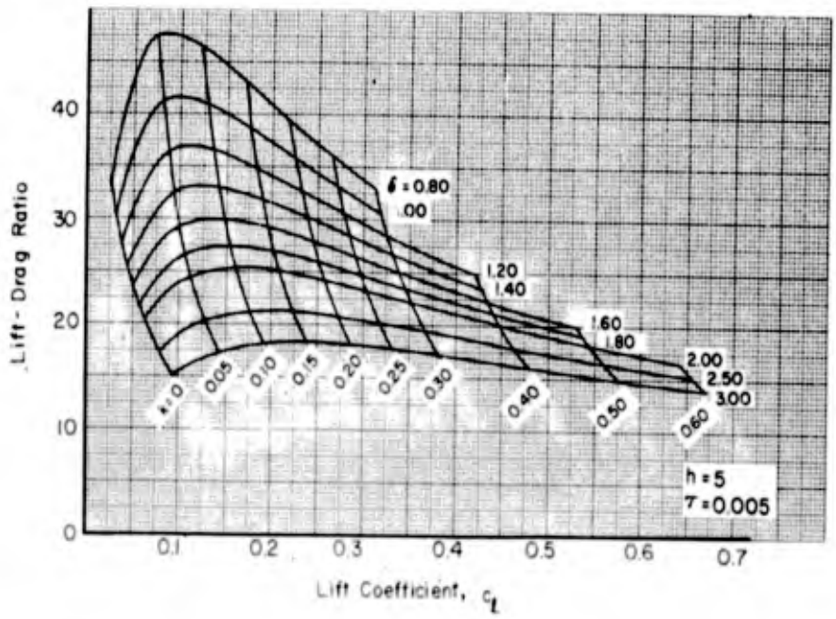

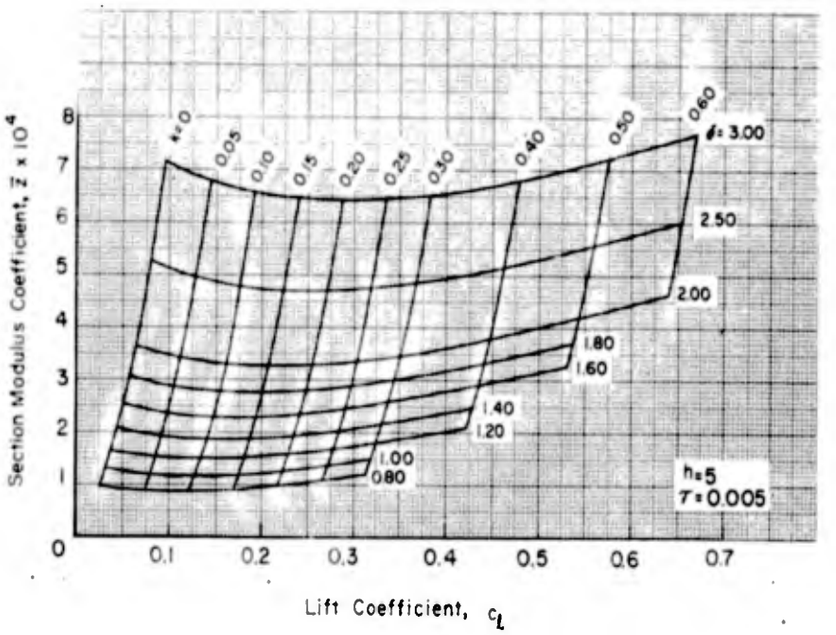

(f) τ = 0.005

FIGURE 15. - (continued)

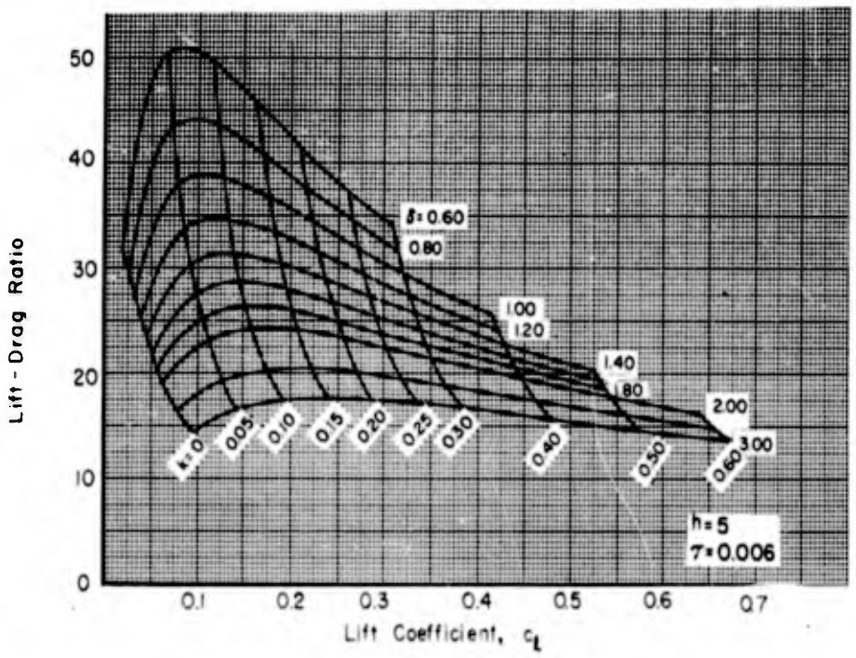

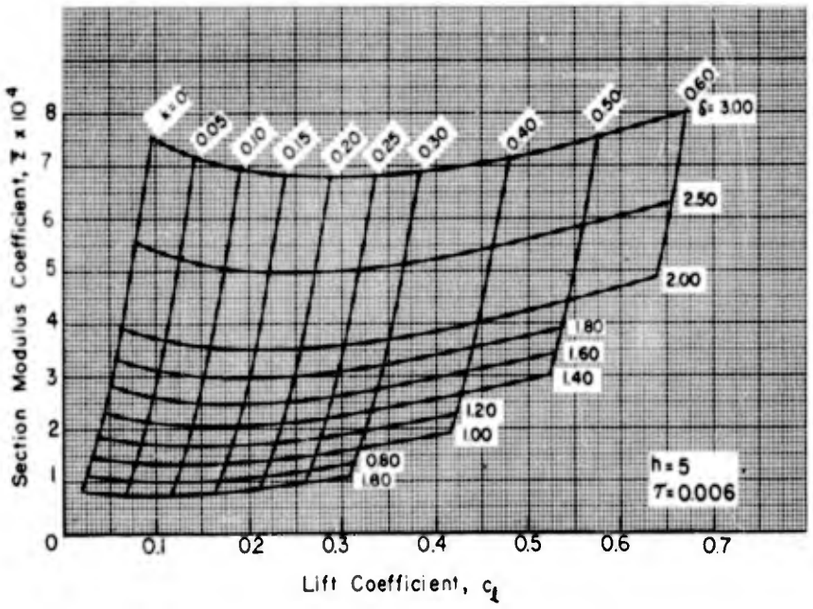

(g) τ = 0.006

FIGURE 15. - (continued)

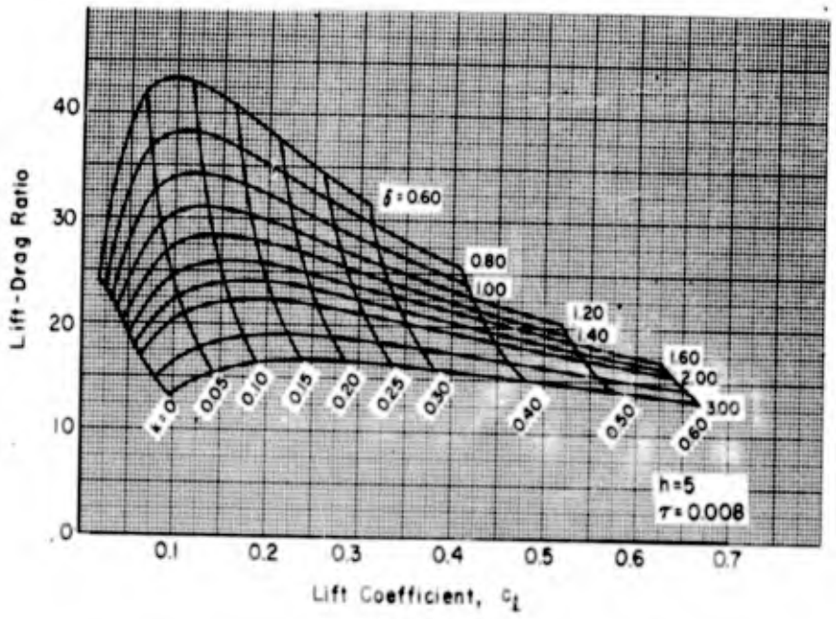

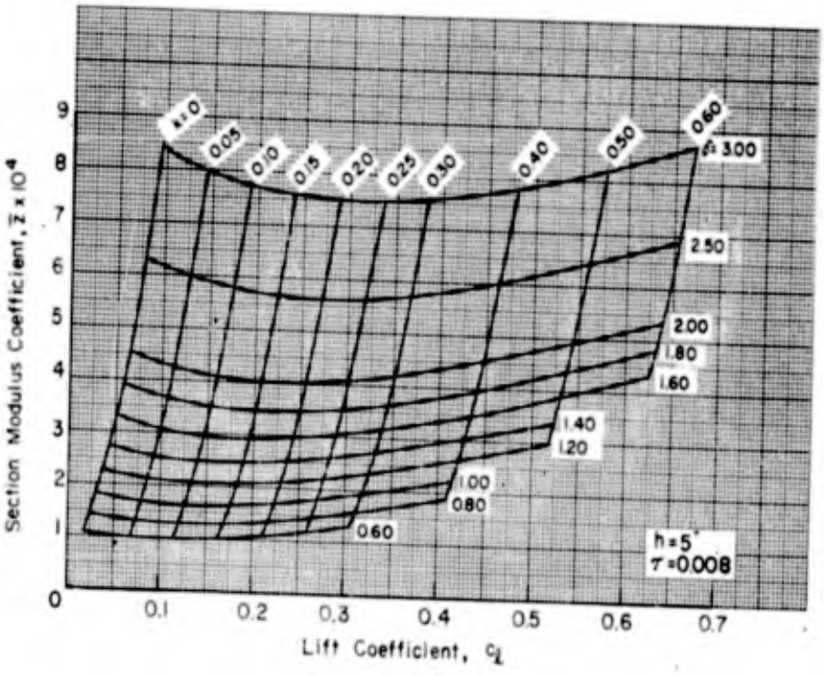

(h) τ = 0.008

FIGURE 15. - (continued)

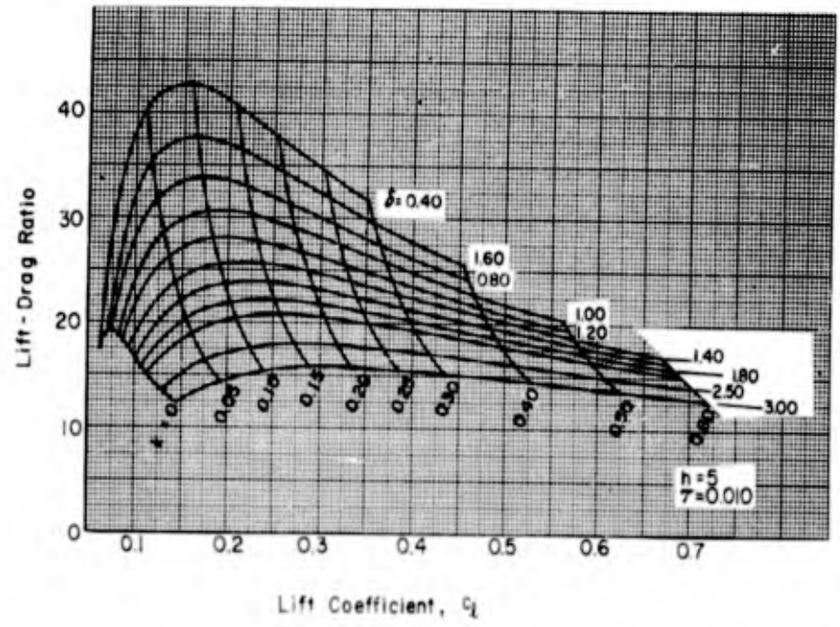

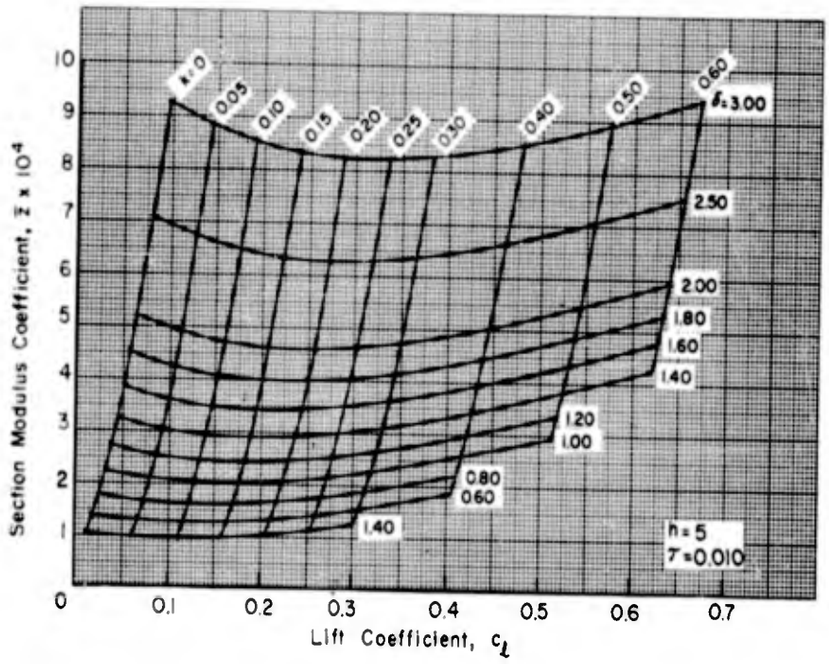

(1) τ = 0.010

FIGURE 15. - (concluded)

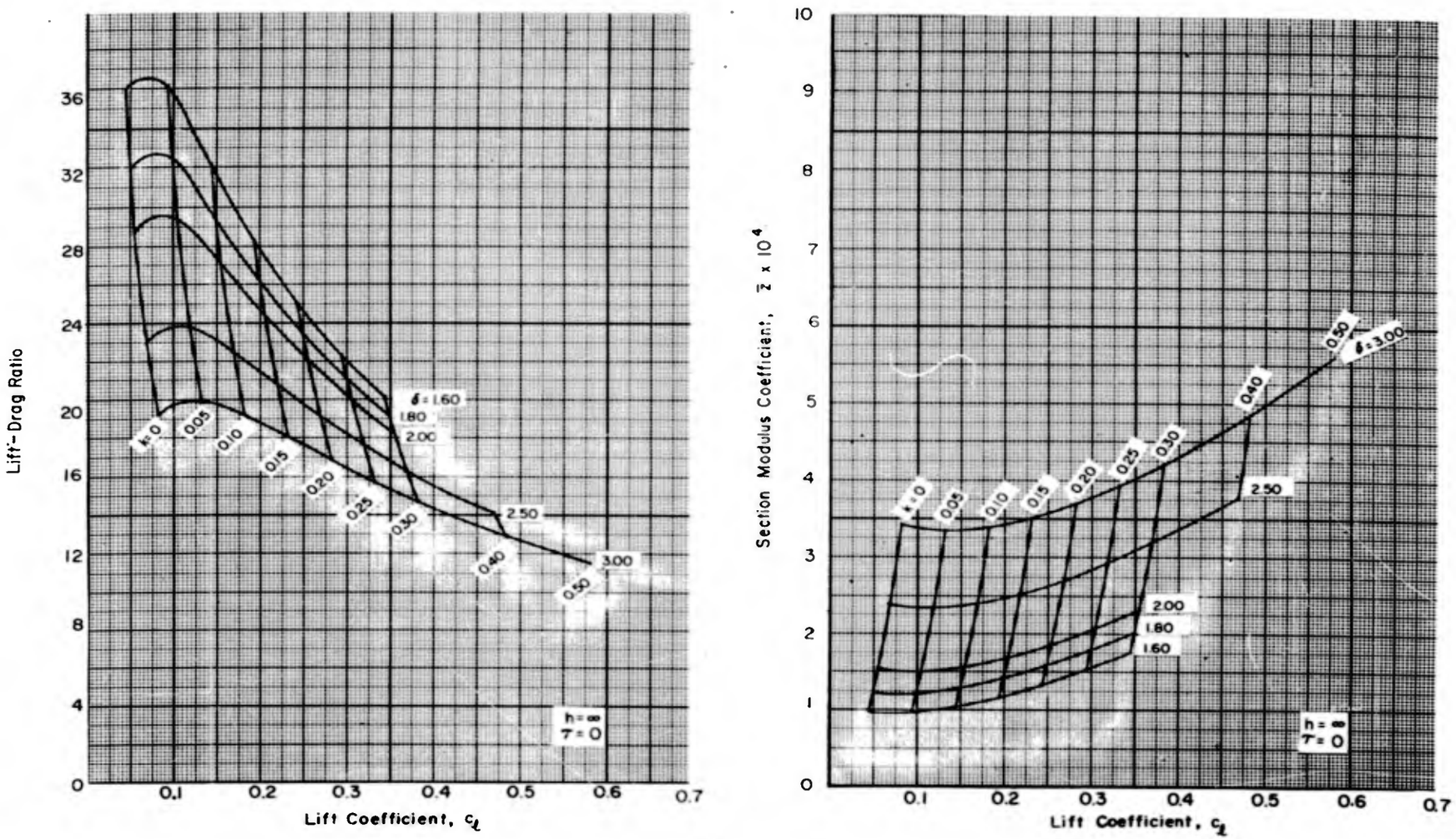

(a) $\tau = 0$

FIGURE 16. - LIFT-DRAG RATIO AND SECTION MODULUS VS. LIFT COEFFICIENT OF TWO-TERM FOILS DESIGNED FOR OPERATION AT INFINITE DEPTH. CONTOURS OF CONSTANT CAMBER INDEX AND ANGLE OF ATTACK.

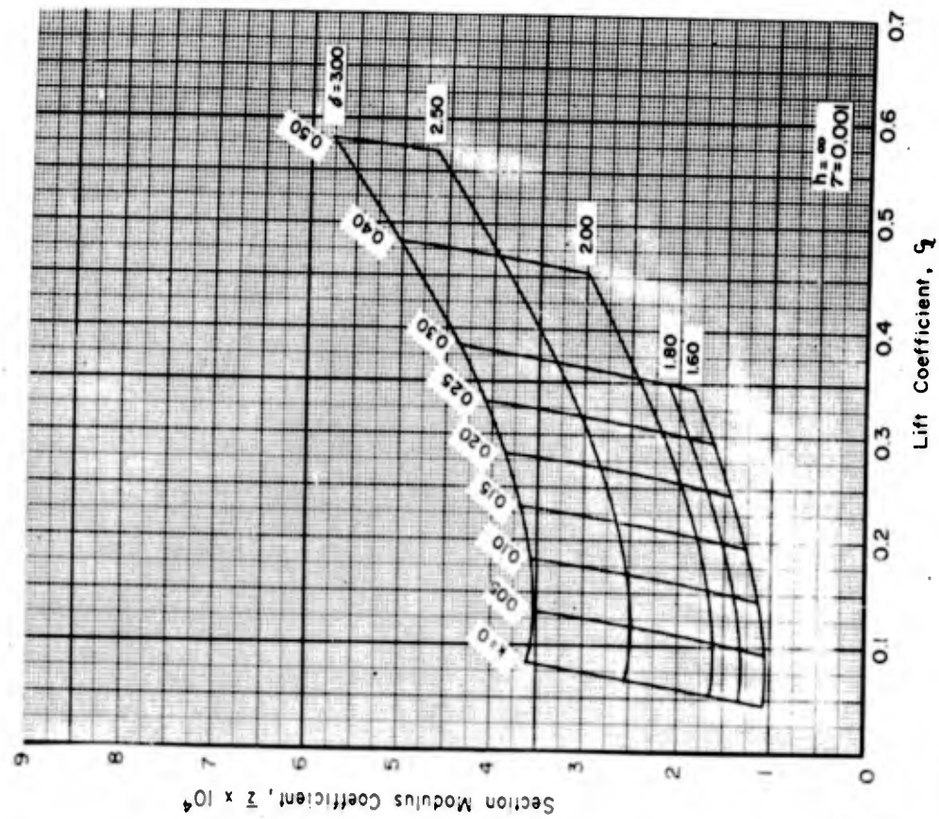

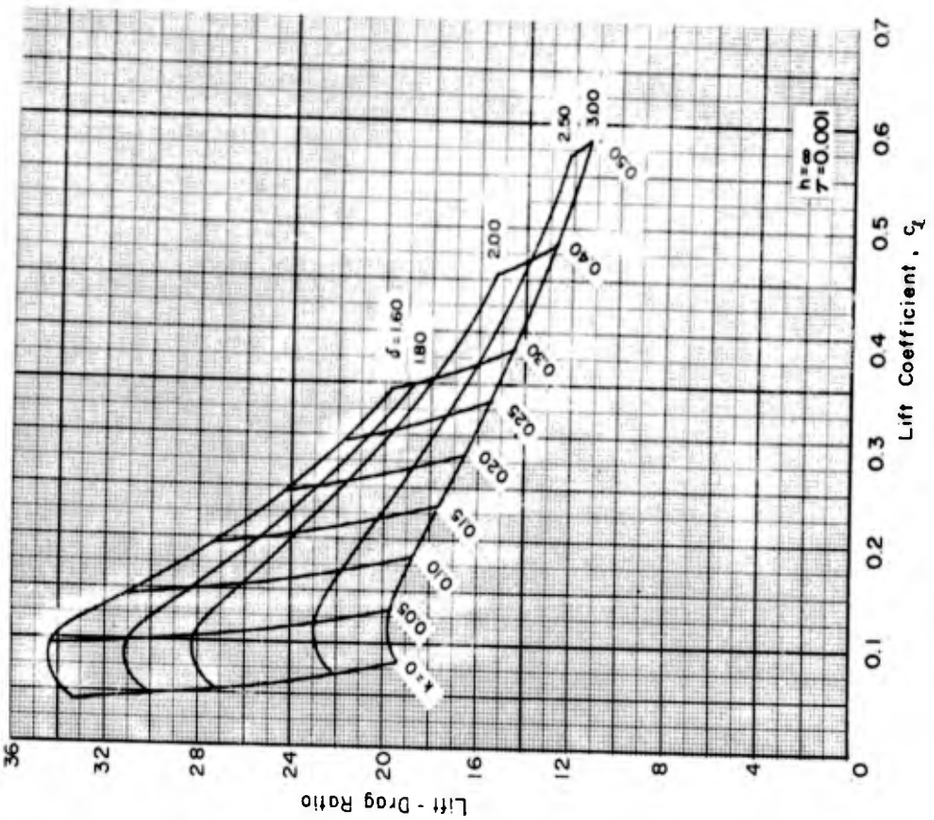

(b) τ = 0.001

FIGURE 16. - (continued)

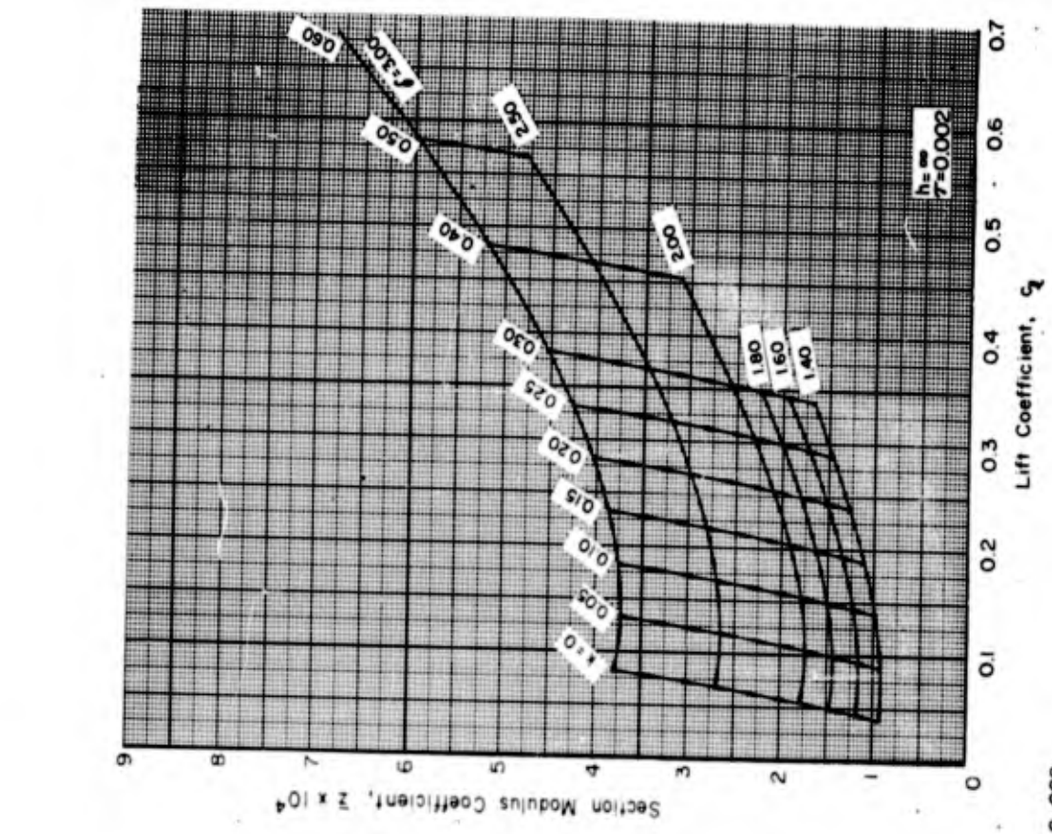

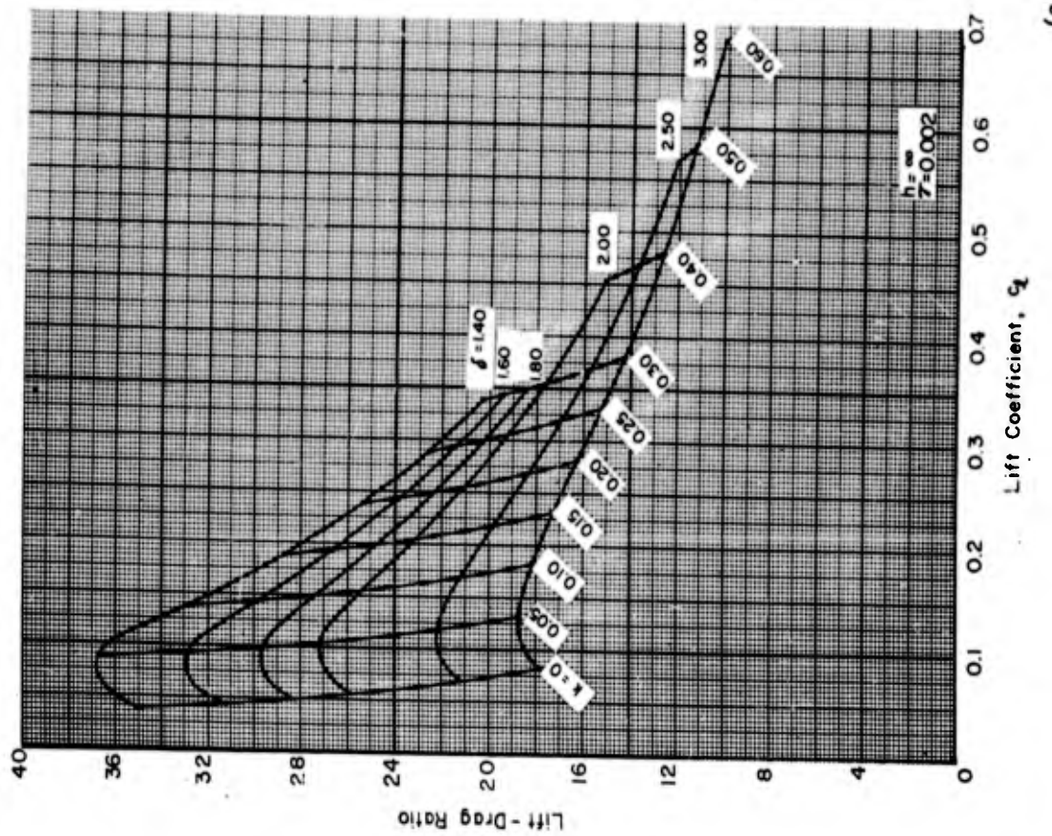

(c) τ = 0.002

FIGURE 16. - (continued)

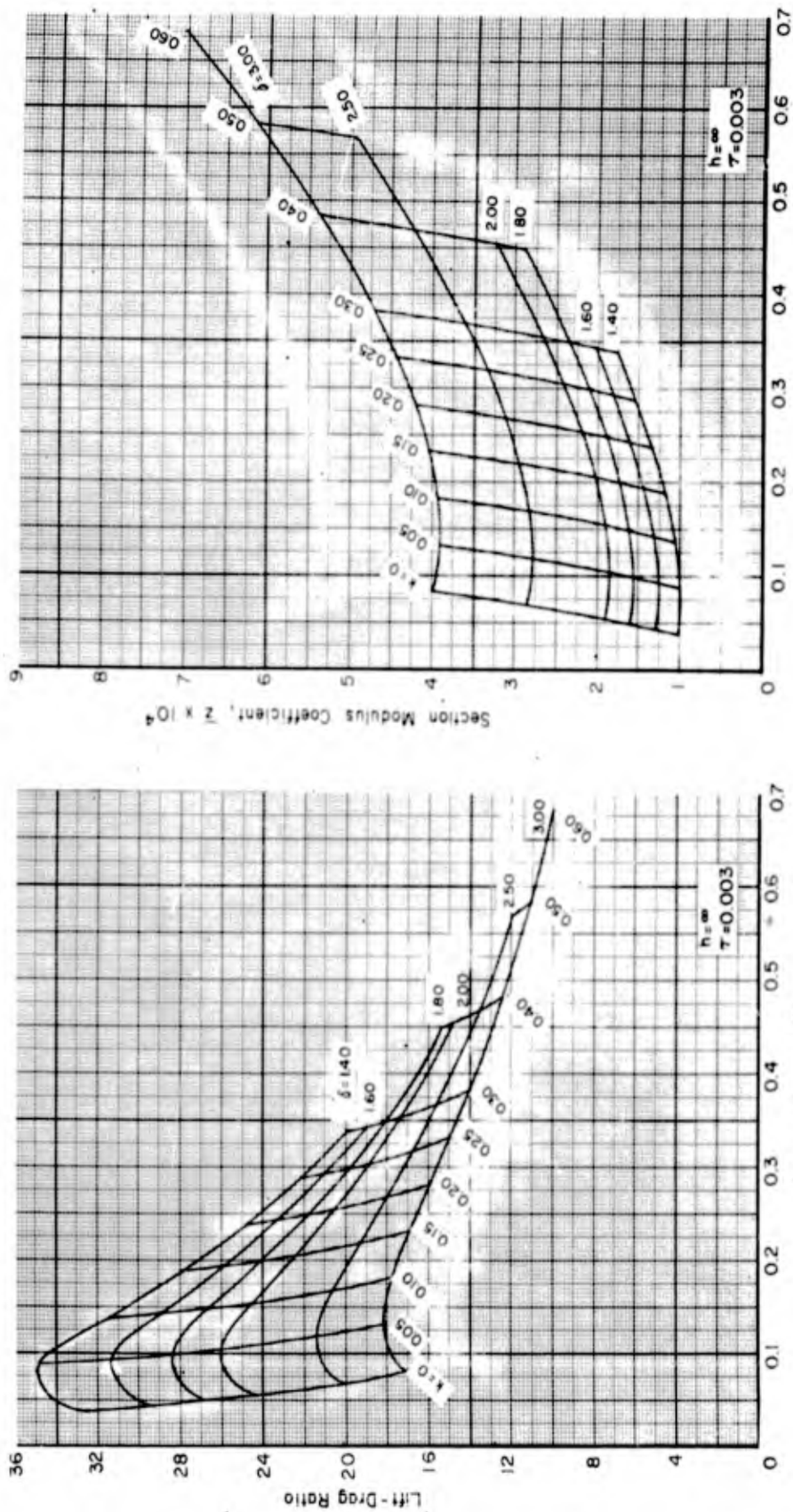

(d) τ = 0.003

FIGURE 16. - (continued)

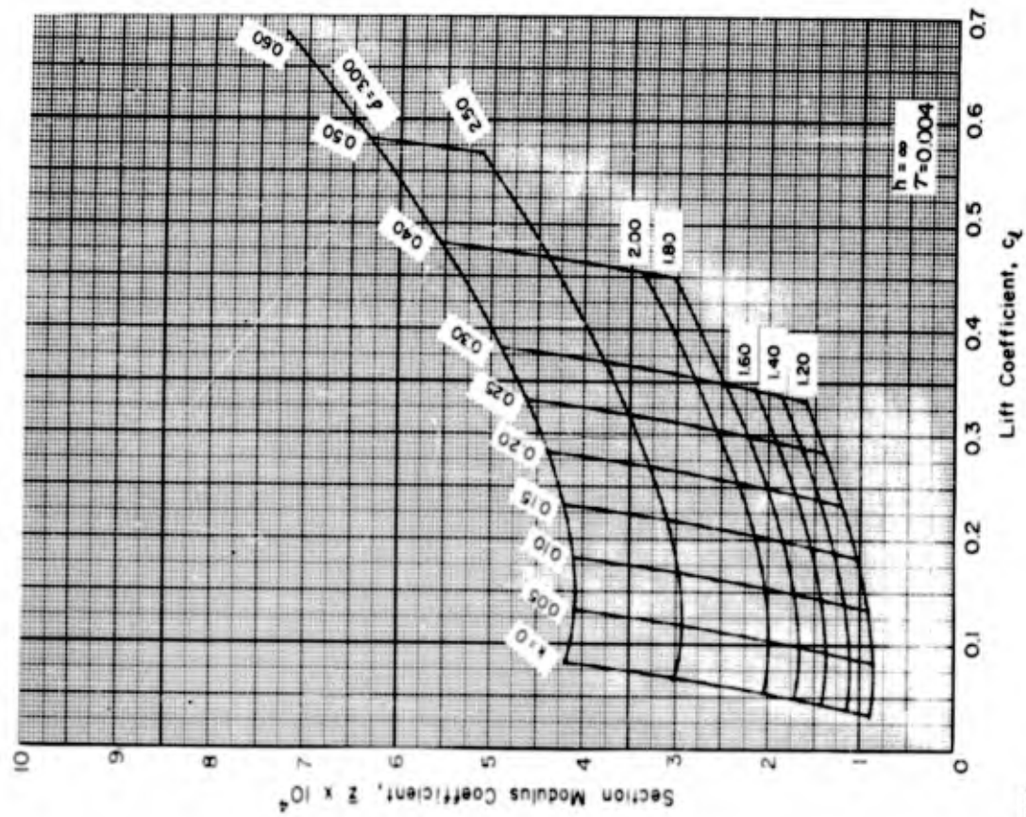

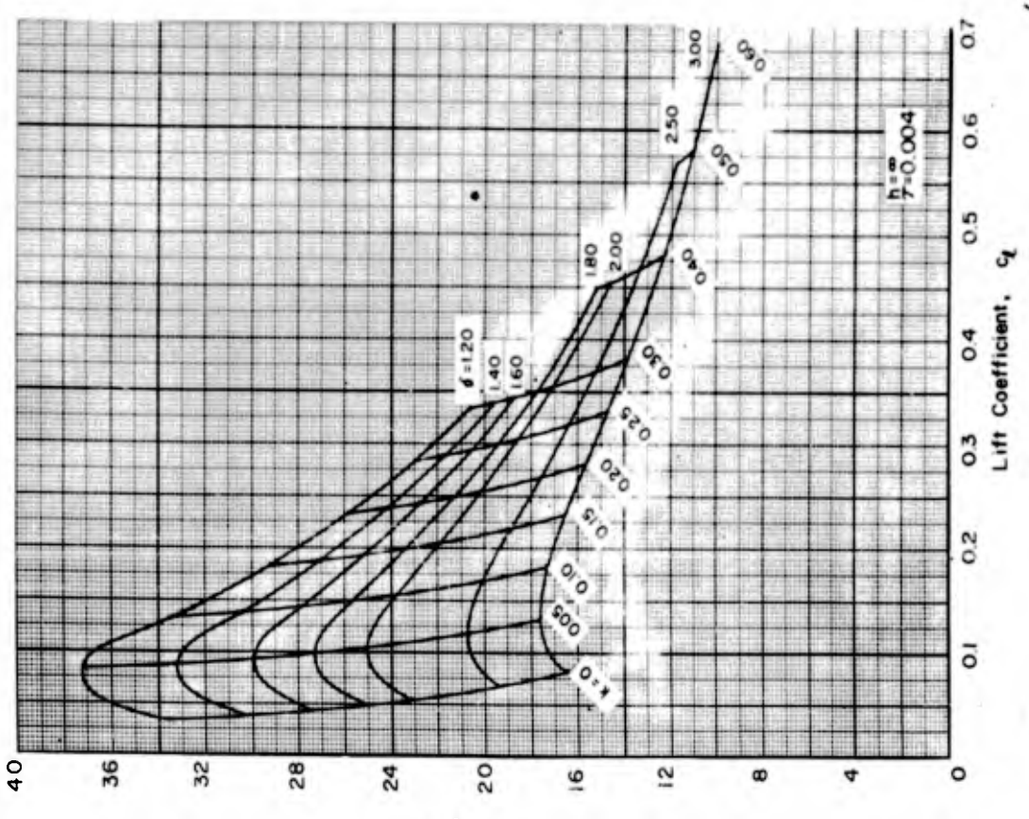

(e) τ = 0.004

FIGURE 16. - (continued)

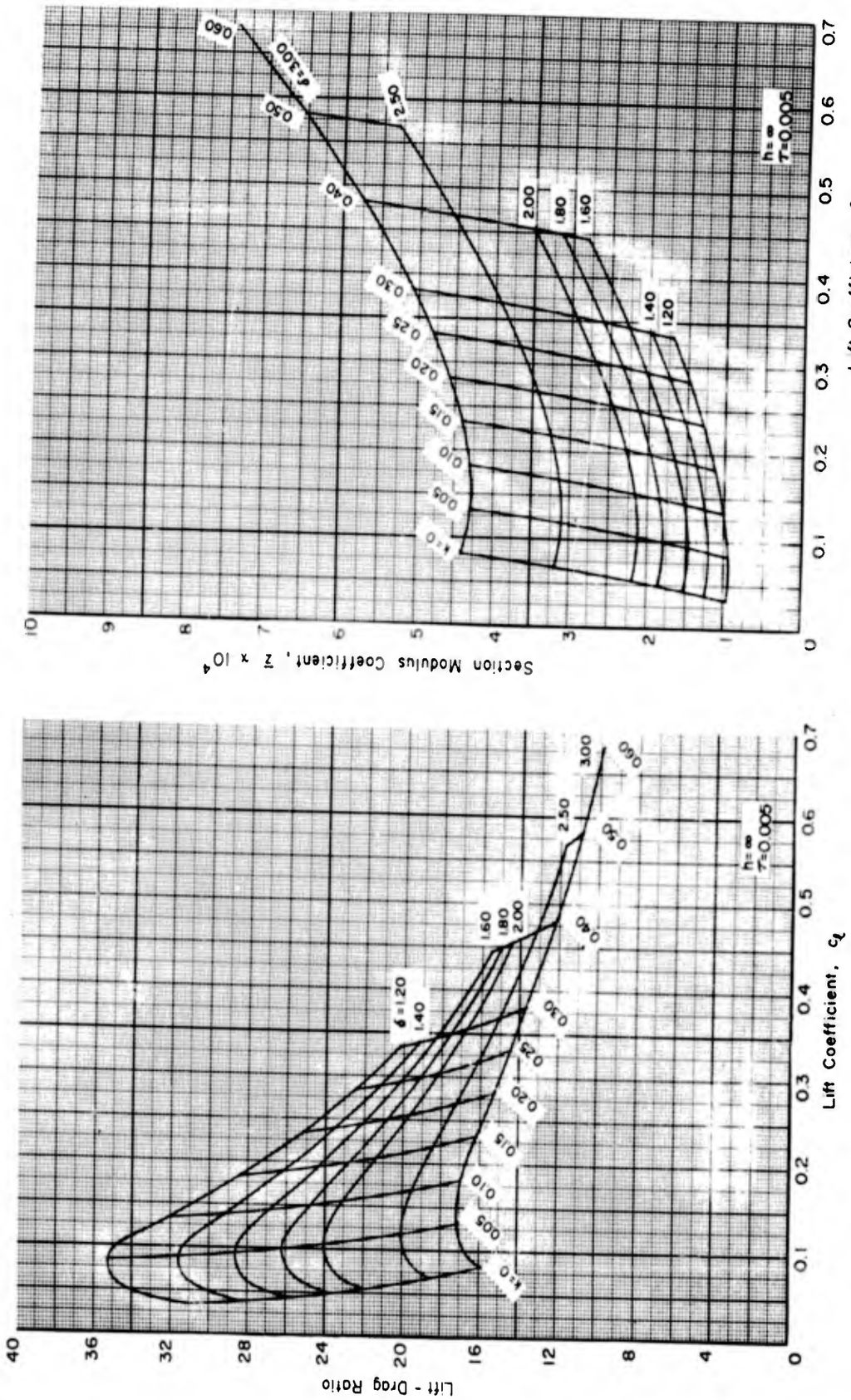

(f) τ = 0.005

FIGURE 16. - (continued)

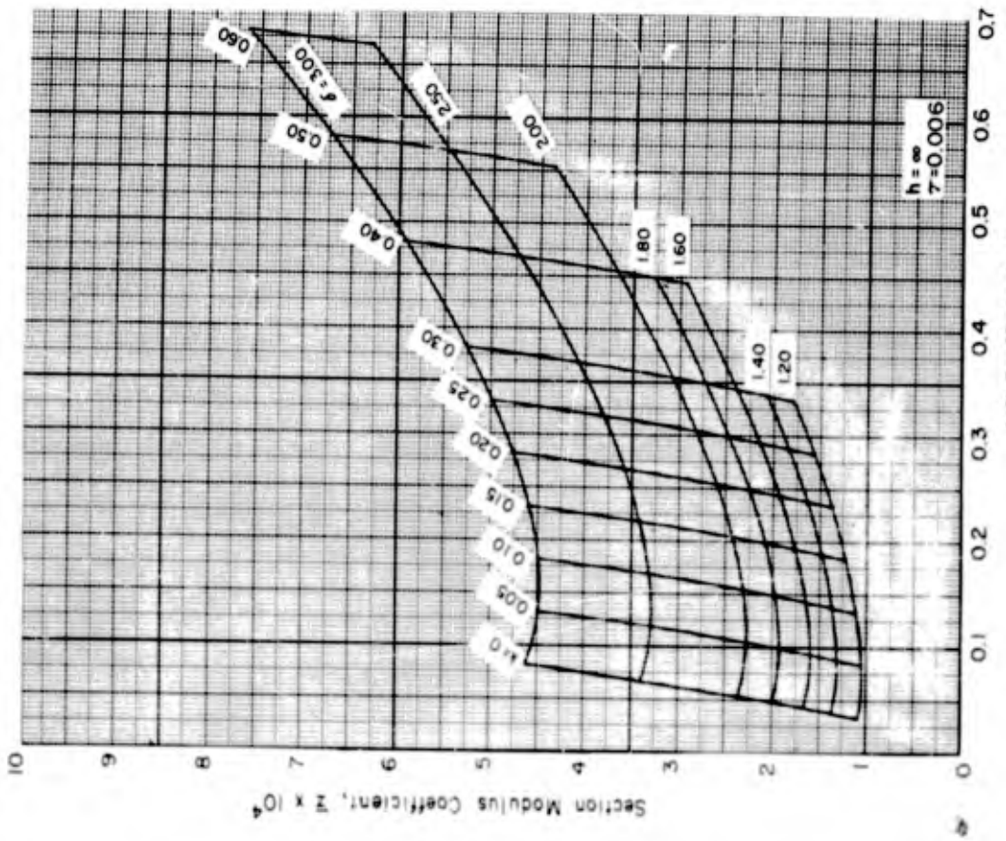

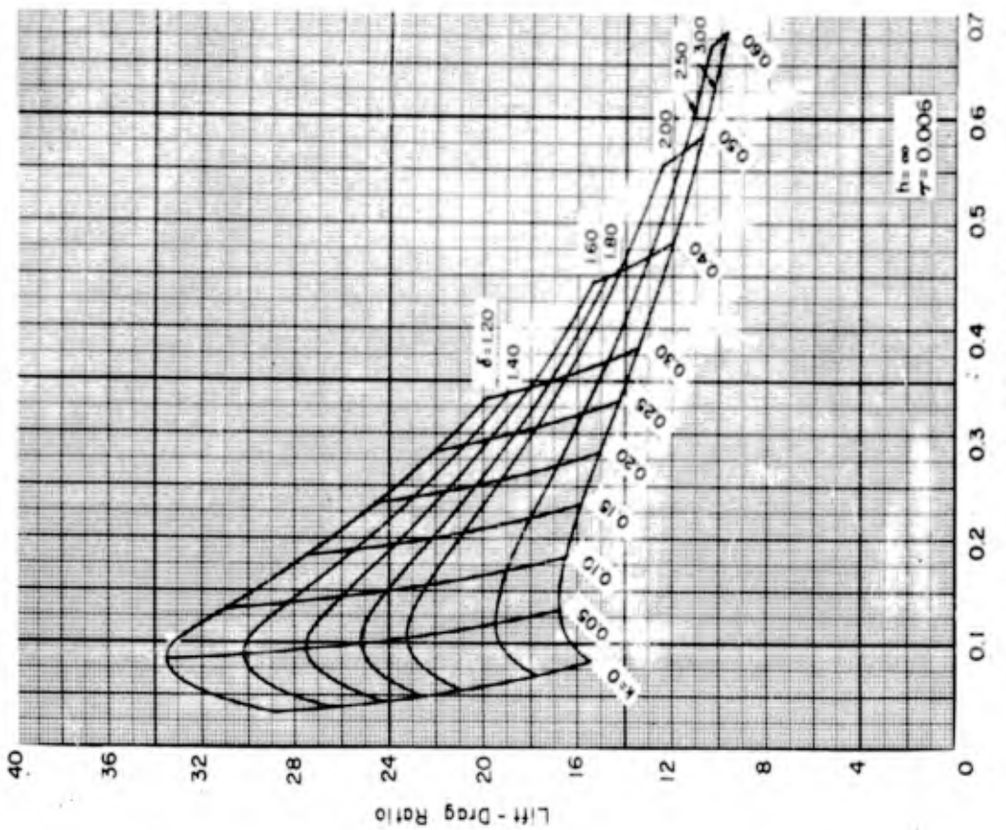

FIGURE 16. - (continued)

(g) τ = 0.006

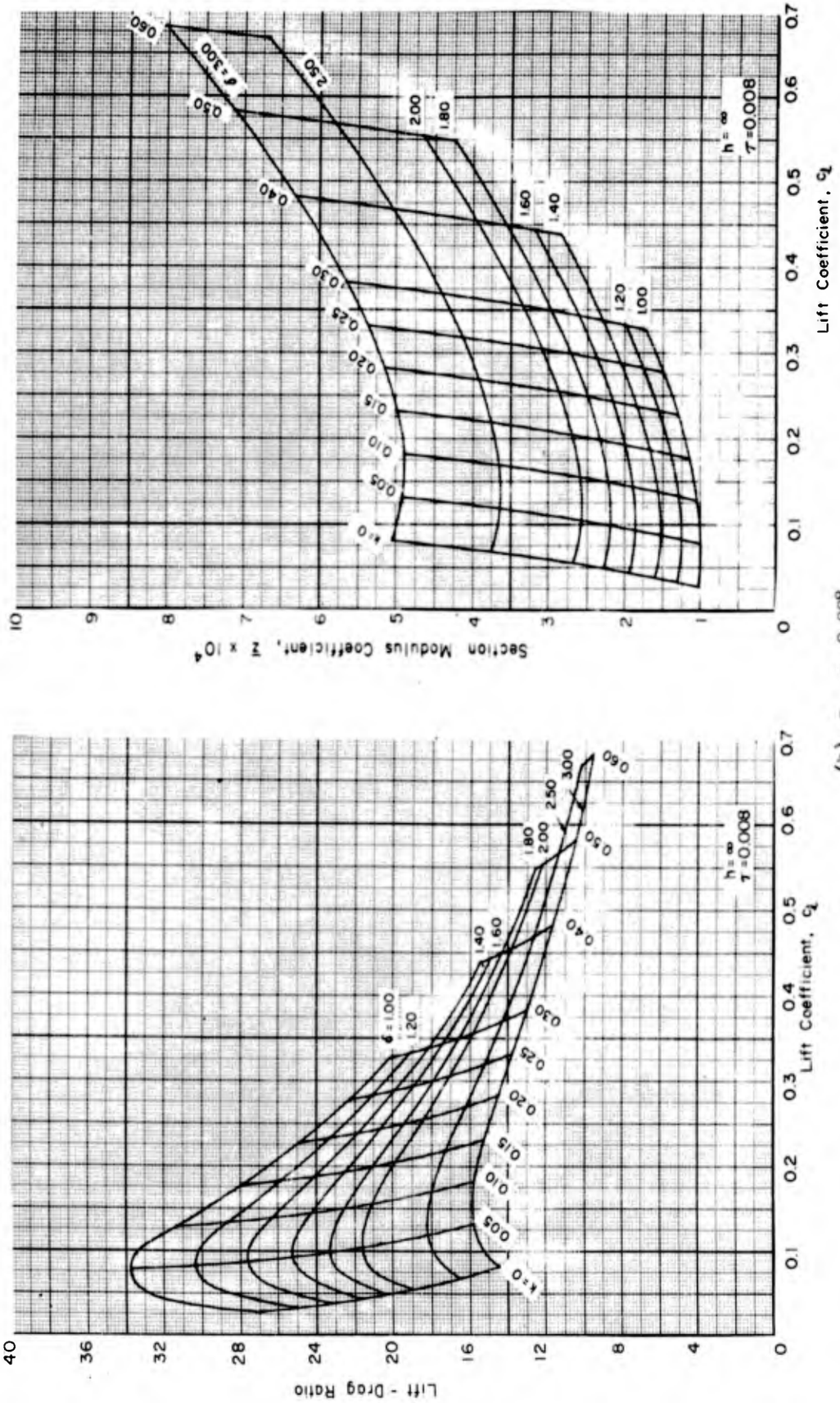

(h) τ = 0.008

FIGURE 16. - (continued)

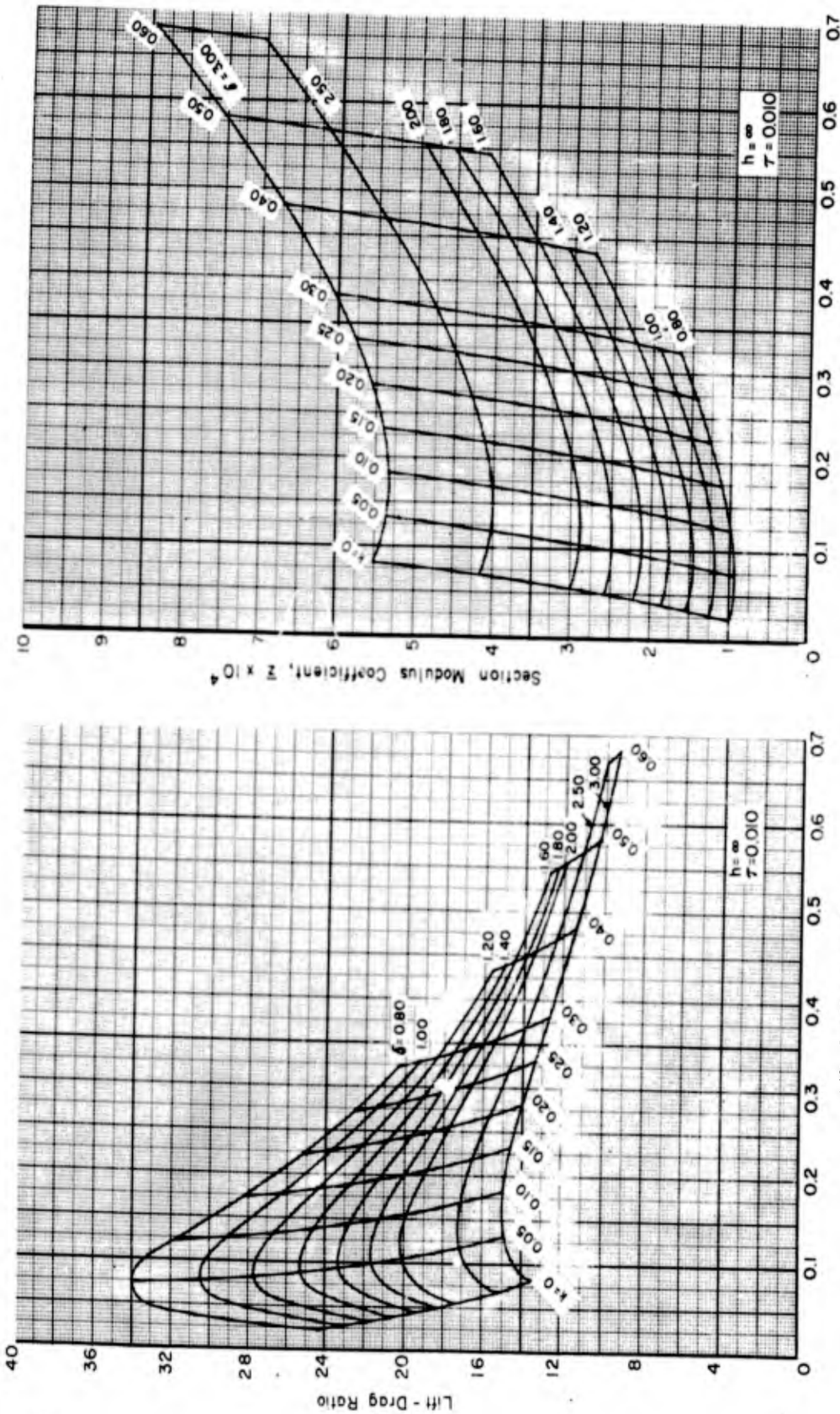

(1) τ = 0.010

FIGURE 16. - (concluded)

HYDRONAUTICS, Incorporated

DISTRIBUTION LIST

BuShips Contract NObs-78396

Chief, Bureau of Ships (60) Navy Department Washington 25, D. C.		
ATTN:	Code 336	1
	Code 335	3
	Code 410	1
	Code 420	53
	Code 442	1
	Code 449	1
Chief, Office of Naval Research (2) Navy Department Washington 25, D. C.		
ATTN:	Code 438	2
Commanding Officer and Director David Taylor Model Basin Carderock, Maryland		
ATTN:	Code 500	1
	Code 513	1
	Code 520	1
	Code 526	1
	Code 530	1
	Code 580	1
Chief, Bureau of Naval Weapons (2) Navy Department Washington 25, D. C.		
ATTN:	Code RAAD-343	1
	Code R-52	1
Commander Armed Services Technical Information Agency Arlington Hall Station Arlington 12, Virginia		
ATTN:	TIPDR	5
Mr. John B. Parkinson Langley Aeronautical Laboratory National Aeronautics and Space Administration Langley Field, Virginia		1
Boeing Airplane Company Aero-Space Division, Box 3707 Seattle 24, Washington		1
California Institute of Technology Pasadena, California		
ATTN:	Professor T. Y. Wu Hydrodynamics Laboratory	1

Convair Hydrodynamic Laboratory
Convair Division
General Dynamics Corporation
San Diego, California 1

Director, Stevens Institute of Technology
Davidson Laboratory
Castle Point Station
Hoboken, New Jersey 1

Grumman Aircraft Engineering Corporation
Marine Engineering Section
Bethpage, Long Island, New York

Hughes Aircraft Company
Systems Development Laboratories
Culver City, California
ATTN: Mr. W. N. Turner 1

The Martin Company
Baltimore 3, Maryland
ATTN: Mr. John D. Pierson 1

Massachusetts Institute of Technology
Department of Naval Architecture and
Marine Engineering
Cambridge 39, Massachusetts 1

Director
University of Minnesota
St. Anthony Falls Hydraulic Laboratory
Hennepin Island
Minneapolis 14, Minnesota 1

Southwest Research Institute
Department of Applied Mechanics
8500 Culebra Road
San Antonio 6, Texas 1

Technical Research Group, Inc.
2 Aerial Way
Syosset, New York

Chief of Naval Operations
Navy Department
Washington 25, D. C.
ATTN: Capt. N. H. Fisher, OP-712 1

UNCLASSIFIED